Summer 2019

Health Monitoring of Liquid Pipelines

Mohammed Hameed Sabhan Al-Tofan

Health Monitoring of Liquid Pipelines

by

Mohammed Hameed Sabhan Al-Tofan

Bachelor of Science
University of Basrah, 2002

Master of Science
University of Basrah, 2006

Bachelor of Arts
University of Basrah, 2010

Master of Science
University of South Carolina, 2017

Submitted in Partial Fulfillment of the Requirements

for the Degree of Doctor of Philosophy in

Civil Engineering

College of Engineering and Computing

University of South Carolina

2019

Accepted by:

M. Hanif Chaudhry, Major Professor

Jasim Imran, Committee Member

Enrica Viparelli, Committee Member

Jamil Khan, Committee Member

Cheryl L. Addy, Vice Provost and Dean of the Graduate School

Dedication

To my lovely wife, Farah Al-Musawi, my son, Hasan, my daughters: Zahraa, Reem, and Judi; and to my great mother, brothers, sisters; and to the spirit of my late father, for their love and support.

Acknowledgments

The author would like to thank the sponsor of this study, the Higher Committee for Education Development in Iraq (HCED), Iraqi Cultural Office in Washington DC, Ministry of Higher Education and Scientific Research, University of Basrah, College of Engineering, and Department of Civil Engineering for their support. Thank is also to the Ph.D. advisor, Dr. M. Hanif Chaudhry for his advice, and to the members of the research committee: Drs. Jasim Imran, Enrica Viparelli, and Jamil Khan for their suggestions. The author also thanks research collaborators Drs. Mohamad Elkholy, Juan Caicedo, Paul Ziehl, John Dickerson, Sahad Khilqa, Lateef Assi, Rafal Anay, and Lindsey LaRocque, and the members of water resources group for their assistance. Thank is also to the administrative staff Karen Ammarell, Jamie Wurdinger, and Brian Hull, for their support. The author also thanks Dennis Corporation for providing an engineering position during the current study, and to the Department of Transportation of Richland County and all the County staff, especially Dr. John Thompson for their support and encouragement throughout the academic training.

Abstract

The crude and refined oil, water, and other liquids are widely transported through pipelines over long distances within geographical boundaries of countries or beyond. Pipeline accidents, however, are frequent, affecting operation and reducing targeted performance. The frequency of these accidents presents a growing concern and necessitates the need for an effective health monitoring plan. This plan requires monitoring of flow conditions and warning of any changes or abnormal conditions. Abnormalities in the flow conditions include changes in the piping system performance due to defects, such as leaks and blockages. These changes can be located and quantified utilizing different approaches. Two effective and economical approaches are: i) observation of pressure oscillations and, ii) acoustic signal monitoring. This may be conducted by comparing the data set for an intact pipe and a pipe with a fault to diagnose the defect and prepare an appropriate course of action.

This work develops two practical approaches to detect abnormal conditions caused by a defect in the pipeline. In the first approach, the transfer matrix method is applied to detect a partial blockage or a leak in liquid pipelines using the first four harmonics of the pressure oscillations produced by a sinusoidal movement of a downstream valve. Unlike most relevant available methods which use a large number of harmonics to analyze the pattern of the frequency response diagram, this study uses only the first four harmonics to investigate the effect of a leak or a partial blockage on the amplitude of pressure head oscillations. A relationship between the location of the blockage or the leak and the amplitude of pressure head oscillation is developed for each lower harmonic in the steady-oscillatory flow. The effects of steady and

unsteady friction and pressure head oscillation nodes are discussed. The results show a satisfactory agreement with those obtained in the time domain using the method of characteristics and with the experimental data reported in the literature.

In the second approach, a primary zone representing the inspected length of the pipe is scanned for potential defects by installing a set of acoustic sensors on the exterior surface of the wall of the pipe. The acoustic signal emitted due to the interaction between the defect and the liquid flow is recorded and analyzed. The characteristics of this signal depend on the location and size of the defect. For instance, the existence of a partial blockage causes a hump in the plot of the relationship between the accumulated signal strength and the sensor location, the height of which is proportional to the blockage size. Following this approach, an application is developed to detect a partial blockage in a simple reservoir-pipe-valve system. The experimental results are verified by computational fluid dynamics (CFD) simulations including solution of the Reynolds-averaged Navier-Stokes equations using the FLUENT commercial package within the ANSYS software. The numerical results show a spike in the plot of the relationship between the sensor location and a number of selected flow parameters in the vicinity of the blockage location in an agreement with the experimental results.

In summary, the two approaches proposed in the current study represent simple techniques that may be used for detection of defects in short or long pipelines. The first approach including measurements of pressure head oscillations at one location may be used in the case of limited access to the entire length of the pipeline, while the second approach including monitoring of the acoustic signal may be used for short pipes with a full access to the entire length of the pipe. The two approaches may be extended to detect defects in pipelines including flow of different fluids, such as gas and steam.

Table of Contents

List of Tables

List of Figures

Chapter 1

Introduction

Two common abnormalities in pipelines transporting liquids are leaks and blockages. Leaks may be detected by direct observations, such as visual or video inspection or by inference methods, such as frequency-domain analysis. However, in some circumstances, there is no access to the entire length of the pipeline which makes it necessary to apply remote detection techniques. On the other hand, blockages in the pipeline always cannot be detected by direct observations regardless of the access to the entire length of the pipeline. Therefore, current study includes two approaches depending on the availability of pipeline access: a pressure monitoring approach with a downstream valve oscillation to detect pipeline abnormalities from one location; and an acoustic-emission approach in which a primary zone of the pipe is scanned for a potential partial blockage detection.

1.1 Research Motivation

Transportation of liquids in pipelines faces considerable challenges including pipeline accidents caused by abnormal conditions. These abnormal conditions may result in considerable safety issues, such as pipe explosion and failure due to significant reduction in the pipeline cross-sectional area or hazardous fluid leakage. For instance, in 2016, the explosion of a major gasoline pipeline in Alabama, which is a crucial fuel supply source for the US East Coast, resulted in death of one worker, injured five others and produced a fuel crisis in many southern states of the USA. It is clear that

pipeline accidents are not only threatening operators' and public life but are more affecting economy. They cause reduction in the flow rate and dissipation of energy. Therefore, these hazardous conditions and their costly remedies necessitate the need for an effective health monitoring plan.

1.2 Pipeline Health Monitoring Approaches

There are many pipeline health monitoring approaches, each with advantages and disadvantages. The cost and risk of implementation are the two most effective parameters for the selection of a certain technique. Among these approaches, the most economical and global are the pressure transients and acoustic wave techniques (Owowo, 2016) in which a pipeline responses to a certain exciter, or a defect interacts with the flow characteristics, producing information about potential abnormalities. These two approaches are adopted in the current study.

1.3 Research Objectives

The main objective of the current work is to develop suitable health monitoring approaches for detecting pipeline abnormalities, including leaks and blockages. Two approaches are traditionally proposed and applied for different piping systems. The first approach includes the pressure head observation of steady-oscillatory flow, while the second approach includes monitoring of the acoustic signal emission. In fact, most of the steady-oscillatory flow methods use several harmonics to excite the liquid flow which requires more operation efforts and safety concerns. In contrast, the approach proposed in the current study requires running the system very few times to extract the required information for abnormalities detection. The second approach includes application of the acoustic signal emission technique in such a way that exploits the

interaction between the pipe abnormality and the steady-flow characteristics to detect the proposed defect in the pipe. It considers a primary zone of the pipe under investigation by installing detection sensors on the external wall of the pipe without any interaction with the liquid flow.

1.4 Research Limitations

The technique presented in Chapters 3 and 5 of this study utilizes the pipeline system response to a set of excitation harmonics, including oscillations under the natural frequency of the pipeline. Oscillating the liquid flow in a pipeline at the natural frequency may cause pressure amplification and resonance. However, care should be taken that the approach is applied within the design limit of the pipeline. For the acoustic emission approach, the noise of the ambient environment must be considered and the approach should be applied in controlled vibrational settings to avoid noise and irrelevant signals interaction.

1.5 Contribution to Knowledge

The technique presented in Chapters 3 and 5 of this study includes the reduction of efforts and requirements for the current steady-oscillatory approaches used for defect detection to only few runs to detect a potential abnormality in liquid pipelines. In addition, the study introduced in Chapter 4 including the acoustic emission approach presents a very simple and economical methodology for blockage detection. Unlike most available techniques which require interaction with the liquid flow in the pipe and cumbersome data analyses, this approach keeps the pipe under normal operation and requires simple data analysis.

1.6 Dissertation Outline

The current dissertation presents two main approaches developed for the health monitoring of liquid pipelines: an acoustic emission technique applied under steady-state flow conditions and a pressure oscillation approach applied under periodic flow conditions. The two approaches are applied successfully for the problem of partial blockage and the first approach is applied for leak detection. This dissertation comprises six chapters including presentations of the two proposed approaches. Chapter 1 includes an introduction in which research motivations, health monitoring approaches, research objectives, research limitations, contribution to knowledge, and dissertation outlines are presented. Chapter 2 includes a brief literature review on the two approaches for blockage detection problem and the second approach for leak detection problem. Chapter 3 presents the technique of using lower harmonics of pressure oscillations for blockage detection in liquid pipelines. This research is published in the Journal of Hydraulic Engineering of the American Society of Civil Engineers (ASCE) (Al-Tofan et al., 2018). Chapter 4 includes application of the acoustic emission technique for blockage detection in liquid pipelines. It also includes flow field description over the primary zone of the pipe and in the vicinity of the blockage location, using the traditional CFD simulations with Reynolds-averaged Navier Stokes equations solved by FLUENT commercial package within the Ansys software. This work is presented in the 60^{th} working group of acoustic emission conference in Charleston, SC on June 19^{th} 2018. Chapter 5 presents the technique of using lower harmonics of pressure oscillations for leak detection in liquid pipelines. Lastly, Chapter 6 includes summary and conclusions of both detection approaches for blockage problem and the pressure oscillation approach for leak detection.

Chapter 2

Literature review

2.1 Blockage Detection by Using Lower Harmonics of Pressure Oscillations

Blockages in pipelines occur for different reasons including, but are not limited to, freezing, hydrate accumulation, chemical deposition, grease build-up, and valve jamming (Wang et al., 2005; Mohapatra et al., 2006; Sattar et al., 2008; Wang et al., 2012; Meniconi et al., 2013). As the blockage protrudes transversely or extends longitudinally, it causes serious problems, such as reduction in the flow rate and dissipation of energy. In addition, it may results in safety issues, such as pipe failure that may occur due to significant reduction in the pipeline cross-sectional area. These hazardous conditions and their costly remedies necessitate the need for an effective pipeline blockage detection plan.

Blockages, unlike other pipeline abnormalities, can not be detected by direct methods, such as visual inspection. However, they may be detected by many other techniques such as hydraulic transient analysis. These techniques are based on different analytical, numerical, experimental and field approaches. Wang et al. (2005), for example, developed a method for partial blockage detection depending on the transient damping caused by a partial blockage. Their work included development of an analytical solution in terms of a Fourier series. Lee et al. (2008) proposed the use of fluid transients as a non-invasive technique for locating blockages in transmission pipelines. They related the oscillatory patterns of the peaks of the frequency response

diagram to the location and size of the blockage and presented a simple analytical expression that can be used to detect, locate, and size discrete blockages. Duan et al. (2011) presented a technique for detecting extended blockages in pressurized pipelines utilizing Frequency Response Method (FRM). Their technique included detection of the extended blockage by examining the resonant peaks in the frequency domain using the transfer matrix method (TMM) and verified by the method of characteristics (MOC). They concluded that the existence of an extended blockage causes a shift in the resonant peaks as compared to those for the original intact pipe with no blockage. Tuck et al. (2013) studied the effect of extended blockages on the fundamental frequency and the maximum pressure head and concluded that, as the pipe diameter reduces with age, the maximum transient response may increase thereby making the pipeline susceptible to fail. They, also, compared the numerical and experimental results with good agreement for the first period of oscillations. Duan et al. (2013) verified experimentally their previously obtained analytical results using six different blockage tests over a range of Reynolds number. Their experiments show a good agreement with the theoretical predictions. Meniconi et al. (2013) conducted experiments on partial blockage detection in pipelines. They performed both pressure signal and frequency response analysis showing that the first analysis is most accurate for locating the blockage, while the second is most accurate for determining the radial constriction and blockage extension. Massari et al. (2014) developed a new algorithm for blockage detection using transient pressures and a stochastic linear approach to estimate the pipe diameter. In a later publication, they compared their algorithm with experimental case studies and showed that a good estimate of the blockage size and extent can be obtained by pressure measurements following a fast valve closure (Massari et al., 2015). Meniconi et al. (2016) analyzed the mechanism of interaction of pressure waves at a discrete partial blockage. Their experiments show two interaction mechanisms: sinuous for partially closed in-line valves and straight for small bore

pipe devices. Scola et al. (2017) proposed a method based on the frequency modeling to detect simultaneous blockages and leaks occurring in the pipeline. They also discussed the effect of the pipe friction in their detection approach and introduced a term to reduce its effect by increasing the excitation frequency.

In fact, many previous detection techniques that use frequency domain analysis either neglect friction effect or consider only steady friction since an accurate universal unsteady friction model is presently unavailable. However, the unsteady friction in the transient analysis is currently a subject for continuous research where several relevant approaches are continuously proposed. These approaches may be classified into three categories: Quasi-2D, instantaneous acceleration based (IAB), and convolution integral methods (Chaudhry, 2014). The first two categories are either computationally intensive, requiring transient simulation of the entire system, or involving calibration of empirical coefficients (Chaudhry, 2014; Khilqa et al., 2017; Duan et al., 2017). The last category involves the development of a weighting function and is suitable for relatively small simple piping systems (Duan et al., 2017). They were introduced by Zielke (1968) for laminar flow and adapted for turbulent flow by many researchers, such as Vardy and Brown (2003), Vitkovsky et al. (2003), and Meniconi et al. (2014). Unlike the IAB models, the convolution-based models utilize the results of a set of previous time steps and hence describe the signal better in turbulent flows at low Reynolds number (Martins et al., 2017). In the current research, both steady and unsteady friction and their effect on the blockage detection approach are considered.

To detect a partial blockage, the frequency response diagram (FRD) of a piping system over a wide range of harmonics for a blocked pipeline may be compared with that of a healthy one. Following this approach, Mohapatra et al. (2006) used the transfer matrix method in the frequency domain with odd harmonics for periodic oscillation of a downstream valve to present a methodology for detecting partial

blockages in single pipelines. The peaks of the pressure frequency response at the oscillating valve was utilized to detect the partial blockage location. They related the odd harmonics FRD pattern with the blockage location. Sattar et al. (2008), on the other hand, used the FRD with even harmonics to detect partial blockage in a pipeline utilizing the troughs of the the pressure head oscillations. They claimed that the system response at even harmonics gives, in some cases, better indication of the blockage existence than the response at odd harmonics depending on the system parameters. In contrast, Gong et al. (2013) compared odd and even harmonics for leak detection and found that the approach using odd harmonics is superior because it eliminates the aliased leak locations. In addition, Sattar et al. (2008) and Meniconi et al. (2013) indicated that a partial blockage reduces the amplitude of the pressure head oscillation at odd harmonics and increases it at even harmonics. Also, Duan et al. (2014) showed that a discrete or an extended blockage changes the amplitude of oscillations in a pressurized water pipeline at resonance for both odd and even harmonics. However, additional investigations are needed to analyze this change in the pressure oscillations for a single frequency with different blockage locations.

As discussed earlier, traditional FRD methods require analyzing the system several times under different modes of oscillation in order to determine the blockage location. For example, the system considered by Mohapatra et al. (2006) requires 100 runs to determine the range of possible blockage locations between 200 and 233 m of a 1600 m long pipeline. More runs are required, with higher harmonics, in order to achieve a greater precision. However, for higher harmonics, the frequency of the valve oscillation is increased, producing higher noise in the acquired signal and requiring serious operational considerations and safety concerns (Lee et al., 2008). In addition, computational deficiencies related to the use of higher harmonics in certain situations require increased computational time to keep a certain level of accuracy. For instance, the satisfactory agreement between considering a tapered pipe *per se*

and a substitute equivalent pipe with a certain number of segments is limited to the fifth harmonic (Chaudhry, 2014). For the number of harmonics greater than five, the analysis requires increasing the number of reaches to get reasonable accuracy. In addition, the damping effect due to the unsteady friction increases and the amplitude of the pressure head oscillation decreases at higher harmonics (Sattar et al., 2008).

In contrast to the traditional FRD methods, the technique proposed by the current study uses lower harmonics for the detection of the partial blockage in liquid pipelines. It utilizes the effect of the blockage location on the amplitude of the pressure head oscillations in a pipeline with liquid flow excited by a sinusoidal opening and closing of a downstream valve at the first four harmonics.

2.2 Blockage Detection by Continuous Emission of Acoustic Signal

One of the most common abnormalities in the liquid transporting pipes is the partial blockage. Partial blockages need to be detected and cleared in order to avoid unnecessary energy losses and flow-rate reductions. Traditionally, there are a number of techniques used to detect partial blockages in liquid pipes. The acoustic technique is one recent approach in which a non-destructive test is applied to detect pipe abnormalities, such as blockages and leaks. Acoustic techniques may include acoustic pulse reflectometry methods or acoustic emission methods. The former includes injection of a small sound pulse into the fluid body and trace the sound wave reflections due to the abnormalities by acoustic sensors, microphone, or hydrophones (Juliano et al., 2012). Reflections of the sound wave may also be caused by fittings along the pipe wall which interfere with the detection approach and increase the method complications. Following acoustic reflectometry technique, Papadopoulou et al. (2008) transmitted the acoustic signal into the fluid in the pipe via a loudspeaker driven by an acoustic pulse generator. They measured the signal reflections by a microphone

and compared its characteristics for different pipe conditions. Even though their results are not conclusive, they provide sufficient justification for a second phase of experiments. In a later research, Silva et al. (2014) conducted experimental acoustic tests supported by numerical simulations considering the acoustic propagation behaviors and their effects on the pipeline system dynamics. Their results show that it is possible to continuously monitor a pipeline remotely to detect a blockage and provide its size and location. In fact, many of the pipe defects occur at or close to the valves. The latter are monitored and analyzed by Yan et al. (2015) who presented an application of AE technique in this regard discussing the AE signal and analyzing its parameters of interest. They concluded that the AE root-mean-square has a strong relationship with the valve and fluid parameters (valve type and size, leakage rate, inlet pressure, and fluid type). However, how the acoustic emission technique is applicable and reliable has been a question for many researchers and a topic for further research and analysis. In this regard, Brunner and Barbezat (2006) recorded AE signals and AE waveforms from sensors mounted on an 60 mm aluminum pipe having fluid flow under operating pressures within the range 5-8 bars for two pipe conditions: an intact pipe and a pipe with a leak. He concluded that the conventional AE signal parameter analysis does not seem suitable for leak detection as compared to the waveform analysis in which distinct high-frequency components of a leaky pipe are obtained as compared to the no-leak condition. In contrast, Giunta et al. (2012) conducted a study to investigate the reliability and applicability of the AE technique for health monitoring of a steel pipeline. They concluded that the rate of the AE energy is strictly related to the density of the source generated by the progressive damage of the pipe material caused by internal fluid pressure. Brunner and Barbezat (2006) also reported that the flow of water in the test system produces a continuous acoustic emission whether there is a leak in the pipe or not. Similarly, for a pipe with a partial blockage, the interaction between the liquid flow and the partial block-

age causes a continuous emission of acoustic signal. This continuous emission of the acoustic signal may be used for detecting a possible partial blockage, as discussed in Chapter 4 of the current study.

2.3 Leak Detection by Using Lower Harmonics of Pressure Oscillations

Leaks in pipelines occur for different reasons including, but are not limited to, earth movement, damage from nearby excavation, sabotage, terrorism, and corrosion. The latter may occur at construction joints, low points of moisture accumulation, or locations of imperfection in the pipes (Boaz et al., 2014). Leaks present a safety and health hazard where pollutants may enter the pipeline if the inside pressures are low. In addition, leaks present an economical concern as they result in energy losses (Colombo et al., 2009). Colombo and Karney (2002) evaluated the impact of leaks on water quality relating the leak size and location to the residence time and discussed the potential entry of contaminated groundwater, pathogens, and soil constituents into the leaky pipes. They also illustrated the potential importance of energy costs of leaky pipes, concluding that the leak is related to the percentage increase in energy cost in a second-order polynomial function. Taking these environmental and economical hazards to consideration allows the preparation and implementation of an effective leak detection plan.

Leaks may be detected by direct observations, such as video inspection or by inference methods, such as frequency-domain analysis (Covas et al., 2005). Numerous papers present an extensive literature review for leak detection in liquid and gas transporting pipes with a variety of methods (Cole, 1979; Black, 1992; Colombo et al., 2009; Puust et al., 2010; Murvay and Silea, 2012; Boaz et al., 2014; Fiedler, 2014; Geiger et al., 2006). As the current leak detection approach is based on the frequency-

domain analysis, only some of the closely relevant works are considered in this section. Mpesha et al. (2001) applied the frequency response method to detect and locate leaks in single, series, parallel, and branched piping systems. They showed that there are secondary pressure amplitude peaks in the frequency response diagram of a piping system with a leak as compared to a healthy system with no leak. They limited their method for pipelines with a friction factor between 0.01 to 0.025 and for a leakage rate of up to 0.5% of the mean discharge with uncertainties in the system parameters not taken in consideration. Covas et al. (2005), on the other hand, proposed a leak detection technique in pipelines using the standing wave difference method, originally used for cable fault location in electrical engineering. They indicated that a leak in a pipeline creates resonance effect in the pressure signal with a secondary superimposed standing wave that can be used for leak detection. They applied this method on different system configurations including a simple reservoir-pipeline-valve and a reservoir-loop-pipe-valve systems. However, their technique requires safety analysis in terms of nodes and antinodes location. In addition, the effect of unsteady friction is not considered in their model. Sattar and Chaudhry (2008) proposed a technique for leak detection utilizing the increase in the amplitude of pressure head oscillations at even harmonics prompted by a leak in the pipeline. They used a simple reservoir-pipe-valve system with a downstream valve that closed and opened in a sinusoidal movement. They verified their results with those obtained in the time domain using the method of characteristics (MOC). They also discussed the effect of steady and unsteady friction on their model results. However, their technique requires extraction of a wide-range of frequency response diagram (FRD) to detect the leak location. The latter requirement presented a growing concern for many operators and researchers. It may be relatively acceptable to oscillate the downstream valve at lower harmonics, but may be impractical and unsafe to oscillate the downstream valve at higher harmonics. The concerns of oscillating the downstream valve at higher harmonics in-

clude, but are not limited to, increase of noise in the acquired signal (Al-Tofan et al., 2018), operational and safety issues (Lee et al., 2008), increased analysis and computational time in some piping systems (Chaudhry, 2014), and increase of damping effect due to unsteady friction (Sattar, 2015).

Due to these concerns, researchers avoid oscillating valves at higher harmonics. One of these attempts is by Lee et al. (2005a) in which a peak-sequencing method is proposed to determine a segment of the pipe length that contains the leak. Their method adopts a comparison of the relative sizes among peaks in the frequency response diagram (FRD) and matching the observed and calculated patterns within a lookup table. They presented this table for the first three odd harmonics in which the resonant peak responses intersect at five locations and divide the pipe length into six unequal regions. This technique presents a reduced effort for leak localization; however, it gives only a range of the pipe length in which the leak exists. Furthermore, the effect of friction on the intersection points of the responses at different harmonics in not analysed. The latter effect may distort the intersection points and mess the classified regions on the pipe length, as discussed later in the current study. In a later research, Gong et al. (2012) presented a leak detection technique in pipelines based on the first three resonant responses. The input signal to their technique requires a bandwidth of up to the fifth harmonic (five times the fundamental frequency of the pipeline). Their results are based on the frequency domain solution with a linearity assumption in the governing equations and are not compared to those obtained in the time domain under non-linear settings. In addition, they used only odd harmonics, reporting in a later research (Gong et al., 2013) that using odd harmonics is superior in comparison to the even harmonics, because it eliminates the aliased leak locations. In contrast, Sattar and Chaudhry (2008) showed that the system response at even harmonics has the advantage in giving better indication of the leak existence over the response at odd harmonics in some cases, depending on the system parameters. This

advantage is in terms of higher value of the leak-induced pattern at even harmonics in some systems with the same leak discharge, as observed in some figures of Covas et al. (2005) and Mohapatra et al. (2006).

The technique proposed in the current study uses lower harmonics for leak detection in liquid pipelines. It utilizes the effect of the leak location on the amplitude of the pressure head oscillations in a pipeline with a liquid flow excited by a sinusoidal opening and closing of a downstream valve at the first four harmonics of the pipeline, two odd harmonics and two even harmonics.

Chapter 3

Use of Lower Harmonics of Pressure Oscillations for Blockage Detection in Liquid Pipelines *

3.1 Introduction

As discussed in Chapter 1, this study , in contrast to the traditional FRD methods, proposes to use lower harmonics for the detection of the partial blockage in liquid pipelines. It utilizes the effect of the blockage location on the amplitude of pressure head oscillations in a pipeline with liquid flow excited by a sinusoidal opening and closing of a downstream valve at the first four harmonics.

3.2 Frequency Domain Analysis

Transient flow in a pipeline shown in Fig. 3.1 may be described by the following continuity and momentum equations after dropping the convective acceleration terms which are typically small in most of the engineering applications and may thus be neglected (Chaudhry, 2015):

*Al-Tofan, M., M. Elkholy, S. Khilqa, J. Caicedo, and M. H. Chaudhry (2018). Use of lower harmonics of pressure oscillations for blockage detection in liquid pipelines. DOI: 10.1061/(ASCE)HY.1943-7900.0001568. *Journal of Hydraulic Engineering* 145 (3), 04018090.

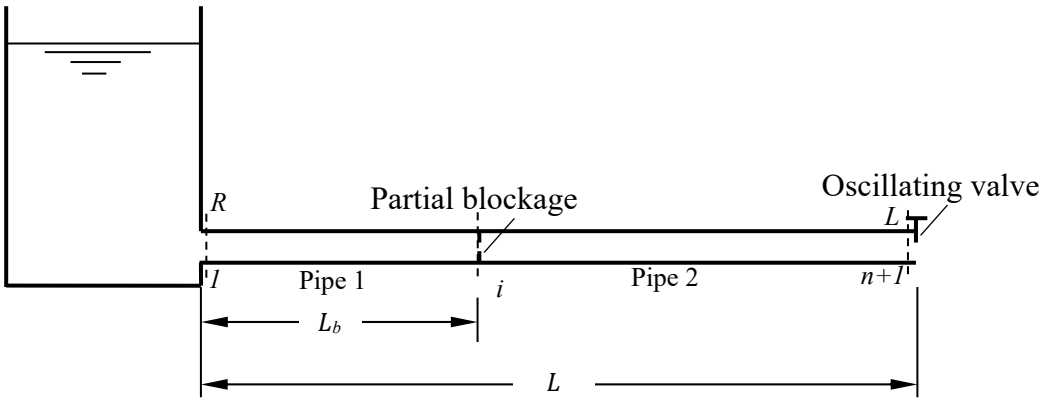

Figure 3.1 Piping system for blockage detection.

$$\frac{\partial Q}{\partial x} + \frac{gA}{a^2}\frac{\partial H}{\partial t} = 0 \tag{3.1}$$

$$\frac{\partial H}{\partial x} + \frac{1}{gA}\frac{\partial Q}{\partial t} + \frac{fQ^2}{2gDA^2} = 0 \tag{3.2}$$

where H is the instantaneous pressure head, Q is the instantaneous flow rate, a is the wave speed, g is the acceleration due to gravity, f is the Darcy-Weisbach friction factor, A is the cross-sectional area of the pipe, x is the distance along the pipeline, positive in the downstream direction, t is the time and D is the pipe diameter.

The instantaneous pressure head H and instantaneous flow rate Q may be expressed as the sum of their mean values, H_0 and Q_0, and their oscillations around the mean, h^* and q^*, as shown in Fig. 3.2 (Chaudhry, 1970). By substituting these into Eqs. 3.1 and 3.2, the following linear equations are obtained

$$\frac{\partial q^*}{\partial x} + \frac{gA}{a^2}\frac{\partial h^*}{\partial t} = 0 \tag{3.3}$$

$$\frac{\partial h^*}{\partial x} + \frac{1}{gA}\frac{\partial q^*}{\partial t} + Rq^* = 0 \tag{3.4}$$

where, $R = fQ_0/gDA^2$ is a linearized resistance term for the turbulent flow. Elimi-

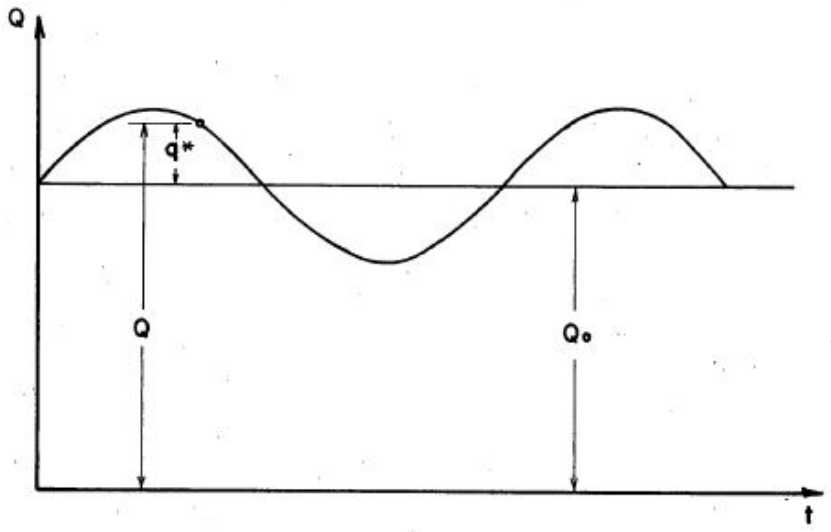

Figure 3.2 Instantaneous and mean discharge. Taken from Chaudhry (1970)

nation of h^* from the previous two equations yields

$$\frac{\partial^2 q^*}{\partial x^2} - \frac{1}{a^2}\frac{\partial^2 q^*}{\partial t^2} - \frac{gAR}{a^2}\frac{\partial q^*}{\partial t} = 0 \tag{3.5}$$

Pressure head and discharge oscillations are assumed to be sinusoidal in time, i.e., $h^* = \mathrm{Re}\,[h(x)e^{j\omega t}]$ and $q^* = \mathrm{Re}\,[q(x)e^{j\omega t}]$, where ω is the angular frequency in radians per second, $j = \sqrt{-1}$, h and q are complex variables and are functions of x only, and Re[ ] stands for the real part.

Substituting these sinusoidal terms into Eq. 3.5, the field matrix, F_i, of the i^{th} pipe may be obtained which is then used to derive blockage detection equations, as discussed in the following section.

Blockage Detection Equations

A partial blockage can be modeled as a partially open, in-line valve with a constant opening. The size of the partial blockage is characterized by the ratio of the pipe diameter at the blockage location to that of the healthy pipeline. The overall extended transfer matrix, U, is obtained by an ordered multiplication of individual extended

field and point matrices and is considered to be characteristics of the piping system. As the partial blockage divides the pipe into two segments, the overall extended transfer matrix, U, for a reservoir-pipe-valve system may be expressed as (Chaudhry, 2014):

$$U = \begin{pmatrix} u_{11} & u_{12} & u_{13} \\ u_{21} & u_{22} & u_{23} \\ u_{31} & u_{32} & u_{33} \end{pmatrix} = F_2 \; P_2 \; F_1 \tag{3.6}$$

where u_{11}, u_{12}, $\cdots$ are elements of the overall transfer matrix; F_1 and F_2 refer to the field matrices of the pipe to the left and to the right of the partial blockage, respectively, and P_2 refers to the point matrix for the partial blockage.

The elements of the overall extended transfer matrix depend on the mode of oscillation of the downstream valve. For instance, u_{11} and u_{12} for a valve oscillating at the 1^{st} (fundamental) harmonic $\left(\omega = \omega_{TH} = \frac{\pi a}{2L}\right)$ may be expressed as (see Appendix A)

$$u_{11} = \frac{2\Delta H_0}{CQ_0} \cos^2\left(\frac{\pi}{2} L_r\right) j \tag{3.7}$$

$$u_{21} = -\frac{\Delta H_0}{Q_0} \sin\left(\pi L_r\right) - C \; j \tag{3.8}$$

where L_r is the relative blockage location (blockage location measured from the upstream reservoir, L_b, divided by the pipe length, L); ΔH_0 is the steady state head loss due to the blockage, and $C = a/(gA)$ is the pipe characteristic impedance.

Utilizing the extended point matrix and the boundary conditions at the valve

$$h_{n+1}^L = u_{21} \; q_1^R + u_{23} \tag{3.9}$$

where q_1^R is the discharge just to the right of the reservoir (i.e., at the first node of the pipe) and h_{n+1}^L is the oscillating pressure head to the left of the valve (i.e., at the last node of the pipe) as shown in Fig. 3.1, q_1^R and h_{n+1}^L can be expanded as (Chaudhry, 2014)

$$q_1^R = -\frac{u_{23} - \frac{2H_0}{Q_0}u_{13} + \frac{2H_0 k}{\tau_0}u_{33}}{u_{21} - \frac{2H_0}{Q_0}u_{11} + \frac{2H_0 k}{\tau_0}u_{31}} \tag{3.10}$$

$$h_{n+1}^L = \frac{\frac{2H_0 k}{\tau_0}}{\frac{2H_0}{Q_0}\frac{u_{11}}{u_{21}} - 1} \tag{3.11}$$

where τ_0 is the initial relative valve opening and k is the amplitude of the sinusoidal valve opening and closing.

Substituting u_{11} and u_{21} from Eqs. 3.7 and 3.8 into Eq. 3.11 gives

$$h_{n+1,1}^L = \frac{\frac{2H_0 k}{\tau_0}}{\frac{4H_0}{Q_0}\frac{\frac{\Delta H_0}{CQ_0}\cos^2\left(\frac{\pi}{2}(L_r)\right)j}{-\frac{\Delta H_0}{Q_0}\sin(\pi L_r) - Cj} - 1} \tag{3.12}$$

Using the same procedure, similar equations can be obtained for a valve oscillating under the 2^{nd}, 3^{rd}, and 4^{th} harmonics as follows:

$$h_{n+1,2}^L = \frac{\frac{2H_0 k}{\tau_0}}{\frac{2H_0}{Q_0}\frac{-1 + \frac{\Delta H_0}{CQ_0}\sin(2\pi(L_r))j}{\frac{2\Delta H_0}{Q_0}\cos^2(\pi(L_r))} - 1} \tag{3.13}$$

$$h_{n+1,3}^L = \frac{\frac{2H_0 k}{\tau_0}}{\frac{4H_0}{Q_0}\frac{-\frac{\Delta H_0}{CQ_0}\cos^2\left(\frac{3\pi}{2}(L_r)\right)j}{\frac{\Delta H_0}{Q_0}\sin(3\pi(L_r)) + Cj} - 1} \tag{3.14}$$

$$h_{n+1,4}^L = \frac{\frac{2H_0 k}{\tau_0}}{\frac{2H_0}{Q_0}\frac{1 - \frac{\Delta H_0}{CQ_0}\sin(4\pi(L_r))j}{-\frac{2\Delta H_0}{Q_0}\cos^2(2\pi(L_r))} - 1} \tag{3.15}$$

Each of the four equations (Eqs. 3.12 through 3.15) gives, for each value of L_r, a complex number the absolute value of which represents the amplitude of the pressure head oscillations. The latter can be normalized using the mean pressure head, H_0, to compute the relative amplitude of the pressure head oscillation, $h_r = \left|h_{n+1}^L\right| / H_0$. The relationship between L_r and h_r for the first four harmonics is used to construct

each corresponding blockage detection curve, as discussed below.

Blockage Detection Curves

A blockage detection curve (BDC) obtained by a sinusoidal motion of a downstream valve at a specified harmonic represents the relationship between the relative blockage location, L_r (on the x-axis) and the relative amplitude of the pressure head oscillation at the downstream end of the pipeline, h_r (on the y-axis) as shown in Fig. 3.3. These curves depend on the system parameters (pipeline length, material, friction, etc.) and can be used to detect a possible blockage location along the pipeline. To construct a blockage detection curve, a relative spatial interval is first selected between 0 and 1 and the coordinates of each detection curve are calculated using Eqs. 3.12 to 3.15. Each relative blockage location gives a complex number, the absolute value of which represents the amplitude of the pressure head oscillation. As shown in Fig. 3.3, the number of the inflection points (points where the 2^{nd} derivative is zero) on each curve increases with the increase in the number of harmonics. Therefore, the 1^{st} harmonic curve gives one possible blockage location for each value of h_r, while the 2^{nd} harmonic curve gives two possible blockage locations except when the blockage is at the mid-length of the pipeline (L_r=1/2), to which one possible blockage location is obtained. This is because of the symmetry feature of the 2^{nd} harmonic BDC. For the 3^{rd} harmonic curve, there are three possible blockage locations except when L_r = 0, 1/3, 2/3, or 1 where two possible blockage locations are obtained. Lastly, for 4^{th} harmonic curve, there are four possible blockage locations except when L_r = 0, 1/2 or 1 where three possible blockage locations are obtained and when L_r = 1/4 or 3/4 where two possible blockage locations are obtained. However, there is only one shared value for the possible blockage location among all the four BDCs which gives the anticipated blockage location. Even though the 1^{st} harmonic BDC is sufficient

to determine the blockage location, the use of additional BDCs is recommended for reconfirmation. The more the number of BDCs used, the more is the accuracy of the blockage location. However, the current approach uses up to the 4^{th} harmonic to avoid the problems of using higher harmonics, as discussed in the Introduction.

3.3 Numerical Application

An examination of the blockage detection equations (Eqs. 3.12 to 3.15) shows that there is a direct relationship between the relative blockage location, L_r, and the absolute value of the pressure head oscillation at the valve, $\left|h^L_{n+1}\right|$. As discussed earlier, the latter term may be represented in the normalized form $h_r = \left|h^L_{n+1}\right| / H_0$ and the relationship between L_r and h_r is used to construct the blockage detection curves for different system parameters.

Figure 3.3 shows the relationship between h_r and L_r for the pipeline system shown in Fig. 3.1 excited at the first four harmonics of the pipeline. Relative amplitude of the pressure head oscillations, h_r, for the 1^{st} and 3^{rd} (odd) harmonics are shown on the y-axis to the left and for 2^{nd} and 4^{th} (even) harmonics are shown on the y-axis to the right. The system is considered frictionless for now with a 65% blocked diameter ($d_r = 0.35$, where d_r is the ratio of the pipeline diameter at the blockage location to that of the healthy pipeline). Other blockage sizes and friction effect on the model output are considered later. The pipe length and diameter are 1600 m and 0.3 m, respectively. The initial steady state discharge is 0.1 m^3/s and the height of water in the reservoir is 50 m. Wave speed, a, is 1000 m/s, initial relative valve opening, τ_0, is 0.9, and the amplitude of the valve oscillations, k, is 0.1.

For the case of 1^{st} harmonic (fundamental frequency) shown in Fig. 3.3, there is only one possible blockage location for each value of the relative amplitude of the pressure head oscillation in the pipeline system. From Eq. 3.12 or by using the curve

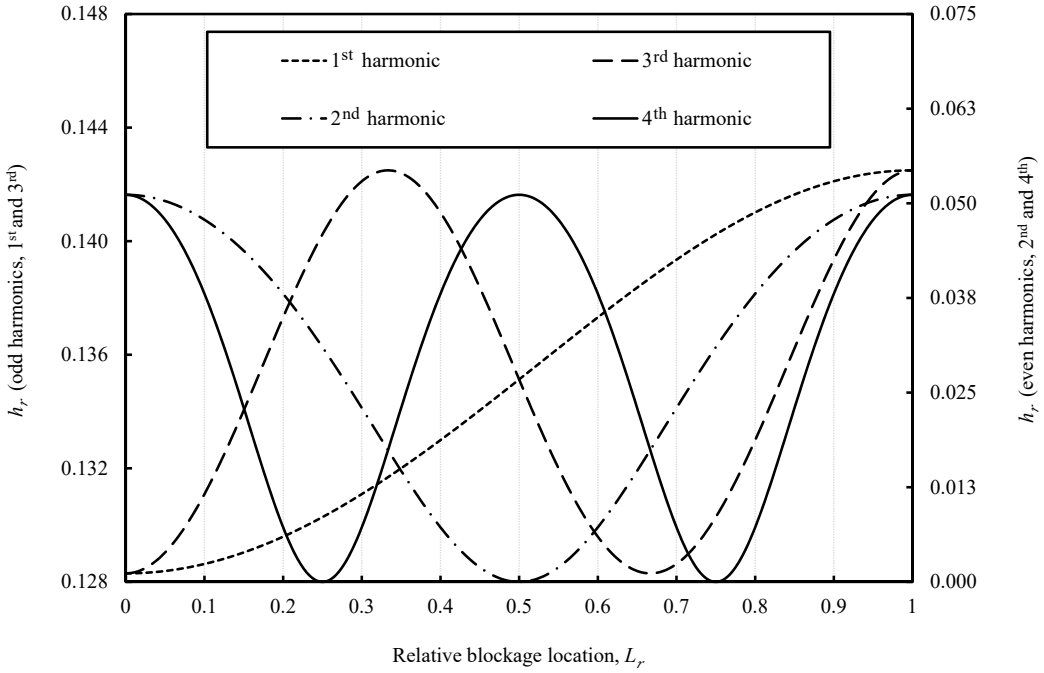

Figure 3.3 Blockage detection curves for the first four harmonics.

of the 1^{st} harmonic in Fig. 3.3, as the partial blockage is moved from the upstream reservoir to the downstream valve (i.e., $L_r = 0$ to 1), the relative amplitude of the pressure head oscillation, h_r, increases gradually from 0.128 to 0.142 or the pressure head increases gradually from 6.4 m to 7.1 m.

For the case of 2^{nd} harmonic, using Eq. 3.13 or the curve of the 2^{nd} harmonic in Fig. 3.3, the amplitude of the pressure head oscillation approaches 0 as the blockage location approaches the pipe mid-length (i.e., $L_r = 0.5$). For a partial blockage away from the pipe mid-length towards the upstream reservoir or towards the downstream valve, h_r increases gradually until it reaches a maximum value at the boundary depending on the size of the partial blockage (0.051 in this example). The curve is symmetrical around the pipe mid-length , i.e., for each value of h_r there are two

possible blockage locations except for the pipe mid-length. This symmetry is also reported by many researchers who used the traditional FRDs (Sattar et al., 2008; Wang et al., 2005; Covas et al., 2005; Lee et al., 2005b). One of the two possible locations is on the reservoir side of the pipe mid-length and the other is on the valve side.

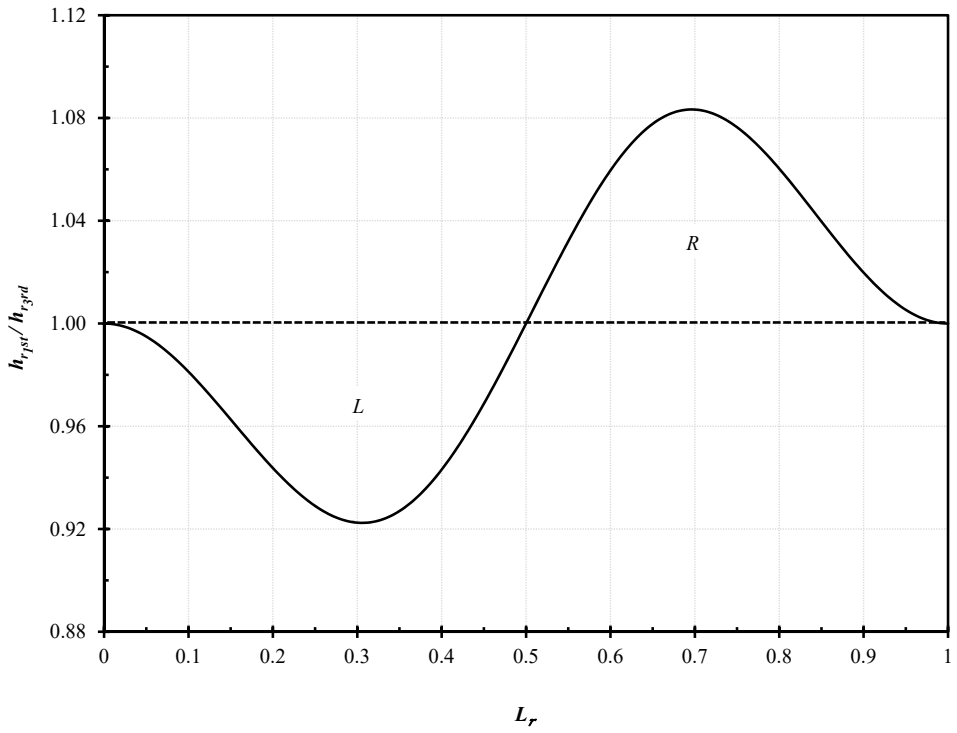

Figure 3.4 Relative amplitude of the pressure head oscillation at first and third harmonics vs. blockage location.

For the case of 3^{rd} and 4^{th} harmonics, there are multiple possible blockage locations for each value of h_r, as discussed earlier. One of these possible locations in each harmonic is the same as that obtained from the first harmonic. However, it is not recommended to use only the 1^{st} harmonic BDC for the reasons discussed in the previous section. For field applications, a combination of the first four harmonics is recommended. One of these combinations is to use the ratio of the amplitude of the pressure head oscillation obtained by oscillating the valve at the 1^{st} harmonic to that

obtained by oscillating the valve at the 3^{rd} harmonic. This ratio is shown in Fig. 3.4 and may be used to determine whether there is a blockage on the reservoir or on the valve side of the pipe mid-length. Region (L) in Fig. 3.4 corresponds to a blockage on the reservoir side of the pipe mid-length, while region (R) corresponds to a blockage on the valve side.

As an example of a blocked pipeline with the above specified parameters, any value of h_r within the range (0.128 to 0.142) may be obtained in a field application depending on an unknown blockage location with the valve oscillating at the first harmonic. Once the value of h_r is obtained, the relationship between h_r and L_r (1^{st} harmonic curve in Fig. 3.3) may be used to locate the partial blockage. An h_r value of 0.132 for example corresponds to L_r of 0.35. Multiplying the latter value by the full length of the pipeline gives a partial blockage location of 560 m from the upstream reservoir. Using Eqs. 3.12 through 3.15 or their corresponding curves in Fig. 3.3, the values in Table 3.1 corresponding to the downstream valve oscillating at the 2^{nd}, 3^{rd}, and 4^{th} harmonics may be determined.

As shown in Table 3.1, there is only one shared location of partial blockage among all the four cases of the modes of oscillation of the downstream valve and this is the anticipated partial blockage location. Furthermore, the ratio between the relative amplitude of the pressure head oscillation resulting from oscillating the valve at the 1^{st} harmonic and that resulting from oscillating the valve at the 3^{rd} harmonic may be utilized to determine the part of the pipeline where the partial blockage exists. From Fig.3.4, as this ratio equals 0.927 (which is less than 1), the partial blockage lies in the reservoir side of the pipe mid-length. Potential field application to detect a partial blockage location using the current approach is discussed later.

Table 3.1 Relative amplitude of pressure head oscillation at the downstream end of the pipeline and the corresponding blockage location for different harmonics.

Harmonic	Relative pressure head oscillation amplitude (h_r)	Possible relative blockage location (L_r)	Actual pressure head oscillation, m	Possible blockage location, m
1^{st}	0.1320	0.350	6.60	560
2^{nd}	0.0145	0.350	0.73	560
		0.650		1040
3^{rd}	0.1424	0.320	7.12	512
		0.350		560
		0.985		1576
4^{th}	0.0235	0.150	1.18	240
		0.350		560
		0.650		1040
		0.850		1360

Effect of Blockage Size

Generally, a partial blockage in a pipeline decreases the amplitude of the pressure head oscillations at the downstream valve at the odd harmonics and increases it at the even harmonics (Mohapatra et al., 2006; Lee et al., 2008; Sattar et al., 2008). Furthermore, the amount of decrease or increase depends on the size of the partial blockage and its location. However, this conclusion is investigated only for a small number of blockage locations in the available literature. In this study, the effect of the partial blockage size on the amplitude of the pressure head oscillation is investigated for all possible blockage locations along the pipeline.

The effect of the blockage size on the relationship between L_r and h_r for three different relative blockage sizes, $d_r = 0.45$, 0.50 and 0.55, in a frictionless system is considered first. Other sizes along with the friction effect are considered later. A higher value of d_r represents a smaller blockage size, and vice versa. The relationship

between L_r and h_r for different blockage sizes for the 1^{st} and 3^{rd} (odd) harmonics is shown in Fig. 3.5. From this figure, it is clear that, as the blockage size increases (d_r decreases), the relative amplitude of the pressure head oscillation decreases for all possible blockage locations. In addition, the 1^{st} harmonic blockage detection curve intersects the 3^{rd} harmonic curve at three locations: upstream end ($L_r = 0$), mid-length ($L_r = 0.5$), and downstream end ($L_r = 1$) of the pipeline. At the point of intersection, the relative amplitude of the pressure head oscillation is the same whether the downstream valve is oscillated at the 1^{st} or 3^{rd} harmonic. The location of the point of intersection and its relation with the steady and unsteady friction is discussed in "Effect of Friction".

The relationship between L_r and h_r for different blockage sizes for the 2^{nd} and 4^{th} (even) harmonics is seen in Fig. 3.6. From this figure, it is shown that the three curves for different blockage sizes intersect at the pipe mid-length in the case of the 2^{nd} harmonic. At the point of intersection, a pressure head oscillation node in which the amplitude of the pressure head oscillation is independent on the blockage size is produced. This may be verified from Eq. 3.13 for $L_r = 0.5$, where the term $\cos^2(\pi L_r)$ equals zero, which makes the amplitude of the pressure head oscillation equal zero regardless of the partial blockage size. For the 4^{th} harmonic, the three curves intersect at two locations ($L_r = 1/4$ and $L_r = 3/4$) producing two pressure head oscillation nodes in term of the blockage size. For locations other than the pressure head oscillation nodes, it is shown that the larger the blockage size, the larger the amplitude of the pressure head oscillations.

Blockage sizes other than the three considered above at different relative blockage locations, as shown in Fig. 3.7 are investigated. Three relative blockage locations are considered: $L_r = 0.25$, 0.5, and 0.75, with the downstream valve oscillating at the first harmonic ($\omega_r = 1$) as an example. For all these three locations, the amplitude of the pressure head oscillation increases as the blockage size decreases (i.e., d_r in-

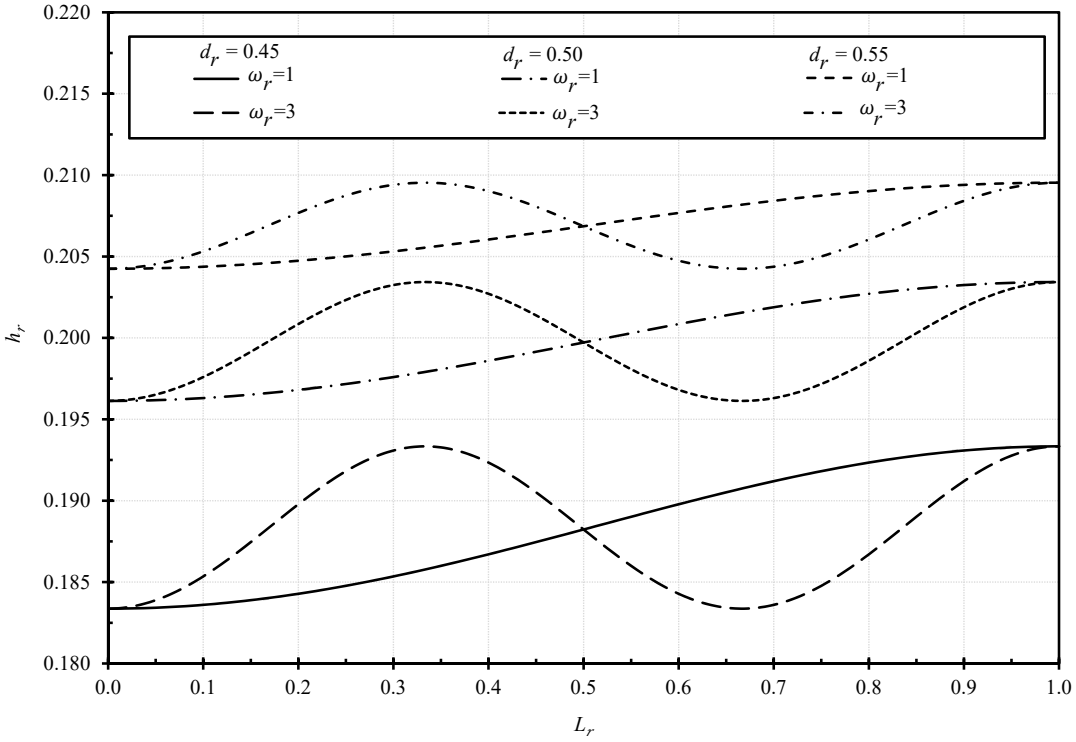

Figure 3.5 Blockage detection curves for first and third harmonics with different blockage sizes.

creases). However, the rate of change of the amplitude of the pressure head oscillation decreases as the blockage size decreases and becomes insignificant as the blockage size approaches the minimum value (i.e, d_r approaches the maximum value of 1). This trend agrees with that reported by Mohapatra et al. (2006) for one selected blockage location at a wide range of harmonics (up to $\omega_r = 100$).

Effect of Friction

Steady and unsteady friction effects on the amplitude of the pressure head oscillations and the interaction among blockage detection curves is discussed in this section. Steady friction effect is first discussed by considering different values of Darcy-Weisbach friction factor, f, as shown in Fig. 3.8. In this figure, the upper two

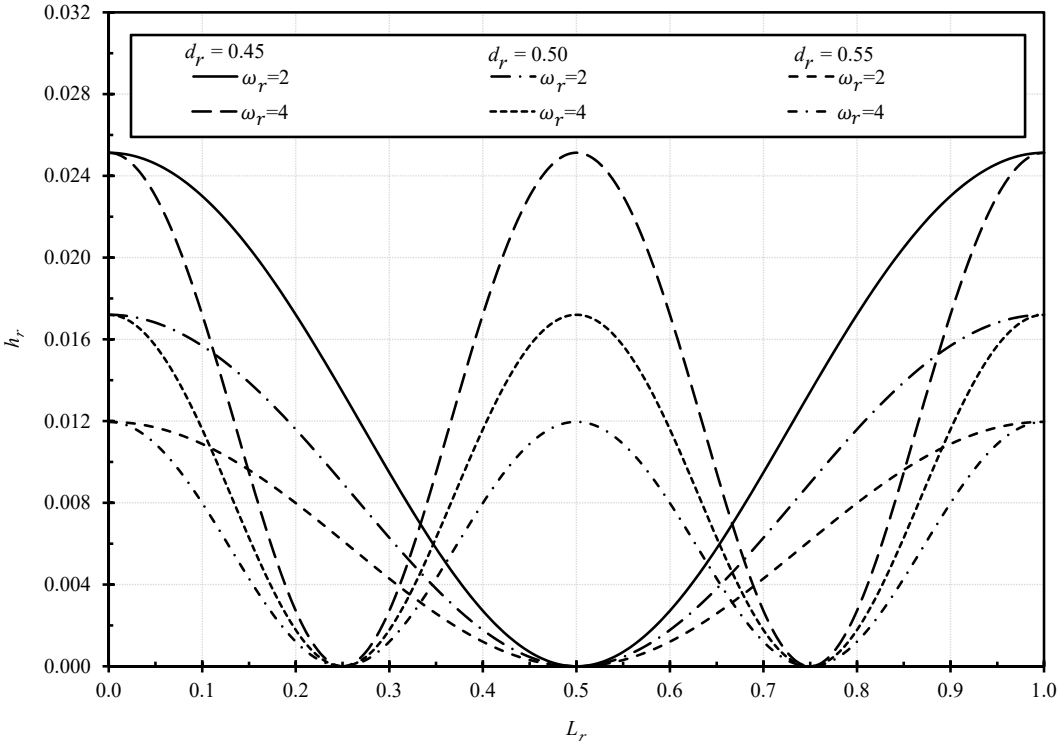

Figure 3.6 Blockage detection curves for second and fourth harmonics with different blockage sizes.

curves represent the relationship between L_r and h_r for the 1^{st} and 3^{rd} harmonics for a frictionless system ($f = 0$), while the lower four curves represent this relationship for a system with $f = 0.01$ and $f = 0.02$, respectively.

It is clear that, as the steady friction losses increase, the amplitude of the pressure head oscillation decreases for all partial blockage locations for both 1^{st} and 3^{rd} (odd) harmonics. Also the range of the relative amplitude of the pressure head oscillations (the difference between h_r at $L_r = 0$ and h_r at $L_r = 1$) decreases as the steady friction losses increase. That means that in the case of 1^{st} and 3^{rd} harmonics, steady friction losses reduce the amplitude of the pressure head oscillations. For the case of 2^{nd} and 4^{th} harmonics, although it is not presented here to conserve space, the amplitude of the pressure head oscillations is proportional to the steady friction losses, i.e.,h_r

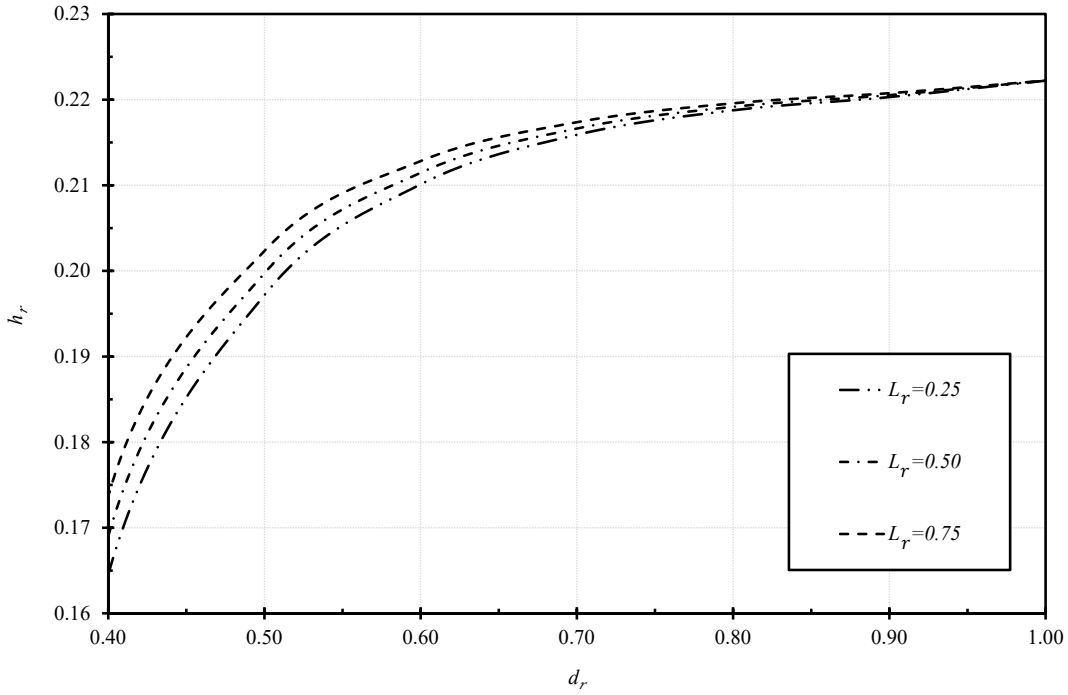

Figure 3.7 Relative amplitude of the pressure head oscillations vs. relative blockage size at 1^{st} harmonic with different relative blockage locations.

increases as f increases.

As mentioned earlier, the 1^{st} harmonic curve for a frictionless system intersects the 3^{rd} harmonic curve at three locations, $L_r = 0$, 0.5, and 1. However, this is not the case if friction is included and the intersection points at $L_r = 0$ and $L_r = 0.5$ are shifted, and there is no intersection at $L_r = 1$. In addition, there are different relative pressure head oscillations for each harmonic at these three locations, i.e., $L_r = 0$, 0.5, and 1, as explained below:

1. Point a_o in inset a of Fig. 3.8 becomes two points, a_1 and a_2 (inset d), and there is a new point of intersection at a_3, slightly away and to the right of the upstream reservoir.

2. Point b_o in inset b of Fig. 3.8 becomes two points, b_1 and b_2 (inset e), and there

is a new point of intersection at b_3, slightly away and to the left of the pipeline mid-length.

3. Point c_o in inset c of Fig. 3.8 becomes two points, c_1 and c_2 (inset f), and there is no intersection between the two curves (the 3^{rd} harmonic curve being below the 1^{st} harmonic curve and any downward shift keeps the two curves apart).

The difference in the amplitude of the pressure head oscillations between a_1 and a_2 is not equal to that between b_1 and b_2 nor to that between c_1 and c_2, but the magnitude of each of these three differences increases as the steady friction loss increases, as shown in insets g, h, and i where the steady friction factor is increased from 0.01 to 0.02. The expansion of the intersection points is because that the shift in each detection curve due to the inclusion of the steady friction depends on the mode of oscillation of the downstream valve. In other words, as the BDCs shift downward due to the inclusion of the steady friction losses, the downward shift of the 3^{rd} harmonic curve is slightly greater than that of the 1^{st} harmonic curve since the effect prompted by the steady friction on the amplitude of the pressure head oscillation is greater in the case of the 3^{rd} harmonic than that in the case of the 1^{st} harmonic. The physical reasoning for such a trend is that the inclusion of the steady friction decreases the excitation response of the system depending on the mode of the downstream valve oscillation and hence leads to a decrease in the amplitude of the pressure head oscillation.

The differential shift between the 1^{st} and 3^{rd} harmonic BDCs due to the inclusion of the steady friction also affects the ratio between the corresponding h_r values used to determine the part of the pipeline in which the partial blockage exists. As discussed earlier, this ratio is less than 1 if the blockage exists in the reservoir side of the pipeline for a frictionless system. However, for a frictional system, there will be two regions of the reservoir side in which this ratio is greater than 1, questioning the possibility

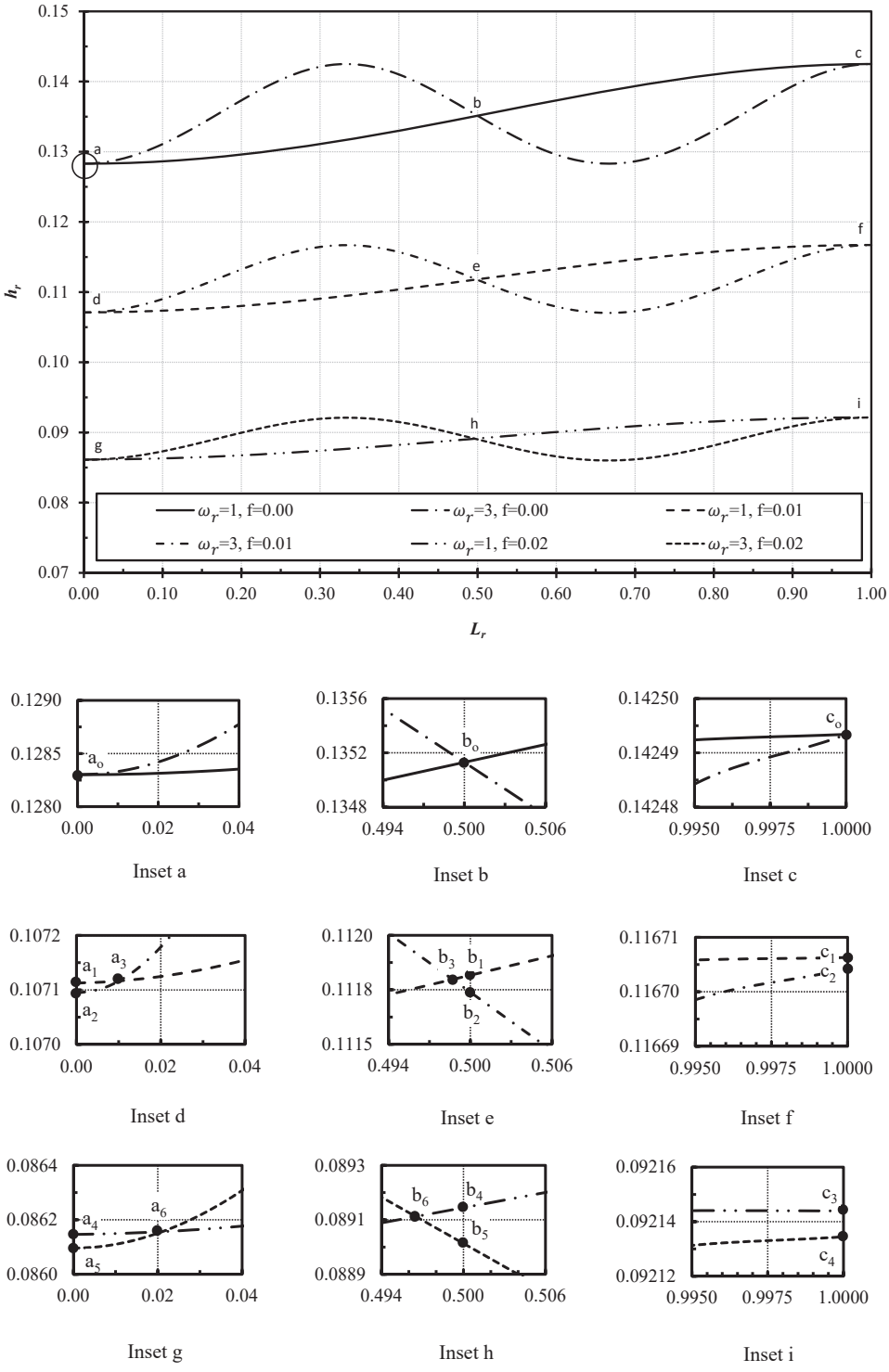

Figure 3.8 Comparison of the first and third harmonic leak detection curves for a system with and without friction with only steady friction included. Insets a through i are enlargements of the interaction points.

of the blockage existence on this side. One of these two regions is in the upstream boundary and the other is just to the left of the mid-length of the pipeline. The extent of these two regions and how much the above mentioned ratio is greater than 1 depend on the amount of the steady friction.

In the steady-oscillatory flow, the unsteady friction is also harmonic dependent (Wang et al., 2005; Sattar et al., 2008) where its effect on the amplitude of the pressure head oscillation increases at higher harmonics. However, the current approach analyzes the variation of the amplitude of the pressure head oscillation for different blockage locations using one harmonic at a time for the first four harmonics. The model of Vitkovsky et al. (2003) for steady-oscillatory flow is used to investigate the effect of unsteady friction on the BDCs proposed in this study. This model suggests adding a component of $\frac{2j\omega}{gA}\left(\frac{1}{C^*}+\frac{j\omega D^2}{4\nu}\right)^{-1/2}$ (in which the shear decay coefficient, $C^* = 7.41/{R_e}^k$, R_e is the Reynold's number, ν is the kinematic viscosity of water, and $k = \log_{10}(14.3/{R_e}^{0.05})$) to the steady friction component to account for unsteady friction effect. The BDCs are reconstructed for two cases: first with only steady friction ($f = 0.02$) and second with both steady and unsteady friction, as shown in Fig. 3.9. From this figure, it is clear that the unsteady friction effect on the BDCs is similar to that prompted by steady friction, while it increases h_r values at even harmonics (bottom and right axes of Fig. 3.9), it decreases h_r values at odd harmonics (bottom and left axes of Fig. 3.9), for all possible blockage locations. However, its effect at 1^{st} and 3^{rd} (odd) harmonics is smaller than that at 2^{nd} and 4^{th} (even) harmonics and it is the greatest when the blockage is located at the points of minimum relative pressure head oscillations of the even harmonic BDCs. Furthermore, the shift of the intersection points between 1^{st} and 3^{rd} harmonic curves when the unsteady friction is included is greater than that in the case if only steady friction is included, as shown in Fig. 3.10. This behavior further affects using the ratio between the corresponding h_r values to determine the part of the pipeline in which the partial blockage exists,

as discussed earlier.

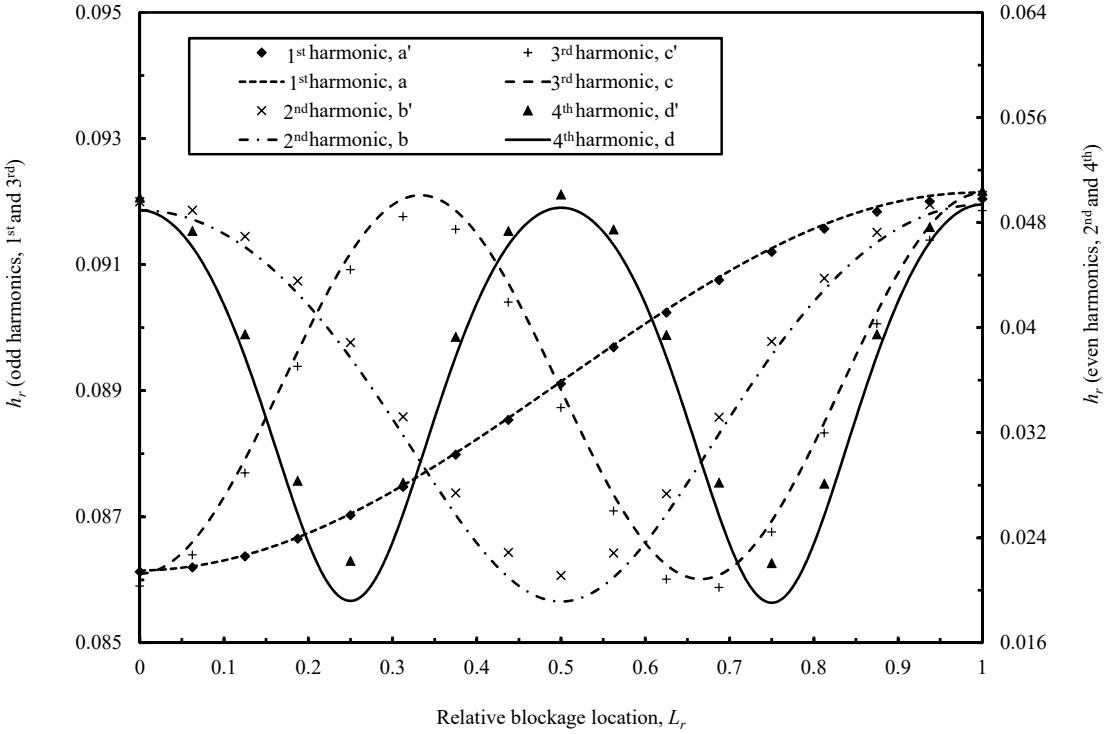

Figure 3.9 Comparison of BDCs with and without unsteady friction (f=0.02) (a,b,c, and d unsteady friction is not included; a',b',c', and d' unsteady friction is included).

3.4 Model Verification

The outputs of the current approach which uses the transfer matrix method (TMM) in the frequency domain to calculate the amplitude of the pressure head oscillations at the downstream end of a pipeline is compared with that obtained by the method of characteristics (MOC) and with the experimental data available in the literature, as discussed in the following paragraphs.

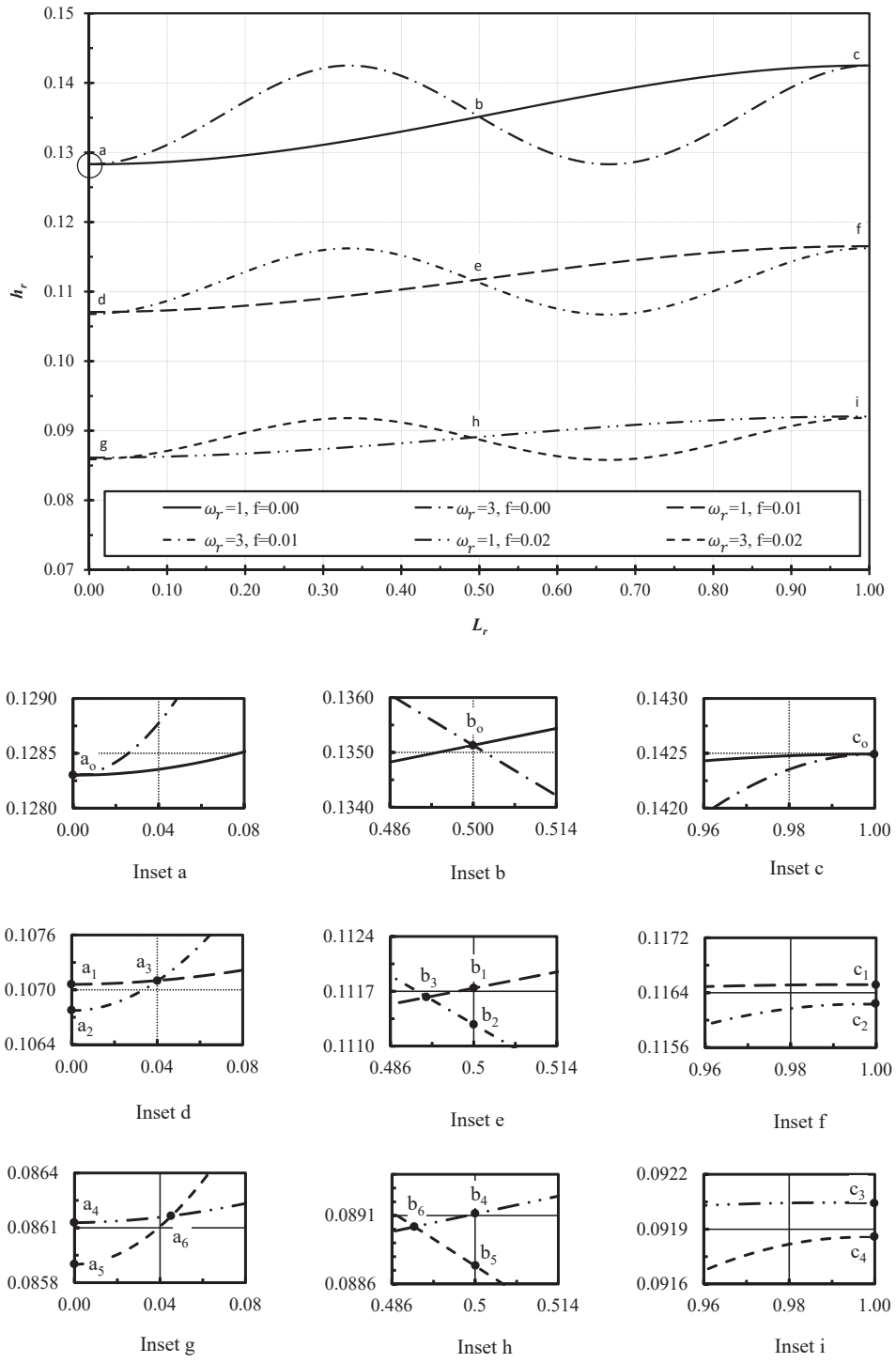

Figure 3.10 Blockage detection curves for 1st and 3rd harmonics, steady and unsteady friction included.

Method of Characteristics

In the method of characteristics, the relationship between time and relative valve opening is first specified for different harmonics of the sinusoidal opening and closing of the valve and simulated as a boundary condition at the downstream end of the pipeline. The relative valve opening, τ, is sinusoidal in time, i.e., $\tau=\tau_0+k$ sin(ω t), in which τ_0 is the mean valve opening, k is the amplitude of the relative valve opening, and ω is the frequency of the oscillating valve. The partial blockage is also identified as an internal boundary condition and located at different locations along the pipeline at 50 m spacing in this study. To ensure that the steady-oscillatory flow has been established, 2800 time steps are considered and the minimum-maximum pressure head difference is taken for the last 400 time steps. All parameters are kept exactly the same as that used in the frequency domain and no noise in the signal is observed. Sample pressure head responses to the 2^{nd} harmonic excitation for three different blockage locations are shown in Fig. 3.11. The relative amplitude of the pressure head oscillation, h_r, is determined as $\Delta H_{L_r}/2H_0$, where ΔH_{L_r} is the maximum-minimum pressure head difference for each corresponding relative blockage location and H_0 is the height of water in the upstream reservoir above the datum.

The process continues for other harmonics of the downstream valve oscillating sinusoidally and for all possible blockage locations. The difference between the relative amplitude of the pressure head oscillations calculated by the MOC and that calculated by the TMM for all possible blockage locations is shown in Fig. 3.12. According to this figure, the amplitude of the pressure head oscillations calculated by the TMM are slightly overestimated as compared to those obtained by the MOC for the 1^{st} and 3^{rd} (odd) harmonics and for all possible blockage locations ($L_r = 0$ to 1). This overestimation may be attributed to the linearity assumption in the TMM solution and it has also been reported by Mohapatra et al. (2006) for a wide range of odd harmonics ($\omega_r = 0$ to 25) for one selected blockage location. However, there is

almost full agreement between the two methods for the 2^{nd} and 4^{th} (even) harmonics.

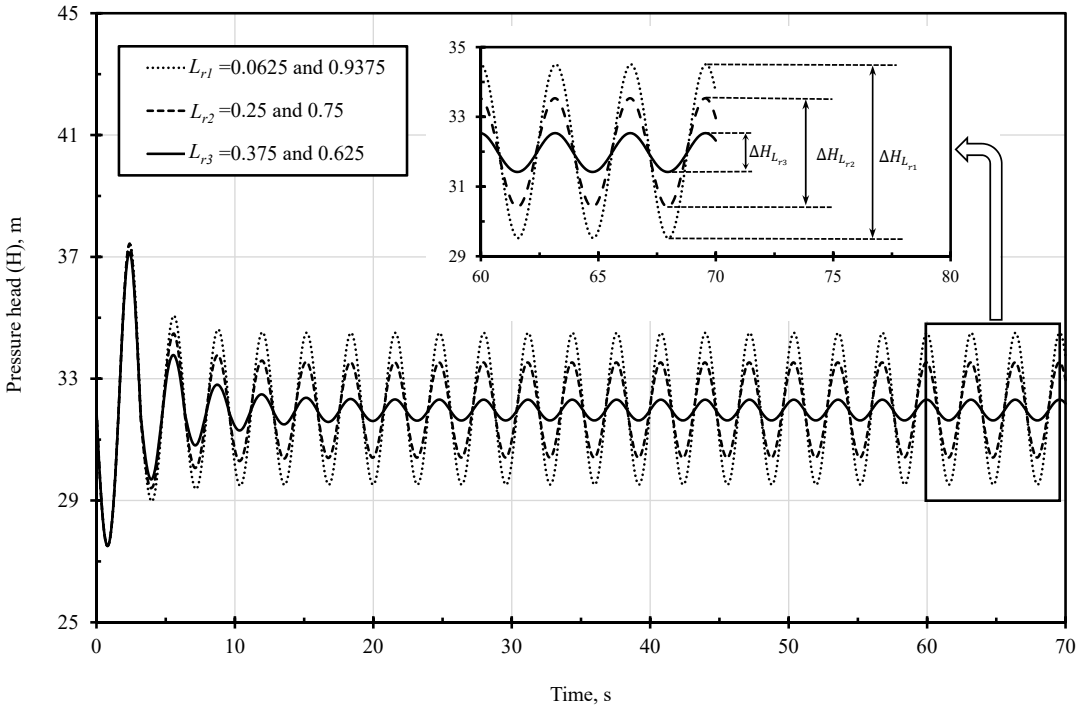

Figure 3.11 Pressure head oscillations of the downstream valve sinusoidal movement at 2^{nd} harmonic for different blockage locations.

Experimental Data

Sattar et al. (2008), in their experimental setup, measured the frequency response of a short pipe and reported the relative amplitudes of the pressure head oscillation corresponding to a set of relative even harmonics up to the 6^{th} harmonic. The system they investigated is similar to that considered in the current study consisting of a constant-level reservoir in the upstream and a sinusoidally oscillating downstream valve. An 80% blockage is placed at the mid-length of a 160 m long copper pipe with 0.0254 m internal diameter. Wave speed and initial steady state discharge are 1000 m/s and 0.000284 m^3/s, respectively. The experimental data points are shown

at the bottom and left axes of Fig. 3.13 (a or b). In this figure, $\Delta\omega_r^{\text{even}}$ represents the oscillation period of the even harmonics of the blockage induced pattern estimated from the experimental data points. Using this period, the relative blockage location ($L_r = L_b/\text{L}$) is estimated as $2/\Delta\omega_r^{\text{even}} = 0.5$ (Sattar et al., 2008). In order to compare this relative blockage location to that estimated by the current approach, two sample BDCs are developed for a similar system. Since there is no data points for the odd harmonics, the 2^{nd} and 4^{th} (even) harmonics BDCs are used as shown on the top and right axes of Fig. 3.13 (a and b).

Fig. 3.13(a) shows the comparison with the 2^{nd} harmonic BDC, while Fig. 3.13(b) shows the comparison with the 4^{th} harmonic BDC. In Fig. 3.13(a), the measured relative amplitude of the pressure head oscillation at the 2^{nd} harmonic is projected horizontally on the 2^{nd} harmonic BDC, then the intersection points are projected vertically to find two anticipated relative blockage locations (L_r=0.47 and 0.53) while four anticipated relative blockage locations (L_r=0.035, 0.47, 0.535, and 0.965) are obtained in Fig. 3.13(b) by projecting the measured relative amplitude of the pressure head oscillation at the 4^{th} harmonic. However, two values of L_r obtained from the two BDCs are almost the same, suggesting two anticipated relative blockage locations of 0.47 and 0.53. Either of these two values gives a good approximation for the actual relative blockage location of 0.5 with a 95% agreement. The 5% difference between the actual and calculated relative blockage locations may be attributed to the uncertainty in the experimental estimation of the system parameters.

3.5 Potential for Field Applications

The blockage detection technique presented in this study may be used in real-life applications for which the model parameters should be verified by a prototype test for the healthy system. The steady-state hydraulic grade line is then computed with all

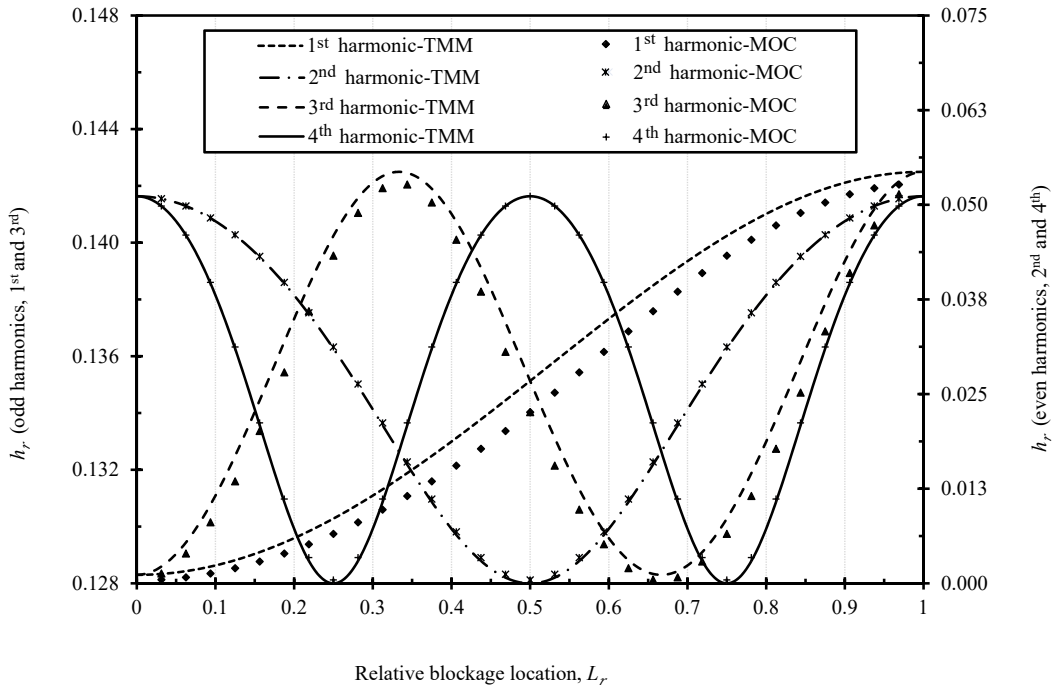

Figure 3.12 Comparison of the blockage detection curves obtained by using method of characteristics and transfer matrix method.

major and minor head losses, including the head loss caused by the partial blockage. The latter may be related to the blockage size and thus the value of d_r is determined. The flow in the pipeline is then excited by oscillating the downstream valve at the 1^{st} harmonic and the relative amplitude of the pressure head oscillation is determined. The amplitude of the pressure head oscillation may be averaged over three to five runs for further accuracy. The relationship between the computed relative amplitude of the pressure head oscillation and the relative blockage location is used to estimate the blockage location. The above procedure is repeated with the valve oscillated at the 2^{nd}, 3^{rd}, and 4^{th} harmonics and the relationship corresponding to each harmonic is used to estimate the possible blockage location. There is one shared value of the relative blockage location among the four modes of oscillation of the downstream valve. This value may differ slightly in each mode of oscillation due to the accuracy

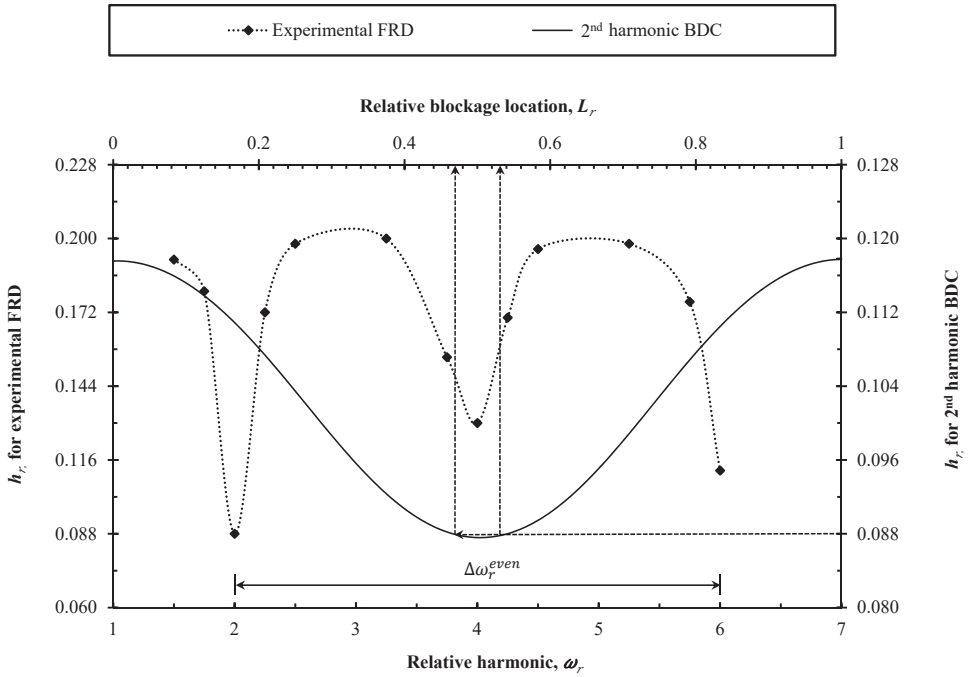

(a) 2nd harmonic

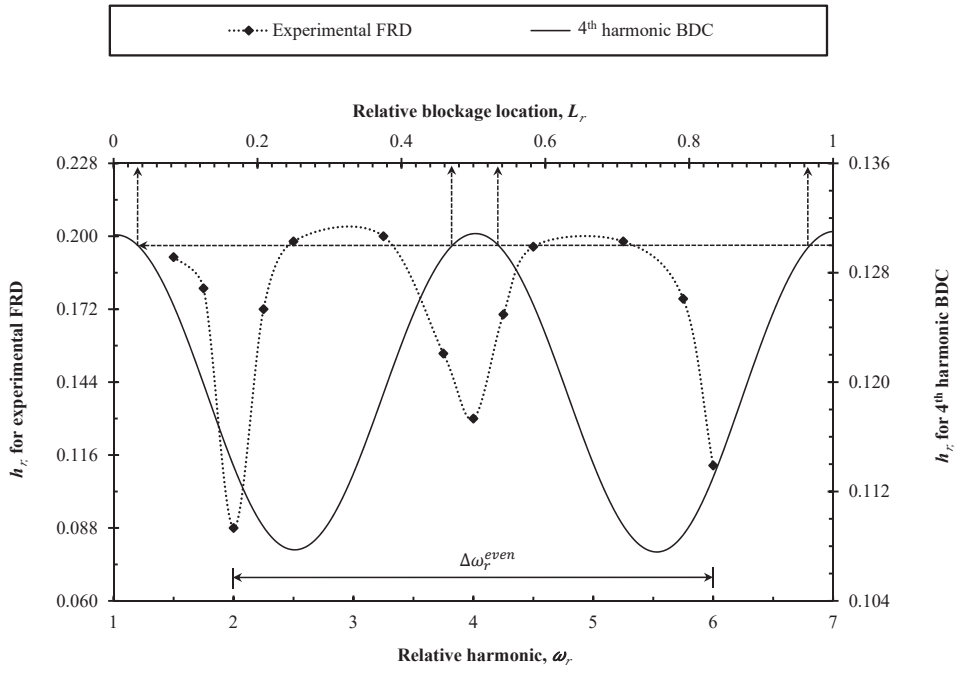

(b) 4th harmonic

Figure 3.13 Comparison of experimentally measured and theoretically computed relative blockage locations.

of measurements but this difference should be small and that makes it easier to determine the blockage location. However, there are a number of uncertainties that need to be taken in consideration. The current model may be used to develop similar detection curves for other pipeline abnormalities, such as leaks.

Chapter 4

Blockage Detection in Pipes by Continuous Emission of Acoustic Signal

4.1 Introduction

Most of the available partial blockage detection techniques involve steps that interfere with the liquid flow and require perforation of the pipe-wall to install the pressure sensors in direct contact with the flowing liquid. In contrast, the approach presented in this chapter utilizes only the interaction between the partial blockage and the steady flow where the blockage emits continuous acoustic signals that can be used for the blockage detection. The emitted signal is produced at the source in the form of a short pulse of elastic and kinetic energy that travels within the pipe-wall and may be detected by sensitive externally-mounted acoustic sensors. A set of detection sensors is used at a pre-defined spacing and moved along the pipe-wall in a suitable tripping distance. The relationship between accumulated signal strength and sensor location is plotted on a curve which shows a hump close to the blockage location. The height of this hump is proportional to the blockage size. Numerical calculations of the turbulence kinetic energy at sensor locations also show a spike of turbulence kinetic energy corresponding to the experimentally recorded hump.

4.2 Acoustic Sensor Selection

Acoustic emission (AE) is defined as the elastic wave produced by the rapid release of energy and may be recorded by acoustic sensors. There are many types of acoustic sensors that manufactured by different companies. Different sensors are tested to check their suitability to the current application, and an integral preamplifier sensor (R6I-AST) of Mistras-Physical Acoustic Corporation is adopted (Fig. 4.1). This sensor is specifically engineered for high sensitivity (117dB, Ref V/m/s) and incorporates low-noise input (<3 μV-RMS RTI). The resonant frequency, operating frequency range and temperature range are 55 kHz (Ref V/m/s), 40 to 100 kHz and -35 to 75 $^{\circ}C$, respectively. Due to its high sensitivity and low resonant frequency, this sensor can be used for applications that involve metal structures, including pipelines.

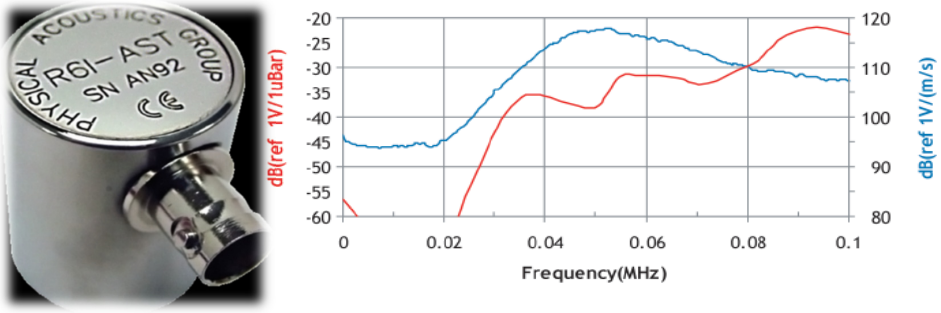

Figure 4.1 AE Sensor.

4.3 Experimental Setup

The acoustic emission test is conducted on a short pipe of 0.0254 m diameter in the Hydraulic Engineering Laboratory of the University of South Carolina. The piping system consists of an upstream reservoir feeding water to a copper pipe which discharges to the atmosphere. The length of the primary zone of the pipe that inves-

tigated for blockage existence is 7.2 m. Seven acoustic sensors are installed on the upper side of the pipe at 1.2 m spacing, starting from the leading edge of the primary zone (Fig. 4.2). Water flow is initiated in the intact pipe first and the acoustic signal is recorded 900 seconds later to ensure that the steady state flow condition is achieved. The emitted signal is recorded for a duration of 80 seconds. The recording duration may be extended for any desired period taking in consideration the amount of data to be analyzed. This time, however, should be sufficient to ensure that no vibrational ambient events are interfering with the recorded signal and to provide enough data record for comparison purposes. The flow is then shut-off and a piece of 0.3048 m long pipe is cut from the pipeline to make the blockage arrangement. Two pieces of the same length are made in advance with two central blockages in such a way that the pipe diameter is reduced by 40% and 60%, respectively. The appropriate fittings are attached for a controlled connection of zero leak and smooth internal water flow. However, to investigate the fittings interaction with the acoustic emission measurements, an intact piece with no blockage is attached first to the pipe and the acoustic signal is recorded under the steady flow conditions (no diameter reduction but only the fittings are attached to the pipe). Thereafter, the experiment is repeated two more times, one with the 40% diameter reduction and the other with 60% diameter reduction. The acoustic signal is recorded for each case: the intact pipe, the pipe with only the fittings attached, the pipe with a 40% diameter reduction, and the pipe with a 60% diameter reduction, all under the steady state flow conditions.

4.4 Experimental Results and Discussion

The accumulated signal strength (in picovolt.second, pV.s) is plotted for the four cases mentioned in the previous section. Figure 4.3 shows this plot for the intact pipe. It is noticed from this figure that the rise of the accumulated signal strength

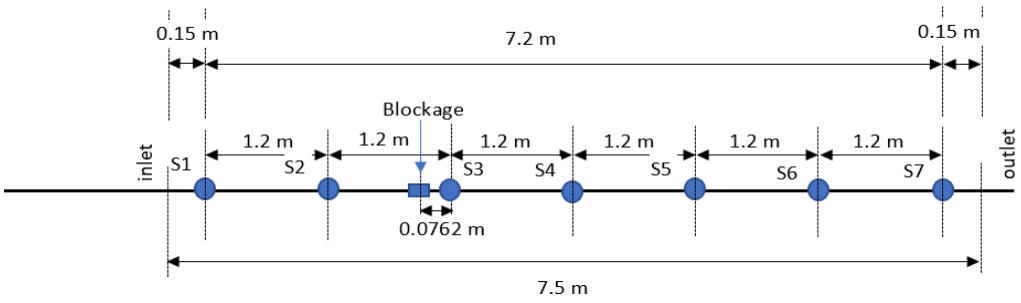

Figure 4.2 Primary Pipe Zone (not to scale).

over time curve increases in the flow direction along the primary length of the pipeline (from sensor S-1 to sensor S-7). However, this increase is very small as compared to that in the case of a blocked pipe where all the curves of the intact pipe signal coalesce to one horizontal line when they are plotted with those of the blocked pipe on the same vertical scale. Figure 4.4 shows the plot of the accumulated signal strength over time for the case with only the fittings attached. It is noticed that the trend of the curve is similar to that of the intact pipe and that the rise of the curve for the case of the pipe with only the fittings attached is insignificant in comparison to that in the case of a blocked pipe, as discussed later.

Figures 4.5 and 4.6 show the accumulated signal strength over time for the partially blocked pipe with 40% diameter reduction. The trend of the accumulated signal strength over time is represented by two separate figures because the rise of the accumulated signal strength over time curve shows two different behaviors, as it approaches or departs the blockage location. Figure 4.5 shows the accumulated signal strength over time at sensors S-1, S-2, and S-3. In this figure, the rise of the accumulated signal strength over time curve increases as the sensor location approaches the blockage location in the flow direction. While in Fig. 4.6, which shows the accumulated signal strength over time curve for sensors S-4, S-5, S-6, and S-7, the rise of

the curve decreases as the sensor location departs farther of the blockage location in the flow direction. The maximum rise occurs in the vicinity of the blockage location (sensor S-3 location). However, for the 60% diameter reduction (larger blockage size), the trend is similar but with higher rise of the curve in the vicinity of the blockage location, as shown in Figs. 4.7 and 4.8. This trend provides information that can be used to detect the blockage location, as discussed in the following section.

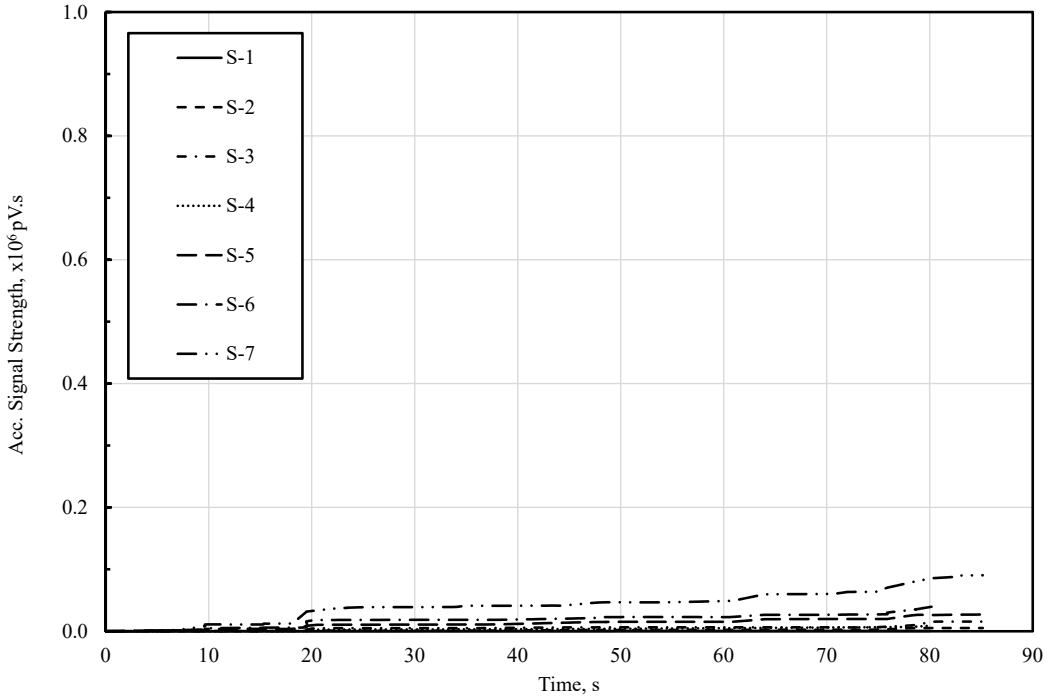

Figure 4.3 Accumulated signal strength over time for an intact pipe.

Final Accumulated Signal Strength

The final accumulated signal strength is the accumulated signal strength from the signal record initialization to the end of the recording duration. As explained previously, the recording duration is taken as 80 seconds in the current study. The final accumulated signal strength is determined for each sensor location and the relationship between these two parameters is plotted, as shown in Fig. 4.9. In this

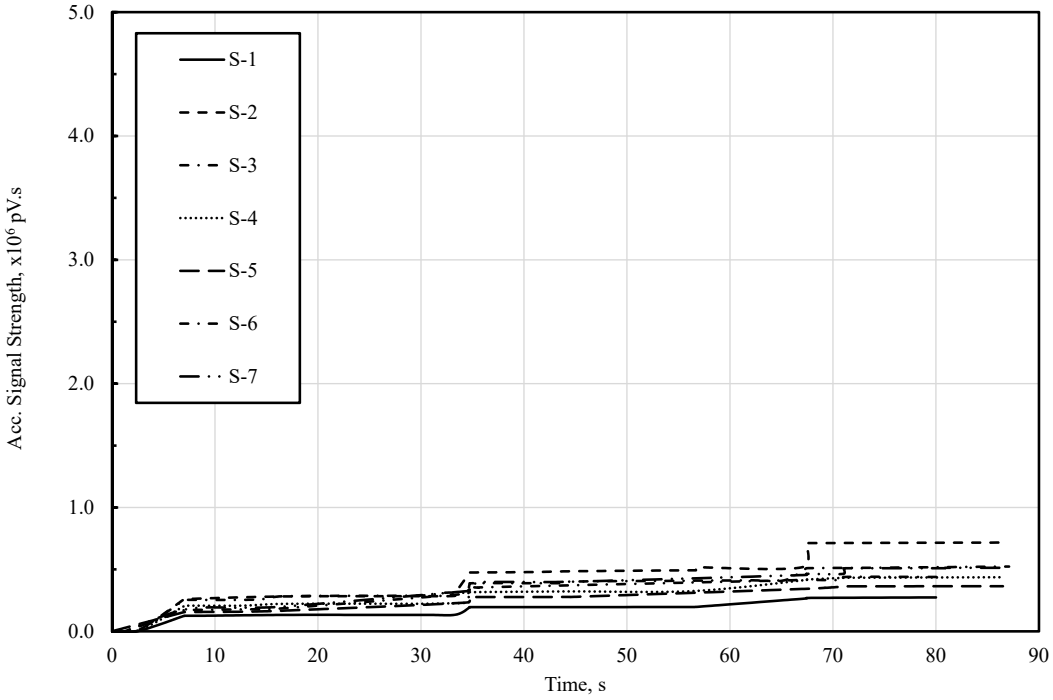

Figure 4.4 Accumulated signal strength over time for a pipe with fittings.

figure, the x-axis represents the sensor location with respect to the blockage location (zero-coordinate), and y-axis represents the final accumulated signal strength. The lower curve in Fig. 4.9 shows the plot for an intact pipe, while the upper two curves show the plot for a pipe with 40% diameter reduction and 60% diameter reduction, respectively. From this figure, it is noted that the plot of the relationship between the final accumulated signal strength and the sensor location represents a horizontal straight line for the intact pipe, while it shows a hump in the vicinity of the blockage location (sensor S-3 location) for the other two partial blockage cases. In addition, the height of the hump is proportional to the percent of the reduction in the pipe diameter, where it is lower in the case of the pipe with 40% diameter reduction than that in the case of 60% diameter reduction. The effect of fittings is insignificant in comparison to the partial blockage cases and hence their effect is no more considered in the following discussions.

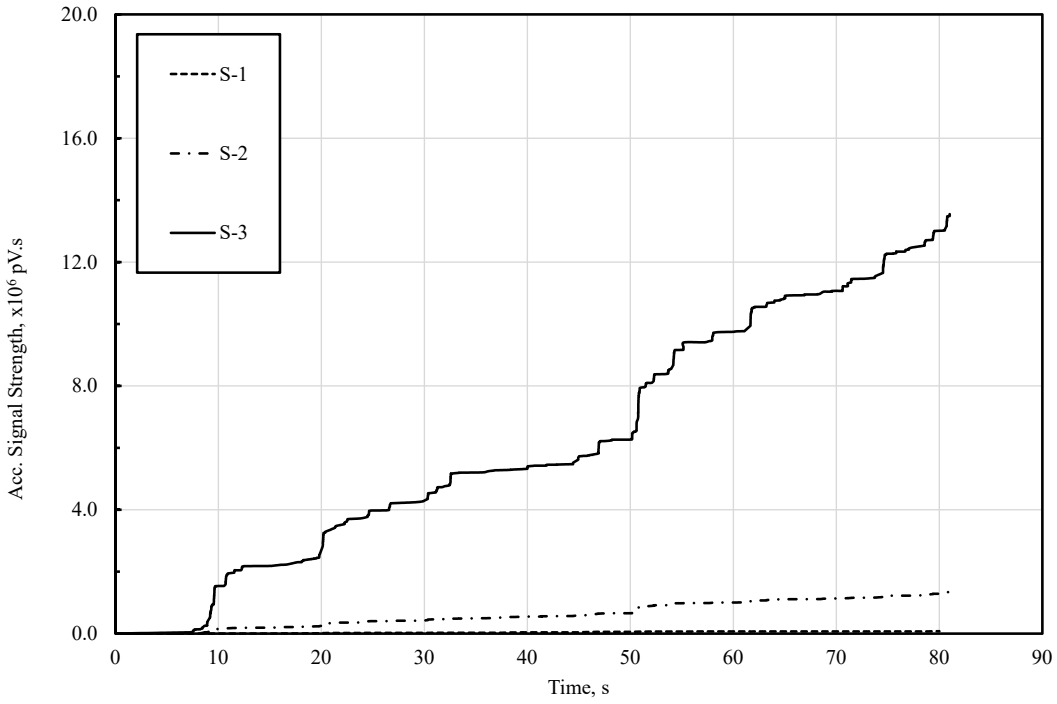

Figure 4.5 Accumulated signal strength over time for a pipe with 40% diameter reduction at sensors S-1, S-2, and S-3.

Final Accumulated Acoustic Emission Energy

In the Acoustic Emission (AE) terminology used in this study, AE energy represents the rectified voltage signal over duration of the AE hit, hence with units of voltage-time. It has a similar definition as the signal strength with a difference in the sensitivity, size, and dynamic range. This parameter is used for comparison purposes and verification with the calculated flow turbulence kinetic energy, as discussed in the following section.

Similar to the definition of final accumulated signal strength, the final accumulated AE energy may be defined as the accumulated AE energy to the end of the recording duration (80 seconds in the current study). Its maximum value for each partially blocked pipe occurs in the vicinity of the blockage location (sensor S-3 location).

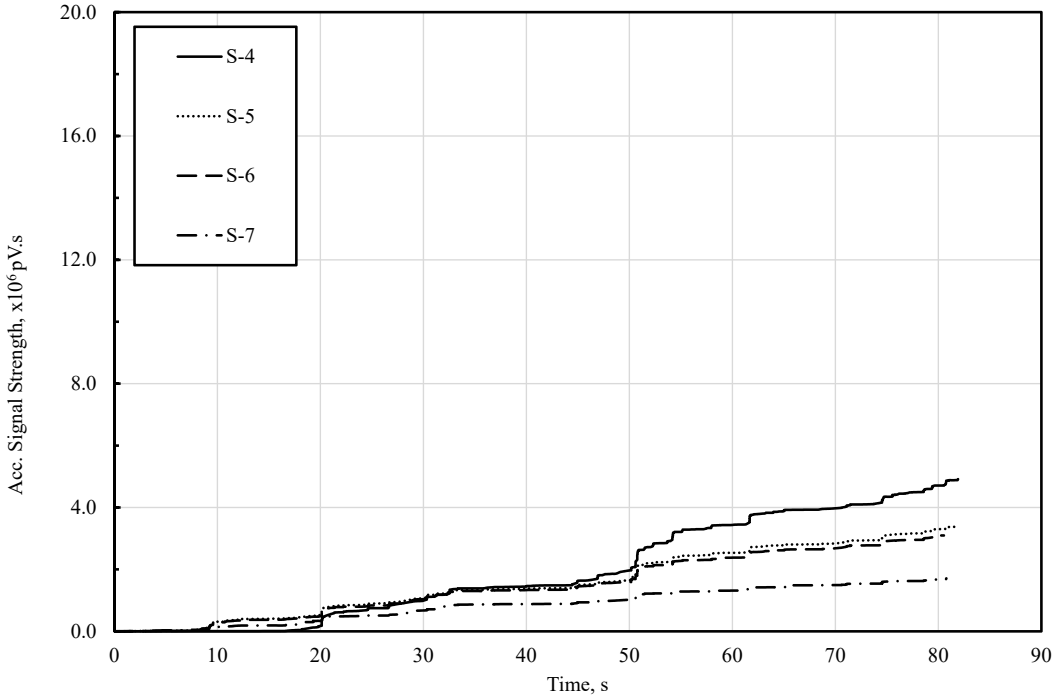

Figure 4.6 Accumulated signal strength over time for a pipe with 40% diameter reduction at sensors S-4, S-5, S-6, and S7.

This maximum value is used to normalize the final accumulated AE energy obtained for each pipe condition at all other sensor locations and the normalized value is called the relative final accumulated AE energy. The behavior of the curves representing the relationship between the sensor location and the final accumulated AE energy is similar to that between the sensor location and the final accumulated signal strength. This relationship is represented by a horizontal straight line for an intact pipe, while there is a hump in the vicinity of the blockage location for a partially blocked pipe. The plot of the relative final accumulated AE energy versus sensor location is verified by the numerical simulation of the flow field in the primary zone of the pipe, as discussed in the following section.

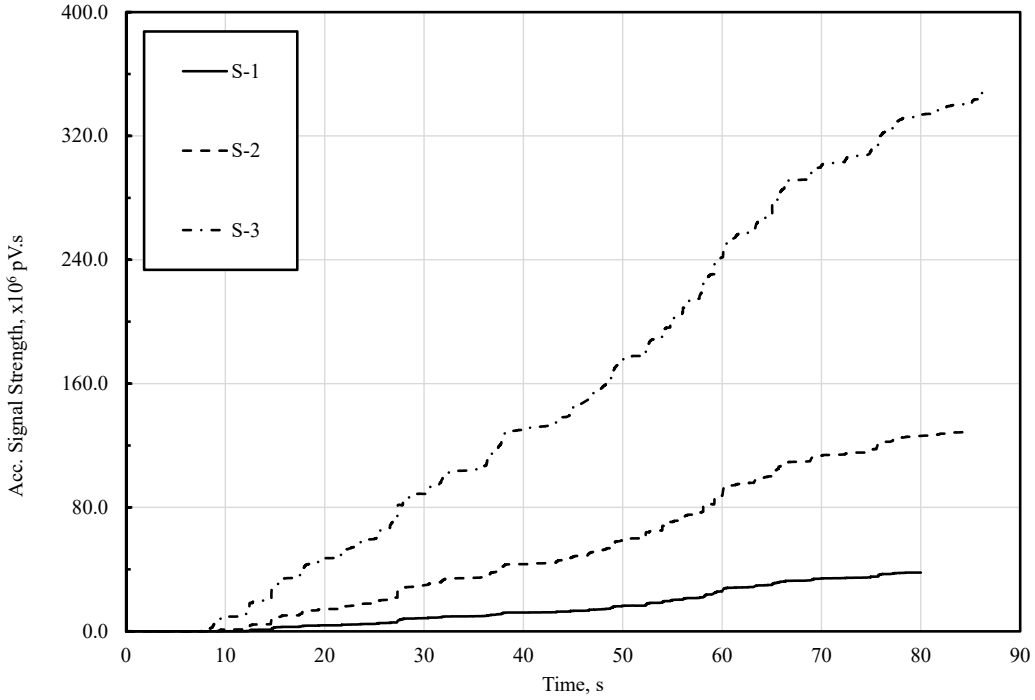

Figure 4.7 Accumulated signal strength over time for a pipe with 60% diameter reduction at sensors S-1, S-2, and S-3.

4.5 Theoretical Verification

The blockage location corresponds to the hump on the curve of the relationship between the relative final accumulated AE energy and the sensor location and is theoretically verified by numerical simulation. The numerical simulation includes analysing the flow characteristics and plotting the velocity profiles at selected sensor locations. In addition, it includes calculations of the relative turbulence kinetic energy of flow and comparing it to the relative final accumulated AE energy. Other parameters representing the flow characteristics are also calculated, as discussed in the following sub-section.

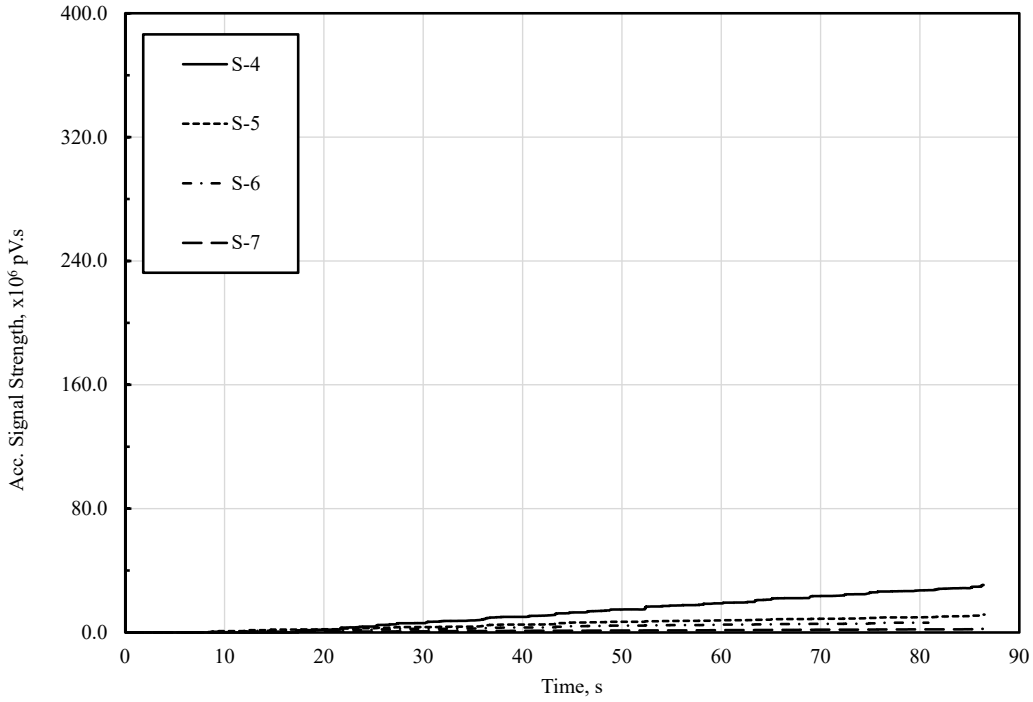

Figure 4.8 Accumulated signal strength over time for a pipe with 60% diameter reduction at sensors S-4, S-5, S-6, and S7.

Numerical Simulation

The flow domain along the primary zone of the pipe is analyzed by solving the three dimensional Reynolds-averaged Navier-Stokes equations using Fluent, a commercial CFD package within the Ansys software. The three dimensional model is used to calculate the parameters of interest at different locations of the pipe including the upper wall on which the acoustic sensors are attached. The parameters of interest include eddy viscosity, turbulent eddy dissipation, and turbulence kinetic energy.

Governing Equations

The Reynolds-averaged conservation equations for mass and momentum may be written as (Ferziger and Peric, 2012):

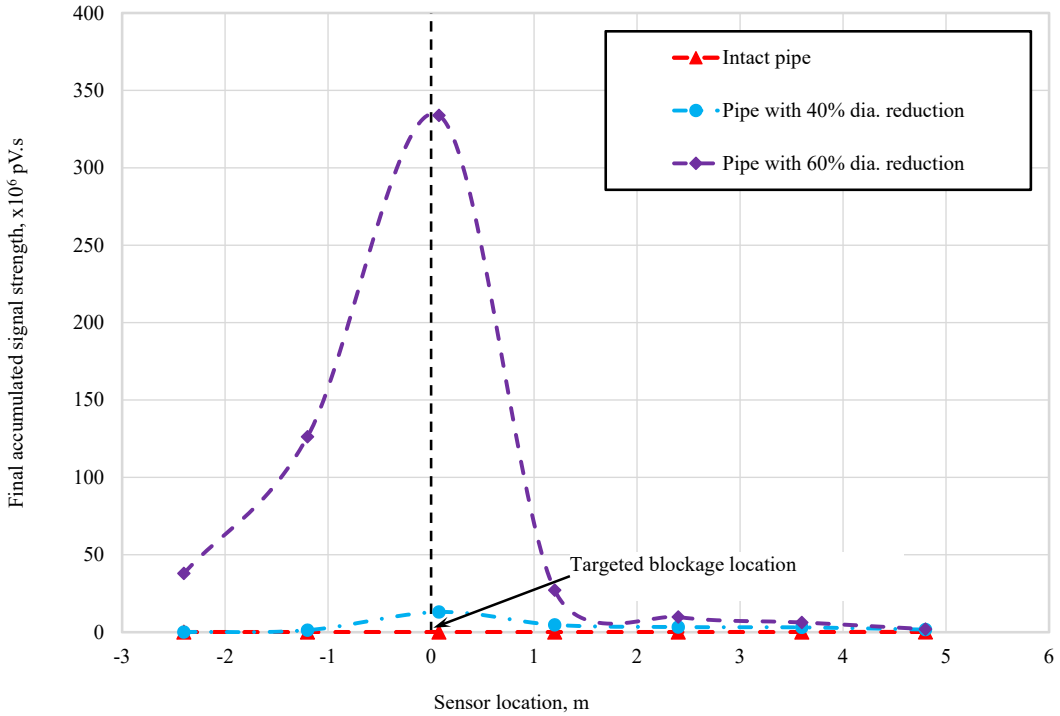

Figure 4.9 Final accumulated signal strength vs. sensor location.

$$\frac{\partial \bar{u}_i}{\partial x_i} = 0 \tag{4.1}$$

$$\frac{\partial \rho \bar{u}_i}{\partial t} + \frac{\partial \rho \bar{u}_i u_j}{\partial x_j} = -\frac{\partial \bar{p}}{\partial x_i} + \frac{\partial}{\partial x_i}[\mu(\frac{\partial \bar{u}_i}{\partial x_j} + \frac{\partial \bar{u}_j}{\partial x_i})] + \frac{\partial \tau_{ij}}{\partial x_j} \tag{4.2}$$

where $\bar{u}_i$ and $\bar{u}_j$ are Reynolds-averaged velocity, x_i and x_j are Cartesian coordinate axes, ρ is the fluid density, $\bar{p}$ is the pressure, t is the time, and μ is the molecular viscosity. The term $\tau_{ij} = -\rho(\overline{u_i u_j} - \bar{u}_i \bar{u}_j)$ is the Reynolds stress.

Flow Turbulence Kinetic Energy Model

The eddy-viscosity model in the Reynolds-averaged approach used by the FLUENT package of Ansys software to solve Navier-stokes equations may be expressed as (Ferziger and Peric, 2012):

$$\tau_{ij} = -\rho \overline{\acute{u}_i \acute{u}_j} = \mu_t \left(\frac{\partial \bar{u}_i}{\partial x_j} + \frac{\partial \bar{u}_j}{\partial x_i} \right) - \frac{2}{3} \rho k \delta_{ij} \tag{4.3}$$

in which k is the turbulence kinetic energy.

In the current study, a bounded second-order central difference scheme is used to solve the governing equations. The $k-\epsilon$ model is used for turbulence closure utilizing two transport equations, as follows:

For turbulence kinetic energy

$$\frac{\partial(\rho k)}{\partial t} + \frac{\partial\left(\rho u_j k\right)}{\partial x_j} = \frac{\partial}{\partial x_j}\left[\left(\mu + \frac{\mu_t}{\sigma_k}\right)\frac{\partial k}{\partial x_j}\right] - G_p - \rho\epsilon \tag{4.4}$$

in which, the eddy viscosity $\mu_t = \frac{C_\mu \rho k^2}{\epsilon}$, C_μ=0.09, and G_p is the turbulence generated due to the gradient of the mean flow velocity, which is defined as

$$G_p = -\rho\overline{\acute{u}_i\acute{u}_j}\frac{\partial u_i}{\partial x_j} = \rho\nu_t\left(\frac{\partial u_i}{\partial x_j} + \frac{\partial u_j}{\partial x_i}\right)\frac{\partial u_i}{\partial x_j} \tag{4.5}$$

where ν_t is the kinematic eddy viscosity.

For turbulence eddy dissipation

$$\frac{\partial(\rho\epsilon)}{\partial t} + \frac{\partial\left(\rho u_j \epsilon\right)}{\partial x_j} = \frac{\partial}{\partial x_j}\left[\left(\mu + \frac{\mu_t}{\sigma_\epsilon}\right)\frac{\partial \epsilon}{\partial x_j}\right] + C_{\epsilon 1}\frac{\epsilon}{k}G_p - C_{\epsilon 2}\rho\frac{\epsilon^2}{k} \tag{4.6}$$

where the values of $C_{\epsilon 1}$, $C_{\epsilon 2}$, σ_k, and σ_ϵ are 1.44, 1.92, 1.0, and 1.3, respectively.

Flow Field General Description

A numerical experiment is performed for a blocked pipe in which the actual pipe diameter is magnified 3 times to provide a clearly captured flow field for discussion purposes. The full-scale pipe parameters are retained in the later calculations used to verify the experimental observations. A partial blockage is added in the pipe by reducing the pipe diameter to the half in the middle of the primary zone to create a clearly captured flow field for discussion purposes.

The fluid body in the primary zone of the pipe is drawn in such a way that the $x - y$ plan coincides with the cross-sectional area of the pipe and z axis coincides with the longitudinal axis of the pipe (as shown in Fig. 4.12).

Fig. 4.10 and Fig. 4.11 show the velocity (color scale) and the velocity vectors, respectively. From these two figures, it is clear that, as the water flow approaches the blockage location, the flow velocity increases until it reaches the maximum value at the vena-contracta (the region where sensor S-3 is located). In addition, flow separation, high turbulence, and flow recirculation occur immediately downstream of the blockage location, as noticed from the direction of the velocity vectors in this region (Fig. 4.11).

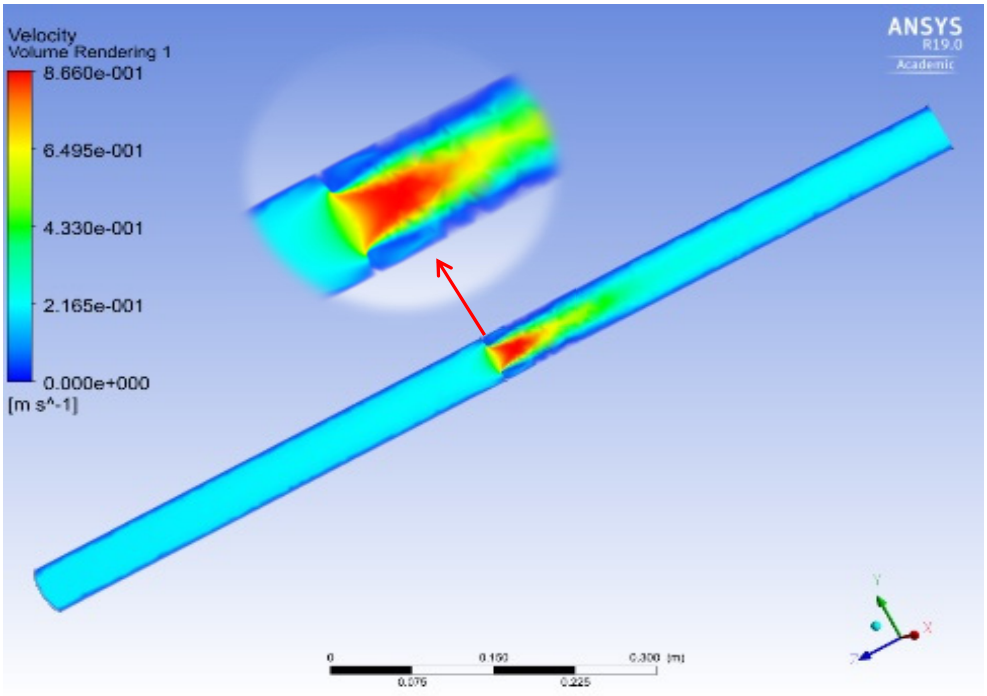

Figure 4.10 Velocity along the primary pipe zone.

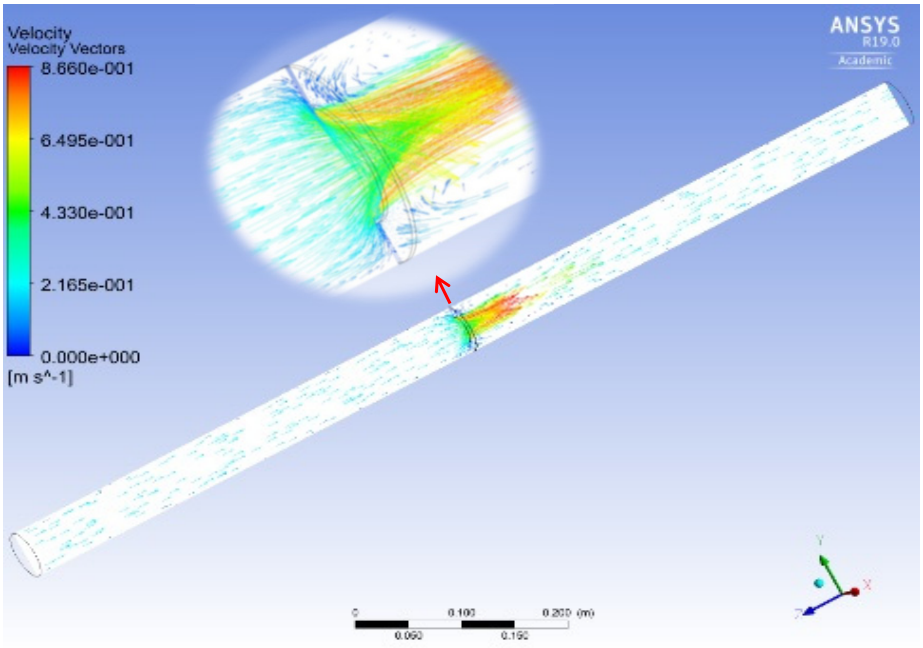

Figure 4.11 Velocity vectors along the primary pipe zone.

Velocity Profiles

Velocity profiles at the location of sensors S-2, S-3, and S-4 (upstream, in the vicinity, and downstream of the blockage location) are shown in Fig. 4.12. From this figure, it is noted that the velocity profiles of the partially blocked pipe at sensors S-2 and S-4 (far away upstream and downstream of the blockage location) are not affected by the blockage and they behave approximately as those of the intact pipe. However, the velocity profile at sensor S-3 (in the vicinity of the blockage location) shows higher velocity in the core of the pipe, as shown in the lower sub-figure to the left of Fig. 4.12 where the flow in the core of the partially blocked pipe is accelerated.

The variation among velocity profiles is attributed to the presence of the partial blockage, which affects the flow characteristics and causes differential flow behaviors in the vicinity of its location. These variations are captured by the numerical simulation and by the acoustic emission experimental results and may be used to locate

the partial blockage.

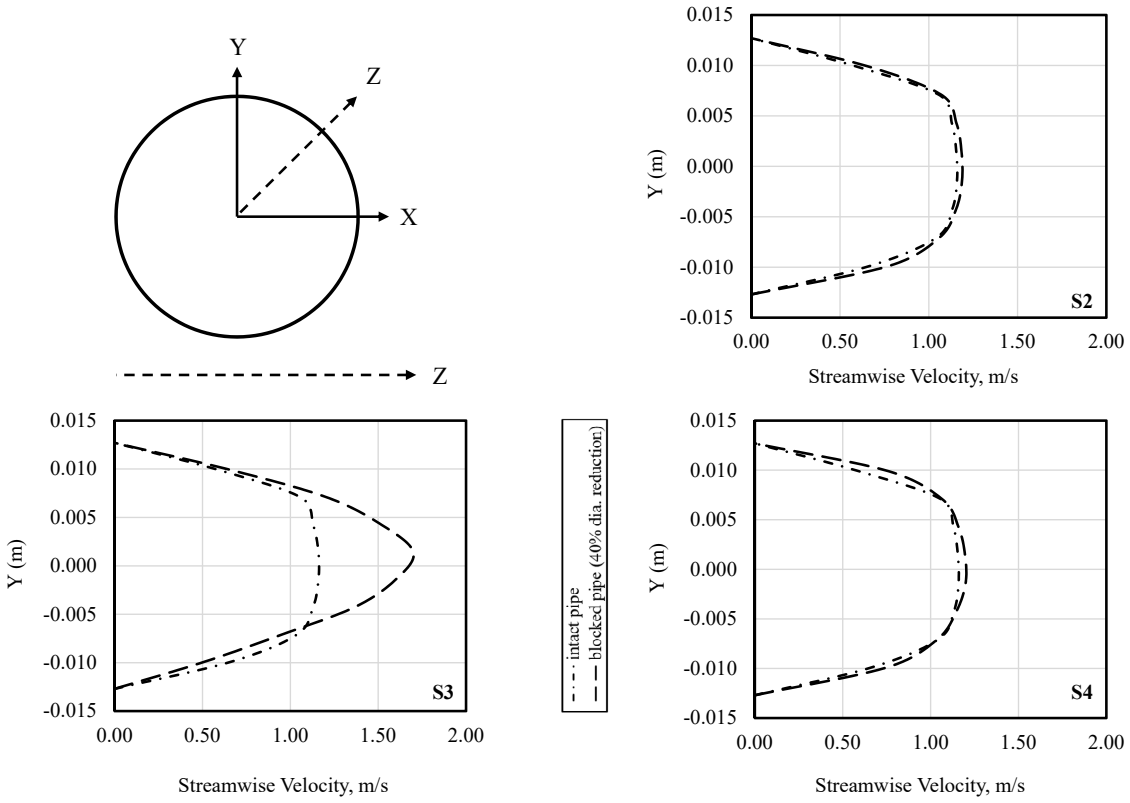

Figure 4.12 Velocity profiles at sensors S-2, S-3, and S-4 for different pipe conditions.

Flow Parameters of Interest

Flow parameters of interest in the current study include some flow characteristic parameters that are affected by the presence of a partial blockage and show abrupt changes close to its location. These include, but are not limited to, eddy viscosity (EV), turbulence eddy dissipation (TED), and turbulence kinetic energy (TKE). Calculations of these parameters are performed to investigate the effect of the blockage existence on each parameter. Figure 4.13, Fig. 4.14, and Fig. 4.15 show the variation of each relevant parameter along the primary zone of the pipe for three different conditions: an intact pipe, a pipe with a 40% diameter reduction, and a pipe with a 60%

diameter reduction. From these figures, it is clear that there is a spike in the vicinity of the blockage location (sensor S-3 location) the height of which is proportional to the percent of diameter reduction. It is also clear that this spike occurs due to the existence of the partial blockage and confirms the experimental results in which a hump is noted at the same location.

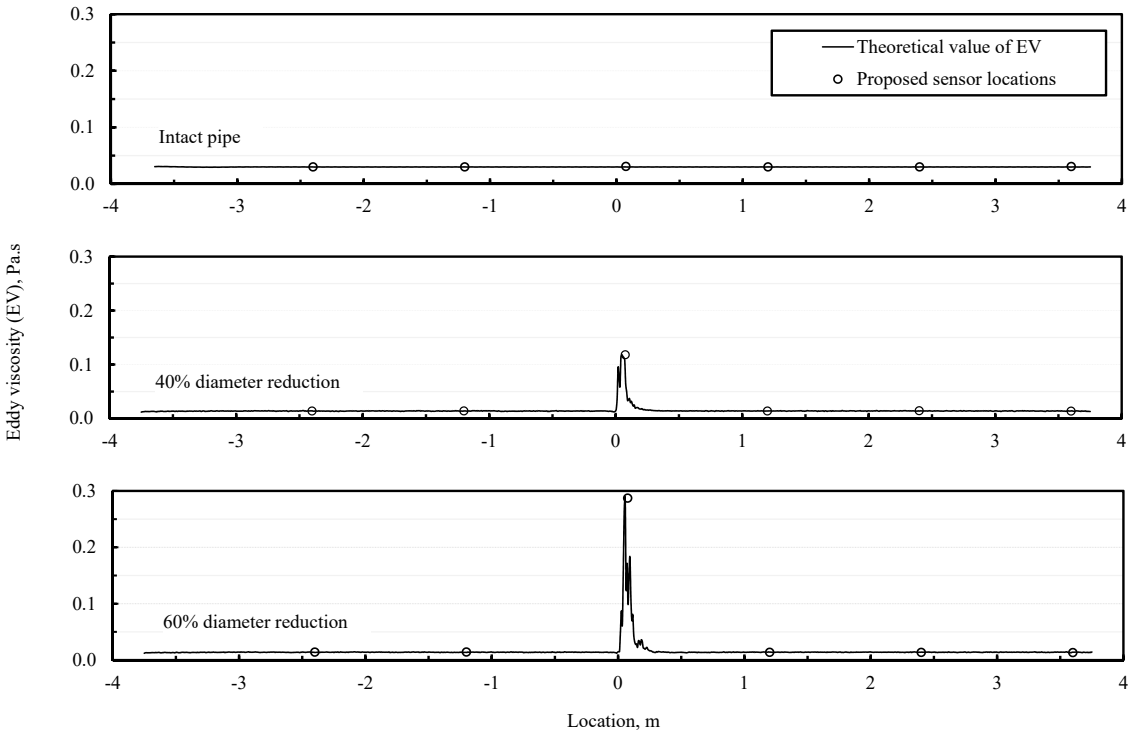

Figure 4.13 Eddy viscosity on the upper-wall of the pipe.

Comparison between Experimental and Numerical Results

The relative final accumulated AE energy during the experiment is compared to the theoretical relative turbulence kinetic energy. As discussed earlier, the relative final accumulated AE energy is obtained by normalizing the final accumulated AE energy using its maximum value for each pipe condition. Similarly, the relative theoretical turbulence kinetic energy is obtained by normalizing the theoretical turbulence kinetic energy using its maximum value for each pipe condition. Figure 4.16 shows the

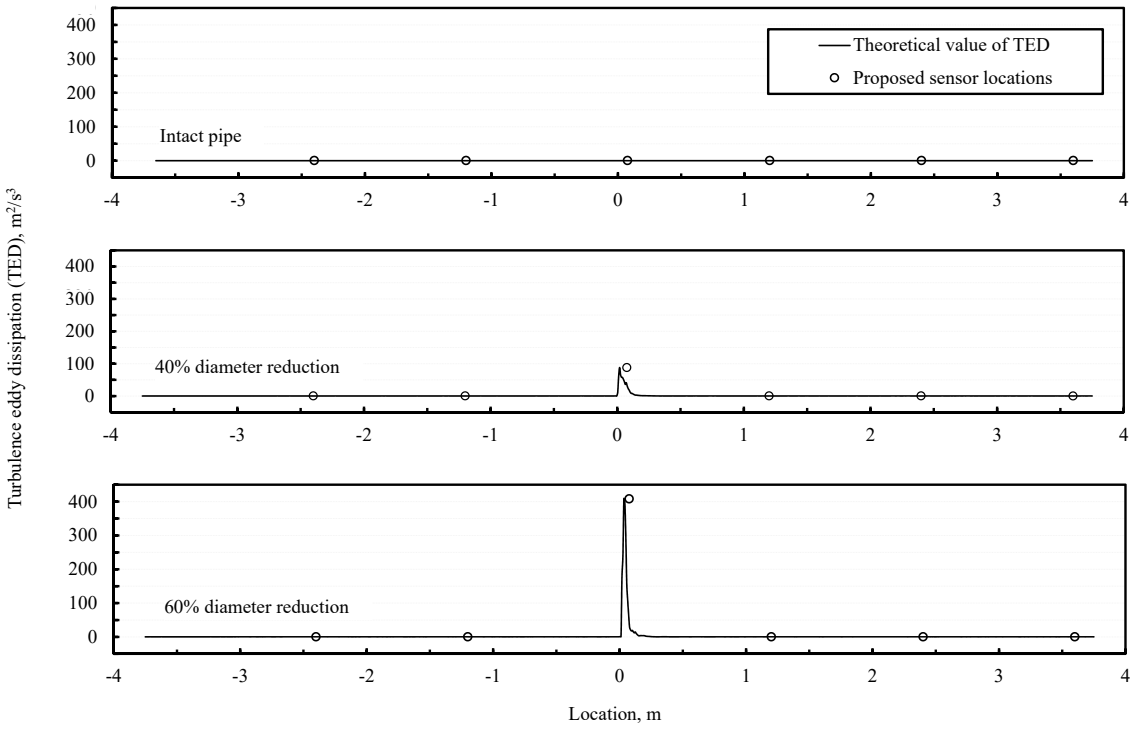

Figure 4.14 Turbulence eddy dissipation on the upper-wall of the pipe.

comparison between the relative final accumulated AE energy and the relative turbulence kinetic energy for the two aforementioned partially blocked pipe conditions. It is clear from this figure that there is an agreement between the theoretical and experimental relative energy plots on showing a hump in the curve of the relationship between the relative energy and the sensor location in the vicinity of the blockage location. It is also important to note that the numerical calculations in which the blockage information is known in advance agree with the experimental findings in which the blockage location is identified from the recorded signal without a prior knowledge.

4.6 Blockage Detection Procedure

This section discusses steps of detecting partial blockage in a pipe having water flow under steady state conditions. A general procedure is introduced; however, the

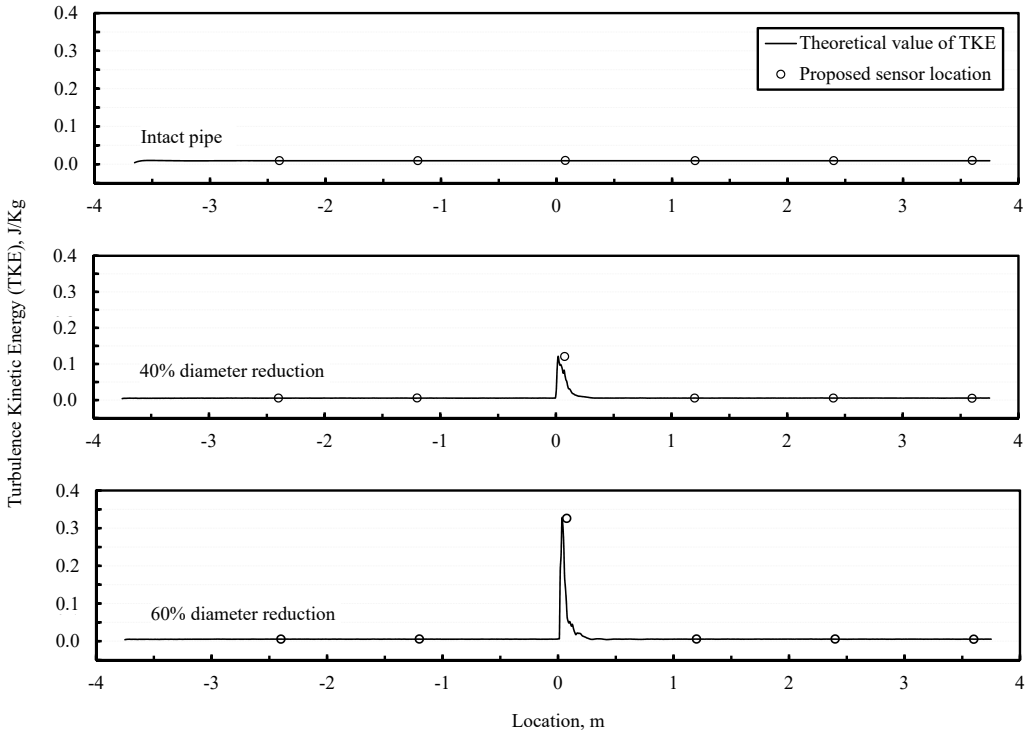

Figure 4.15 Turbulence kinetic energy on the upper-wall of the pipe.

approach is applied only on the current problem settings. Modifications are needed for application on different system settings. A minimum number of 5 sensors is proposed to be used for current approach application. The following steps may be used as a guideline for the detection process:

1. Select the primary zone of the pipe under investigation.

2. Equally divide the primary zone into two parts.

3. Define the sensors spacing, S, as follows (see Fig. 4.17):

   $S = L/2(N-1)$

   where L is the length of the primary zone and N is the number of sensors.

4. Place the sensors at the selected spacing, starting from the leading edge of the primary zone.

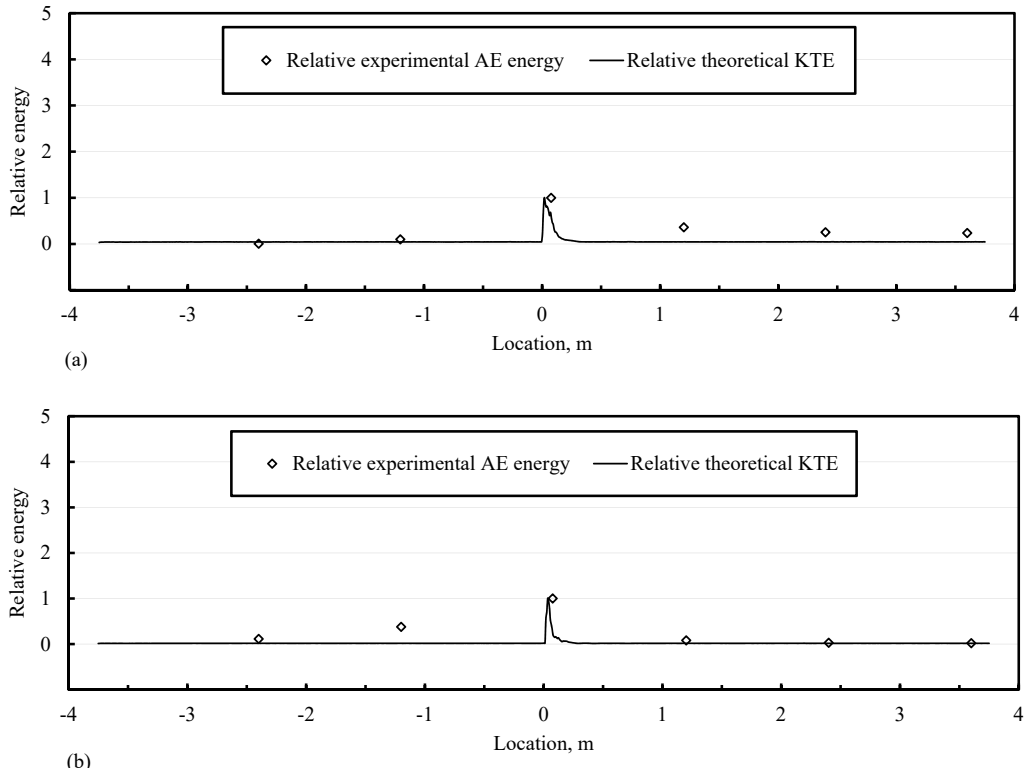

Figure 4.16 Experimental relative accumulated AE energy vs. numerical relative turbulence kinetic energy; (a) 40% diameter reduction, (b) 60% diameter reduction.

5. Record the acoustic signal for the desired accumulation time (80 seconds).

6. Shift the row of sensors for the specified tripping distance in the flow direction.

7. Repeat steps 5 and 6 until the end of the primary zone is reached.

8. Draw the accumulated signal strength versus sensor location for each tripping distance.

9. Locate the hump on the curve which represents the approximate blockage location.

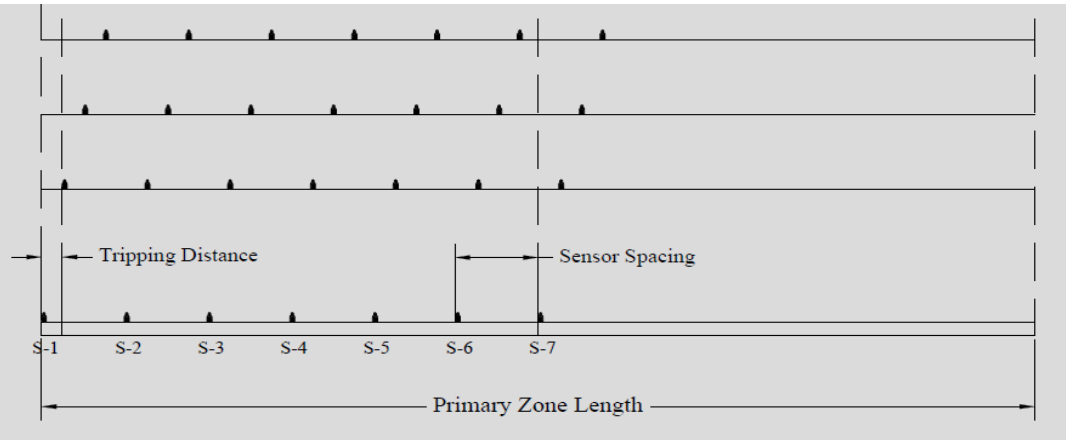

Figure 4.17 Blockage detection procedure.

Chapter 5

Use of Lower Harmonics of Pressure Oscillations for Leak Detection in Liquid Pipelines

5.1 Introduction

A simple technique for leak detection in liquid pipelines is presented in this chapter. The governing equations are solved in the frequency domain using the transfer matrix method (TMM). A direct relationship between the relative leak location and the amplitude of pressure head oscillation is obtained. This relationship is utilized to construct leak detection curves (LDCs) the characteristics of which are discussed briefly. Unlike the relevant frequency response diagram (FRD) methods, the current approach requires minimum efforts since it uses only the first four harmonics instead of a large set of harmonics. The comparisons with the time domain solution by the method of characteristics (MOC) and with the experimental data from the literature show a satisfactory agreement.

5.2 Frequency Domain Analysis

The governing equations describing transient flow in the simple piping system shown in Fig. 5.1 are (Chaudhry, 2015):

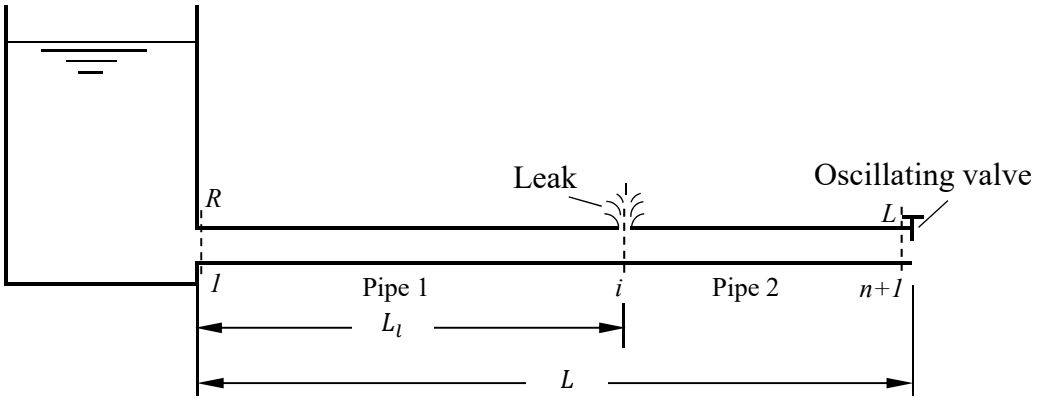

Figure 5.1 Piping system for leak detection.

$$\frac{\partial Q}{\partial x} + \frac{gA}{a^2}\frac{\partial H}{\partial t} = 0 \tag{5.1}$$

$$\frac{\partial H}{\partial x} + \frac{1}{gA}\frac{\partial Q}{\partial t} + \frac{fQ^2}{2gDA^2} = 0 \tag{5.2}$$

in which, a is the wave speed, g is the acceleration due to gravity, f is the Darcy-Weisbach friction factor, A is the cross-sectional area of the pipe, x is the distance along the pipeline, positive in the downstream direction, t is the time, and D is the pipe diameter. The variables H and Q are instantaneous pressure head and instantaneous flow rate, which may be expressed as the sum of their mean values, H_0 and Q_0, and their oscillations around the mean, h^* and q^*, as shown in Fig. 3.2 (Chaudhry, 1970).

The substitution of $H = H_0 + h^*$ and $Q = Q_0 + q^*$ into Eqs. 5.1 and 5.2 yields the following linear equations

$$\frac{\partial q^*}{\partial x} + \frac{gA}{a^2}\frac{\partial h^*}{\partial t} = 0 \tag{5.3}$$

$$\frac{\partial h^*}{\partial x} + \frac{1}{gA}\frac{\partial q^*}{\partial t} + Rq^* = 0 \tag{5.4}$$

in which, the linearized resistance term for the turbulent flow, R, equals fQ_0/gDA^2. The pressure head oscillation around the mean, h^*, may be eliminated from the previous two equations, yielding

$$\frac{\partial^2 q^*}{\partial x^2} - \frac{1}{a^2}\frac{\partial^2 q^*}{\partial t^2} - \frac{gAR}{a^2}\frac{\partial q^*}{\partial t} = 0 \tag{5.5}$$

The pressure head and discharge oscillations may be assumed as sinusoidal in time, i.e., $h^* = \mathrm{Re}\,[h(x)e^{j\omega t}]$ and $q^* = \mathrm{Re}\,[q(x)e^{j\omega t}]$, where ω is the angular frequency in radians per second, $j = \sqrt{-1}$, h and q are complex variables which are functions of x only, and Re[ ] stands for the real part. These sinusoidal terms may be substituted into Eq. 5.5 to obtain the field matrix, F_i, of the i^{th} pipe which is then used to derive the leak detection equations, as discussed in the following section.

Leak Detection Equations

A leak detection equation represents the relationship between the relative leak location and the amplitude of pressure head oscillation. It may be derived for each excitation frequency of the downstream valve which produces a sinusoidal pressure head oscillation in the pipeline. The piping system is simulated in the frequency domain and the governing equations are solved by using the transfer matrix method (TMM). The leak is simulated as an orifice. The leak discharge is characterized by its ratio to the mean discharge in the pipeline. The leak separates the pipeline into two segments and the overall transfer matrix of the pipeline may be expressed as (Chaudhry, 2014)

$$U = \begin{pmatrix} u_{11} & u_{12} & u_{13} \\ u_{21} & u_{22} & u_{23} \\ u_{31} & u_{32} & u_{33} \end{pmatrix} = F_2\ P_2\ F_1 \tag{5.6}$$

where u_{11}, u_{12}, $\cdots$ are elements of the overall transfer matrix; F_1 and F_2 refer to the field matrices of the pipe to the left and to the right of the leak, respectively, and P_2 refers to the point matrix for the leak.

The elements of the overall extended transfer matrix for a leaky pipe, u_{11} and u_{12}, with a valve oscillating at the 1^{st} (fundamental) harmonic $\left(\omega = \omega_{TH} = \frac{\pi a}{2L}\right)$ may be expressed as (see Appendix B)

$$u_{11} = -\frac{Q_{l0}C}{4\Delta H_0} \times \text{versin}\,(\pi L_r)\, j \tag{5.7}$$

$$u_{21} = \frac{C^2 Q_{l_0}}{4\Delta H_0} \sin(\pi L_r) - C\ j \tag{5.8}$$

where, L_r is the relative leak location (leak location measured from the upstream reservoir, L_l, divided by the pipe length, L); Q_{l_0} is the steady state leak discharge for the head at the leak, ΔH_0, $\text{versin}\,(\pi L_r) = 2\sin^2\left(L_r \frac{\pi}{2}\right)$, and $C = a/(gA)$ is the pipe characteristic impedance.

As shown in Appendix B, the following equations represent the relationship between the relative leak location and the pressure head oscillation for the first four harmonics of the valve oscillation

$$h^L_{n+1,1} = \frac{\dfrac{2H_o k}{\tau_o}}{\dfrac{2H_o}{Q_o} \times \dfrac{\dfrac{CQ_{l0}}{4\Delta H_o} \times \text{versin}\,(L_r\pi)\, j}{\dfrac{C^2 Q_{l0}}{4\Delta H_0} \sin(\pi L_r) - Cj} - 1} \tag{5.9}$$

$$h^L_{n+1,2} = \frac{\dfrac{2H_0 k}{\tau_0}}{\dfrac{2H_0}{Q_0} \times \dfrac{-1 + \dfrac{CQ_{l0}}{4\Delta H_0} \times \sin(2\pi L_r)\, j}{\dfrac{C^2 Q_{l0}}{2\Delta H_0} \sin^2(\pi L_r)} - 1} \tag{5.10}$$

$$h^L_{n+1,3} = \frac{\dfrac{2H_0 k}{\tau_0}}{\dfrac{2H_0}{Q_0} \times \dfrac{-\dfrac{CQ_{l0}}{4\Delta H_0} \times \text{versin}\,(3\pi L_r)\, j}{\dfrac{C^2 Q_{l0}}{4\Delta H_0} \sin(3\pi L_r) + Cj} - 1} \tag{5.11}$$

$$h^L_{n+1,4} = \frac{\dfrac{2H_0 k}{\tau_0}}{\dfrac{2H_0}{Q_0} \times \dfrac{1 - \dfrac{CQ_{l0}}{4\Delta H_0} \times \sin\left(4\pi L_r\right) j}{-\dfrac{C^2 Q_{l0}}{2\Delta H_0} \sin^2\left(2\pi L_r\right)} - 1} \tag{5.12}$$

The amplitude of pressure head oscillations may be normalized using the mean pressure head, H_0, to compute the relative amplitude of pressure head oscillation, $h_r = \left|h^L_{n+1}\right| / H_0$. The relationship between L_r and h_r for the first four harmonics of the pipeline is used to construct each corresponding leak detection curve.

Leak Detection Curves

A LDC represents the relationship between the relative leak location, L_r, and the relative amplitude of pressure head oscillation, h_r. The LDCs for the first four harmonic are shown in Fig. 5.2. The left axis of this figure shows the ordinates of the odd (1^{st} and 3^{rd}) harmonics, while the right axis shows the ordinates of the even (2^{nd} and 4^{th}) harmonics. LDCs may be constructed in a similar way as that used to construct the blockage detection curves (BDCs), introduced by Al-Tofan et al. (2018), and has a similar number of inflection points. However, LDCs differ from BDCs in their trends and location of maxima and minima. It may be noted from Fig. 5.2 that the maximum value of h_r for the 1^{st} harmonic LDC is obtained when the leak is located at the upstream end of the pipeline. In addition, there is only one value of the leak location that corresponds to each value of h_r. However, for the 2^{nd} harmonic LDC, two values of the leak location are obtained for each value of h_r, except when the leak is located at the mid-length of the pipeline, where only one value of the leak location is obtained. This is because of the symmetry feature of the 2^{nd} harmonic LDC. For the 3^{rd} harmonic LDC, there are two maxima (when the leak is located at $L_r = 0$ and $2/3$) and two minima (when the leak is located at $L_r = 1/3$ and 1).

For all other locations, there are three values of the leak location that correspond to each value of h_r. For the 4^{rd} harmonic LDC, there are two maxima (when the leak is located at $L_r = 1/4$ and $3/4$) and three minima (when the leak is located at $L_r =$ 0, 1/2, and 1). For all other locations, there are four values of the leak location that correspond to each value of h_r. However, as in the BDCs, there is only one shared value for the possible leak location which can be obtained by using the 1^{st} harmonic LDC and reconfirmed by using the other three LDCs. Using additional LDCs (higher than 4^{th} harmonic) results in problems related to using higher harmonics, as discussed in the Introduction.

5.3 Numerical Application

Equations 5.9 through 5.12 show that there is a direct relationship between the relative leak location, L_r, and the absolute value of the pressure head oscillation at the valve, $\left|h^L_{n+1}\right|$. As discussed earlier, the latter may be normalized using the mean pressure head in the pipeline to give the relative amplitude of pressure head oscillation, h_r. The relationship between L_r and h_r is used to construct LDCs for the first four harmonics of the pipeline. In the current numerical application, a frictionless system is considered first with a relative leak discharge, $q_r = 0.1$ (where q_r is the ratio of the leak discharge to the initial discharge in the pipeline). The effect of friction and leak discharge are considered later. The pipe length, L, pipe diameter, D, initial steady-state discharge, Q_0, mean pressure head, H_0, wave speed, a, initial relative valve opening, τ_0, and the amplitude of the valve oscillations, k, are 1600 m, 0.3 m, 0.1 m^3/s, 50 m, 1000 m/s, 0.9, and 0.1, respectively.

The leak detection curves for a system with the aforementioned parameters are constructed, as shown in Fig. 5.2. It can be noticed from the 1^{st} harmonic LDC that there is only one leak location for each value of the relative amplitude of pressure head oscillation in the piping system. In addition, as the leak location is changed

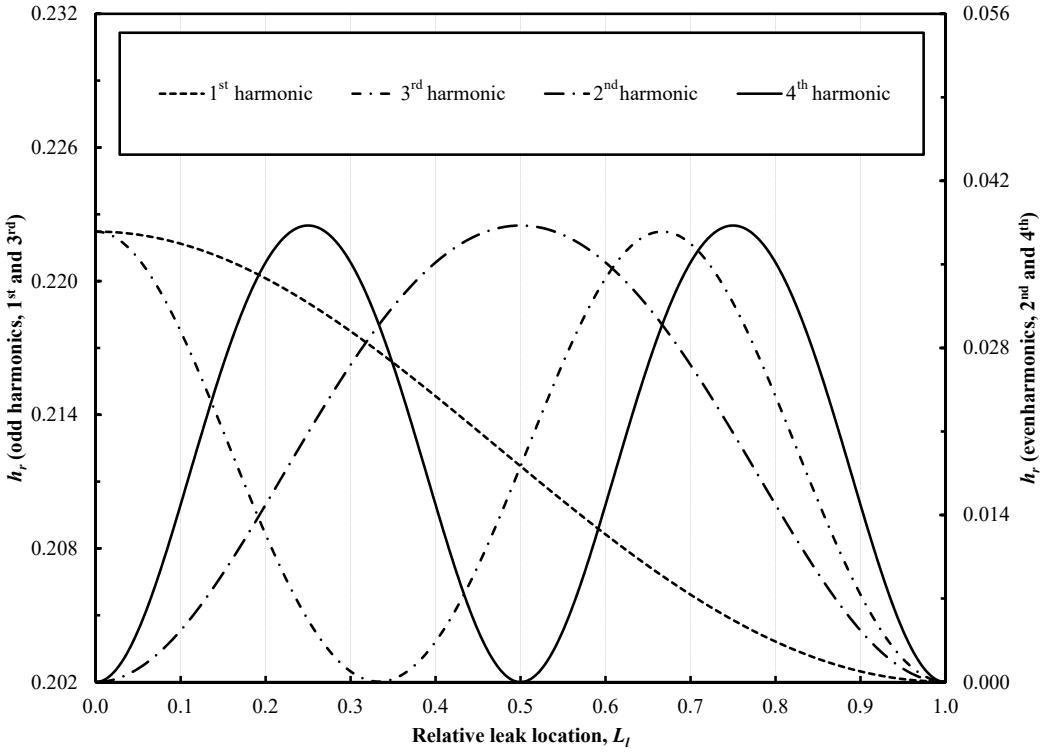

Figure 5.2 Leak detection curves for the first four harmonics.

from the upstream reservoir towards the downstream valve (i.e., $L_r = 0$ to 1), the relative amplitude of pressure head oscillation, h_r, decreases gradually from 0.222 to 0.202 or the amplitude of pressure head oscillation decreases gradually from 11.1 m to 10.1 m.

For the 2^{nd} harmonic LDC, as the leak location approaches the pipe mid-length (i.e., $L_r = 0.5$), the amplitude of pressure head oscillation approaches its maximum value depending on the leak discharge (0.01 m^3/s in this example). For a leak location away from the pipe mid-length towards the upstream reservoir or towards the downstream valve, h_r decreases gradually until it reaches its minimum value at the boundary. In addition, the curve is symmetric around the pipe mid-length i.e., for each value of h_r, there are two possible leak locations except for the pipe mid-length. One of these two locations is on the reservoir side of the pipe mid-length and the

other is on the valve side.

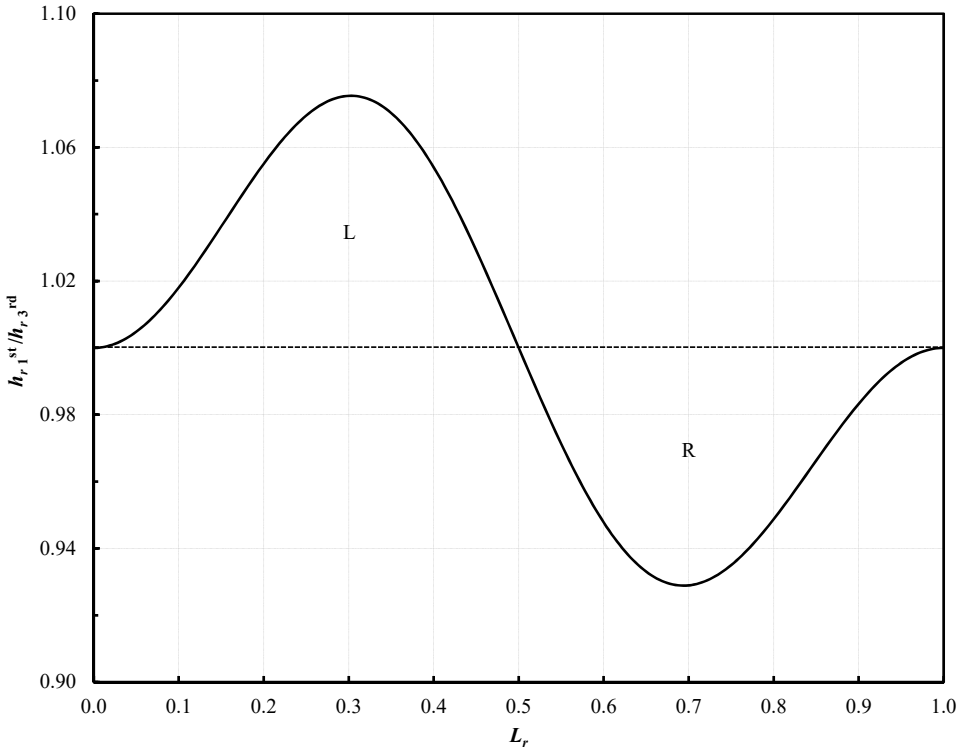

Figure 5.3 Relative amplitude of pressure head oscillation at first and third harmonic vs. leak location.

For the 3^{rd} and 4^{th} harmonic LDCs, there are multiple leak locations for each value of h_r, except at the points of maxima and minima. One of these possible locations obtained from each LDC is the same as that obtained from the 1^{st} harmonic LDC. However, it is not recommended to use only the 1^{st} harmonic LDC; a combination of the first four harmonics is recommended. One of these combinations uses the ratio of the amplitude of pressure head oscillation obtained from oscillating the downstream valve at the 1^{st} harmonic to that obtained from oscillating the downstream valve at the 3^{rd} harmonic. This ratio is shown in Fig. 5.3 and may be used to determine whether the leak exists on the reservoir side or on the valve side of the pipe mid-length. Region (L) in Fig. 5.3 (in which this ratio is greater than 1) corresponds to a leak on the reservoir side of the pipe mid-length, while region (R) (in which this

ratio is less than 1) corresponds to a leak on the valve side.

According to the LDC for the 1^{st} harmonic of the current example, any value of h_r within the range 0.222 to 0.202 may be obtained in a field application depending on the location of an unknown leak. Once this value is obtained, the 1^{st} harmonic LDC may be used to locate the leak. For example, an h_r value of 0.2148 corresponds to the L_r value of 0.4. The latter may be multiplied by the full length of the pipeline to give a leak location of 640 m from the upstream reservoir. For the 2^{nd}, 3^{rd} and 4^{th} harmonic LDCs, the values in Table 5.1 are obtained.

Table 5.1 Relative amplitude of pressure head oscillation at the downstream end of the pipeline and the corresponding leak location for different harmonics.

Harmonic	Relative pressure head oscillation amplitude (h_r)	Possible relative leak location (L_r)	Actual pressure head oscillation, m	Possible leak location, m
1^{st}	0.2148	0.4	10.74	640
2^{nd}	0.03516	0.4 0.6	1.758	640 960
3^{rd}	0.20382	0.269 0.4 0.931	10.191	430.4 640 1489.6
4^{th}	0.01487	0.1 0.4 0.6 0.9	0.7435	160 640 960 1440

It can be noticed from this table that there is only one shared leak location among all the four LDCs ($L_r = 0.4$). In addition, the ratio between the relative amplitude of pressure head oscillation resulting from oscillating the valve at the 1^{st} harmonic to that resulting from oscillating the valve at the 3^{rd} harmonic is greater than 1, which reconfirm that the leak is on the reservoir side of the pipe mid-length.

Effect of Leak Size

Three different leak discharges are considered to discuss the effect of the leak discharge on the LDCs. Leak discharge is expressed by its relative value, q_r, representing the leak discharge, Q_l, divided by the mean discharge in the pipeline, Q_0. Figure 5.4 shows the 1^{st} and 3^{rd} (odd) harmonics LDCs for three values of q_r (0.15, 0.25, and 0.35) using the same system settings and parameters from the "Numerical Application". According to this figure, for the 1^{st} harmonic, the relative amplitude of pressure head oscillation, h_r, decreases as the relative leak discharge, q_r, increases for all possible leak locations except when the leak is located at the upstream end of the pipeline ($L_r = 0$). At this location, a pressure head oscillation node in terms of the leak size is created in which the relative amplitude of the pressure head oscillations is the same for all leak discharges. For the 3^{rd} harmonic, two pressure head oscillation nodes in terms of the leak size are created (at $L_r = 0$ and $L_r = 2/3$). For all other possible locations, the relative amplitude of pressure head oscillation, h_r, decreases as the relative leak discharge, q_r, increases.

The effect of the leak size on the 2^{nd} and 4^{th} (even) harmonics is shown in Fig. 5.5. From the 2^{nd} harmonic LDC presented in this figure, it is seen that there are two pressure head oscillation nodes in terms of the leak size: at $L_r = 0$ and at $L_r = 1$. However, for the 4^{th} harmonic, there are three pressure head oscillation nodes in terms of the leak size: at $L_r = 0$, $L_r = 1/2$, and $L_r = 1$. For all other possible locations, and unlike the case of the odd harmonics, the relative amplitude of pressure head oscillation, h_r, increases as the relative leak discharge, q_r, increases.

Effect of Friction

In this section, the effect of steady and unsteady friction on the amplitude of pressure head oscillation and subsequently on the LDCs is discussed.

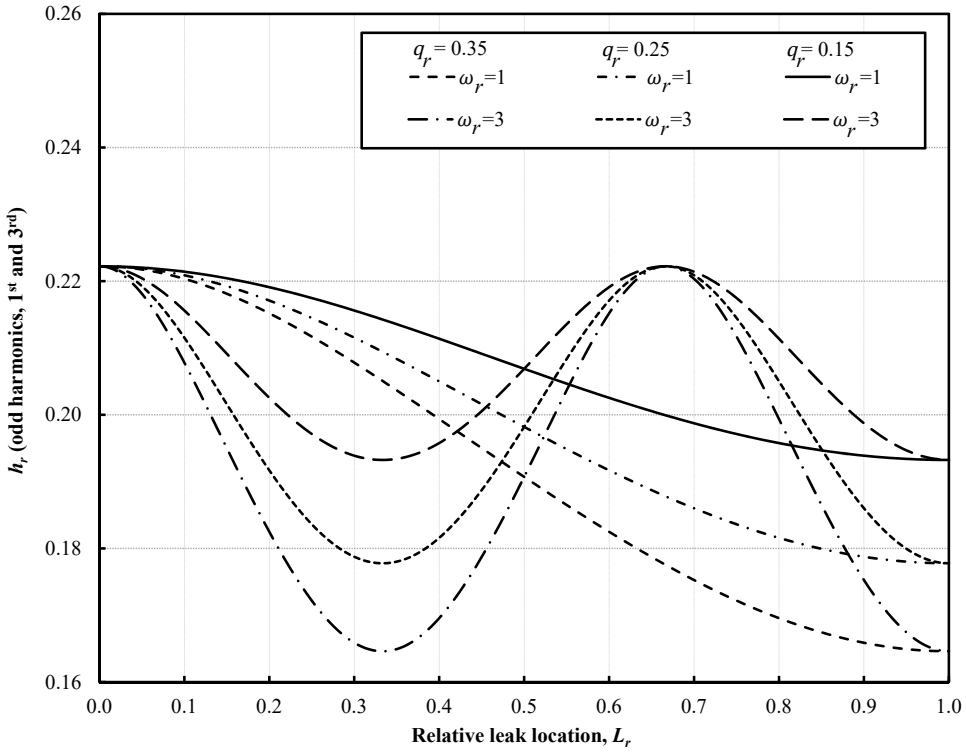

Figure 5.4 Leak detection curves for first and third harmonics with different leak sizes.

Steady Friction

As an example, steady friction effect represented by Darcy-Weisbach friction factor, f, on the relationship between L_r and h_r for the 1^{st} and 3^{rd} harmonics is discussed as follows. Three values of f (0, 0.01, and 0.02) are considered, as shown in Fig. 5.6. In this figure, the upper two curves represent the 1^{st} and 3^{rd} harmonic LDCs for a frictionless system, while the lower four curves represent the 1^{st} and 3^{rd} harmonic LDCs for a system with f =0.01 and f = 0.02, respectively. The lower part of this figure shows enlargements for the interaction points between the 1^{st} and 3^{rd} harmonic LDCs.

It is noticed that the amplitude of pressure head oscillation is inversely proportional to the steady friction factor, f, for all possible leak locations and for both 1^{st} and 3^{rd} (odd) harmonics. In addition, the 1^{st} and 3^{rd} harmonic LDCs for the friction-

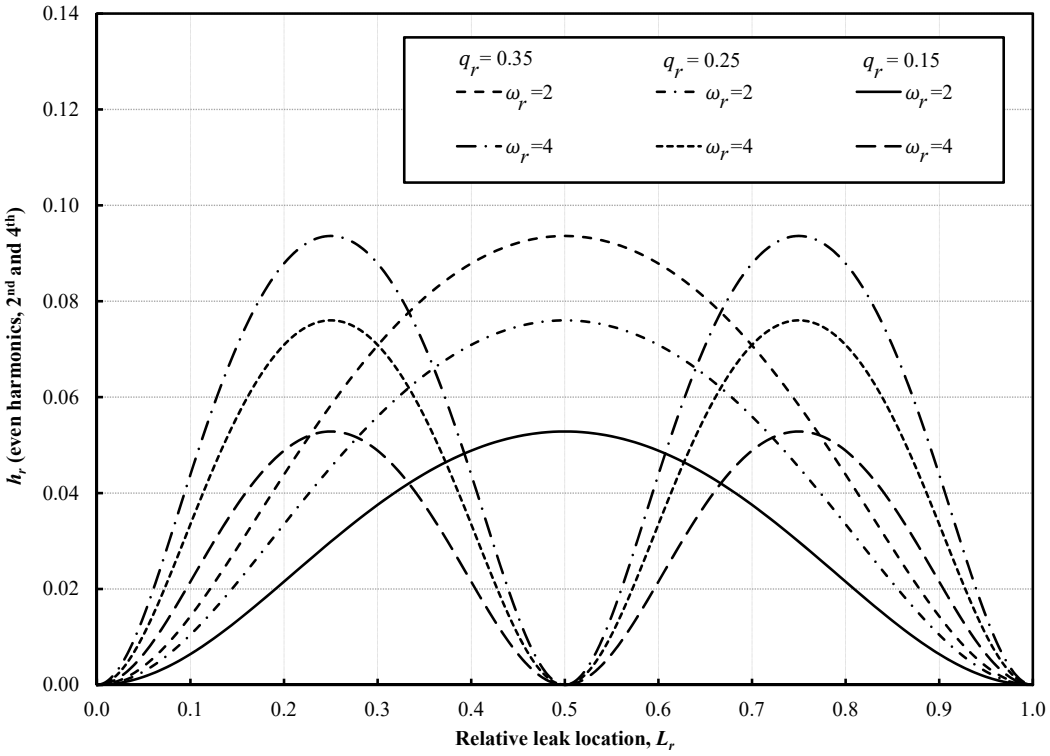

Figure 5.5 Leak detection curves for second and fourth harmonics with different leak sizes.

less system intersect at three locations: L_r =0, 0.5, and 1 (points a, b, and c in the upper part of Fig. 5.6). That means that the pressure head oscillation is the same whether the downstream valve is oscillated at the 1^{st} or 3^{rd} harmonic. The location of these intersection points, however, is changed as the steady friction is included in the calculations, as shown in the lower four curves of Fig. 5.6 (insets d, e, f, g, h, and i). The intersection between the 1^{st} and 3^{rd} harmonic LDCs for a system including friction occurs only at two locations: slightly to the left of the downstream boundary and slightly to the left of the pipeline mid-length. Point a_o in inset a becomes two points, a_1 and a_2 (inset d), and there is no more intersection between the two curves (the 3^{rd} harmonic curve being below the 1^{st} harmonic curve and any downward shift resulting from increasing steady friction keeps the two curves apart). Point b_o in inset b becomes two points, b_1 and b_2 (inset e), and there is a new point of intersection

at b_3. Point c_o in inset c becomes two points, c_1 and c_2 (inset f), and there is a new point of intersection at c_3.

The amplitude of pressure head oscillation at points a_1, b_1 and c_1 is greater than that at points a_2, b_2 and c_2, respectively. However, the difference in the amplitude of pressure head oscillation between each two corresponding points (a_1 and a_2, for example) is not the same as that between any other corresponding points (b_1 and b_2, or c_1 and c_2), but the difference between each two corresponding points increases as steady friction factor increases, as shown in insets g, h, and i. The change in the intersection points that occurs due to the inclusion of steady friction may be attributed to the proportional relationship between steady friction and the number of harmonics. In other words, the effect of steady friction on the amplitude of pressure head oscillation is greater in the case of oscillating the downstream valve at the 3^{rd} harmonic than that in the case of oscillating the downstream valve at the 1^{st} harmonic. This differential effect changes the ratio between the amplitude of pressure head oscillation resulted from oscillating the downstream valve at the 1^{st} harmonic to that from oscillating the downstream valve at the 3^{rd} harmonic, which is used to determine the side of the pipe mid-length in which the leak exists. As discussed previously for a frictionless system, this ratio is greater than 1 when the leak exists on the reservoir side of the pipe mid-length and less than 1 when the leak exists on the valve side. For a frictional system, however, this is not true for all possible leak locations. For a short section near the downstream valve, this ratio is greater than 1 in spite of that the leak is on the valve side. In addition, for a short section to the left of the pipe mid-length this ratio is less than 1 in spite of that the leak is on the reservoir side. The extent of these two regions and the above mentioned ratio deviation from 1 increases as steady friction increases.

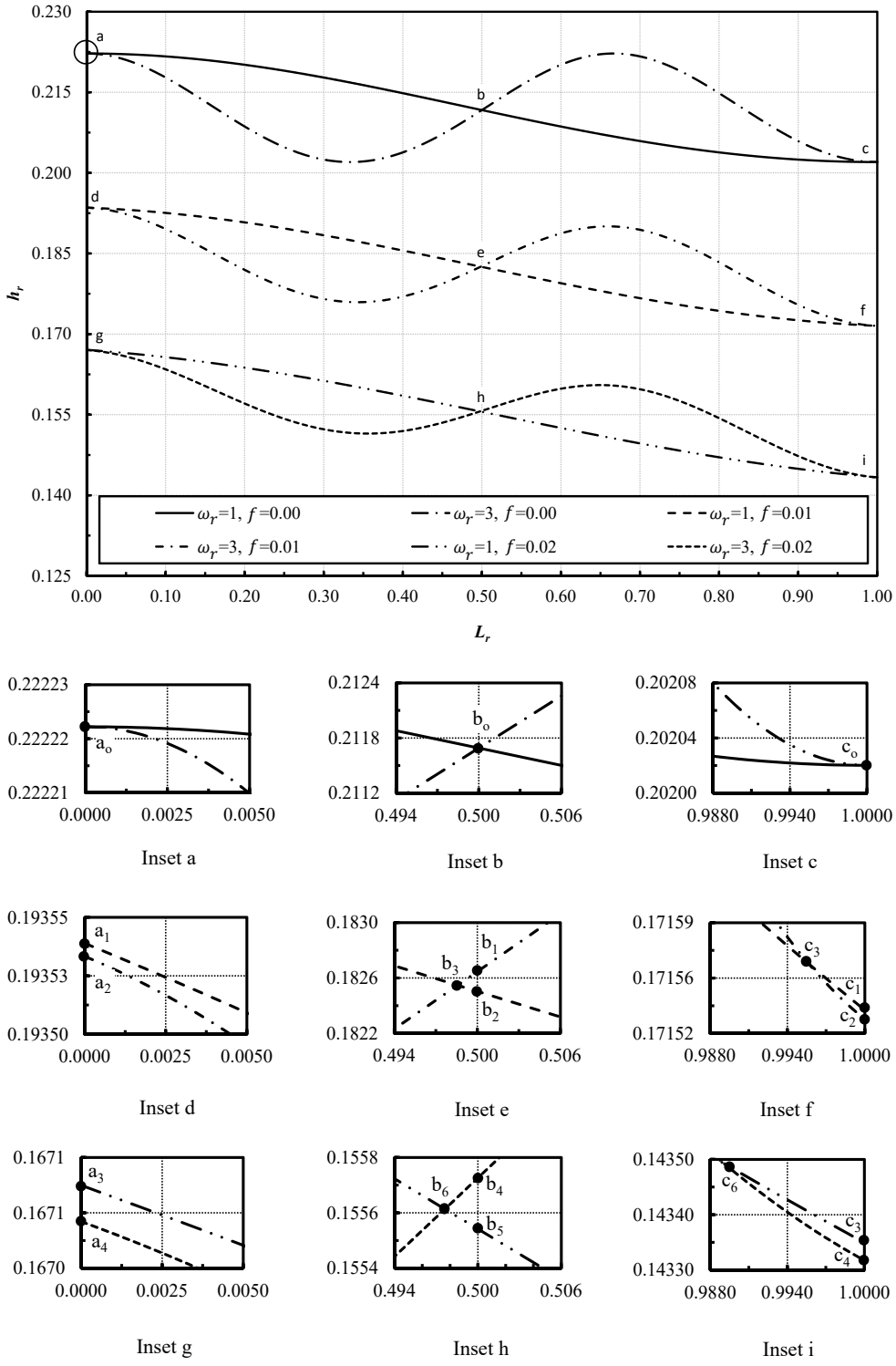

Figure 5.6 Comparison of the first and third harmonic leak detection curves for a system with and without friction; only steady friction included. Insets a through i are enlargements of the interaction points.

Unsteady Friction

The effect of inclusion of unsteady friction in the calculations of pressure head oscillation and the subsequent effect on the leak detection curves is discussed in the following paragraphs. Numerous models for investigating the effect of unsteady friction on the pipelines transient flow are proposed in the literature. However, the model of Vitkovsky et al. (2003) is used in the current study for its simplicity and suitability for simple reservoir-pipeline-valve system. According to this model, the steady friction is increased by an amount of $\frac{2j\omega}{gA}\left(\frac{1}{C^*}+\frac{j\omega D^2}{4\nu}\right)^{-1/2}$ (in which the shear decay coefficient, $C^* = 7.41/{R_e}^k$, R_e is the Reynold's number, ν is the kinematic viscosity of water, and $k = \log_{10}(14.3/{R_e}^{0.05})$) to account for unsteady friction. The LDCs are reconstructed by including this amount in the calculation of pressure head oscillation and compared to those constructed with only steady friction included (taking f as 0.01), as shown in Fig. 5.7. From this figure, it can be seen that the inclusion of unsteady friction results in a minor shift of the leak detection curves. This shift occurs in two different ways: either downward (in the case of the odd harmonics) or upward (in the case of the even harmonics). In addition, for odd harmonics, this shift is greater in the case of 3^{rd} harmonic than that in the case of 1^{st} harmonic. Similarly, for even harmonics, this shift is greater in the case of 4^{th} harmonic than that in the case of 2^{nd} harmonic. However, the current approach considers one harmonic at a time (up to the 4^{th} harmonic) to analyze the variation of the amplitude of pressure head oscillation for different leak locations.

5.4 Model Verification

The outputs of the current approach are compared with those obtained in the time domain using the method of characteristics (MOC) and with the experimental data available in the literature, as discussed in the following paragraphs.

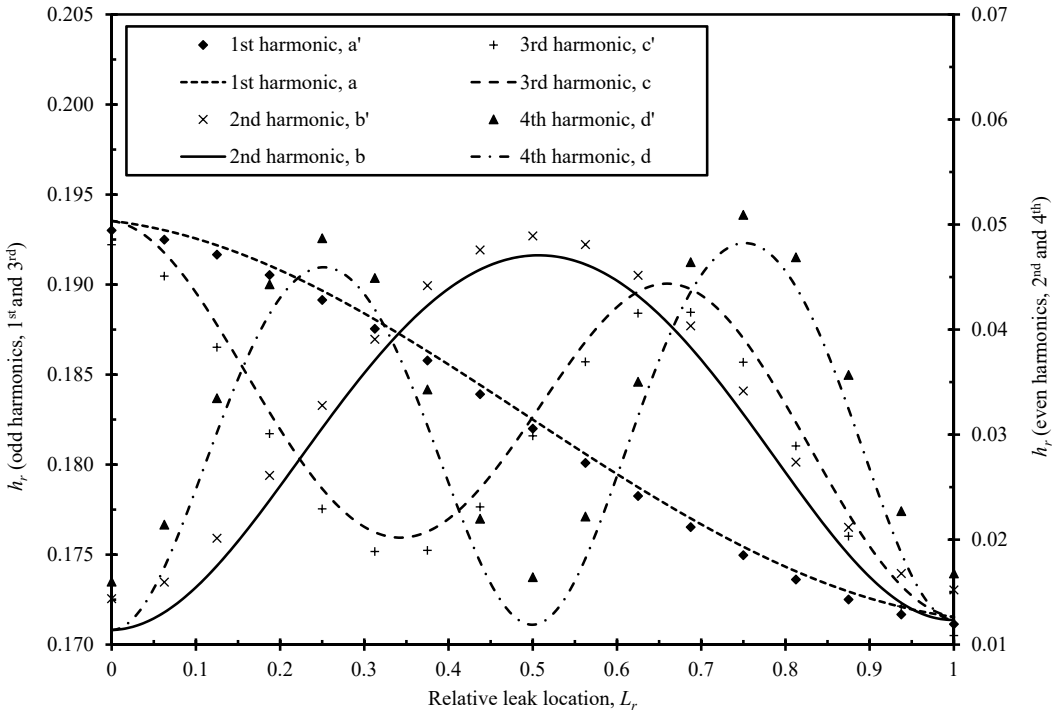

Figure 5.7 Comparison of the leak detection curves with and without including of unsteady friction ($f = 0.02$) (a, b, c, and d unsteady friction is not included; a', b', c', and d' unsteady friction is included).

Method of Characteristics

Leak detection curves proposed in the current study are reconstructed in the time domain using the method of characteristics (MOC). A simple system is used consisting of an upstream reservoir, a pipeline, and a downstream valve. The upstream reservoir supplies 0.0001 m^3/s of water to the pipeline which leaks at a rate of 0.000025 m^3/s (q_r=0.25). One leak is considered at a time and placed at different locations at 50 m spacing along a 1600 m long pipeline. All other parameters are kept the same as those considered in the Numerical Application. The downstream boundary is applied by relating the relative valve opening, τ, to time, t, in a sinusoidal relationship such that $\tau = \tau_0 + k \sin(\omega t)$, in which τ_0 is the mean valve opening, k is the amplitude of

the relative valve opening, and ω is the frequency of the oscillating valve. The leak is also simulated as an intermediate boundary condition at each of the above specified locations. Computations are done for 2800 time steps with each time step equal to 0.025 seconds in order to ensure that the steady-oscillatory flow is established and the amplitude of pressure head oscillation is constant. The maximum-minimum pressure head difference is taken for the last 10 seconds and no noise in the signal is observed. As an example, the downstream valve is oscillated at the 2^{nd} harmonic and the pressure head response at the downstream end of the pipeline is calculated with the leak existing at different locations, one at a time, as shown in Fig. 5.8. The relative amplitude of pressure head oscillation, h_r, is determined as $\Delta H_{L_r}/2H_0$, where ΔH_{L_r} is the maximum-minimum pressure head difference for each corresponding relative leak location and H_0 is the mean pressure head.

The calculations are done for the other leak locations with the downstream valve oscillations at other harmonics to construct the LDCs for the first four harmonics. The LDCs obtained by the TMM (in the frequency domain) are compared with those obtained by the MOC (in the time domain), as shown in Fig. 5.9. From this figure, it is clear that the amplitude of pressure head oscillations are slightly higher by the TMM than those obtained by the MOC for the 1^{st} and 3^{rd} (odd) harmonics and for all possible leak locations ($L_r = 0$ to 1). This overestimation may be attributed to the linearity assumption in the TMM solution. However, there is almost full agreement between the results computed by the two methods for the 2^{nd} and 4^{th} (even) harmonics.

Experimental Data

The presence of a leak in a pipeline produces an oscillatory pattern in the system frequency response diagram (FRD). This oscillatory pattern has a period that

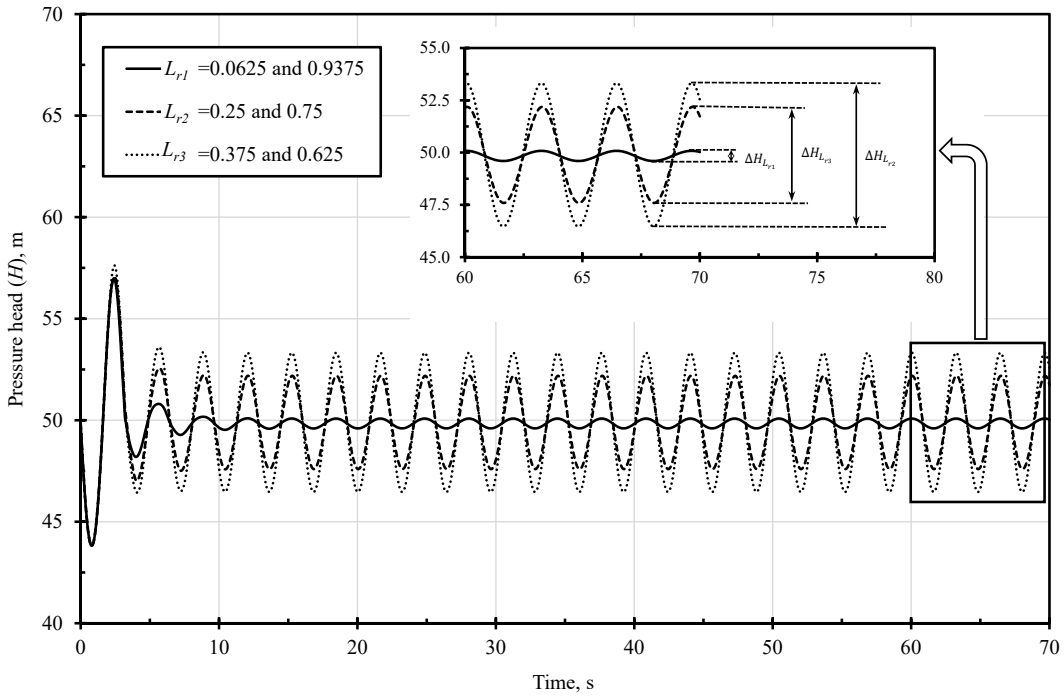

Figure 5.8 Pressure head oscillations of the downstream valve sinusoidal movement at the second harmonic for different leak locations.

may be related to the leak location. Sattar (2015) presented this relationship as $L_l/L = 2/\Delta\omega_r^{\text{even}}$ in which L_l is the leak location from the downstream valve, L is the pipe length, and $\Delta\omega_r^{\text{even}}$ is the period of the even harmonics leak induced oscillation pattern in the FRD. He extracted the FRD for a short pipe in order to determine this oscillation period. His data points include the relative amplitude of pressure head oscillations, h_r, corresponding to a set of relative frequencies up to the 6^{th} harmonic, as shown in the bottom and left axes of Fig. 5.10 (a or b). The piping system he used consists of a constant-level upstream reservoir, a pipeline, and a downstream valve. The height of water in the reservoir is 7.19 m and the mean discharge supplied to the pipe is 0.000284 m^3/s. The pipe length and diameter are 156 m and 0.0254 m, respectively. The pipe is leaking through an orifice of a relative area opening, A_{orf}/A_p, of 0.004 (where A_{orf} is the area of the leak orifice and A_p is the cross-sectional area of the pipe). Using a typical orifice equation, the leak discharge can be determined as

$Q_L = C_d A_{orf} \sqrt{2gH_L}$ (in which Q_L is the leak discharge for the head on the leak, H_L, and C_d is the coefficient of the discharge). The leak orifice is located at a distance of 72.12 m from the downstream valve. Using the proposed relationship between the even harmonics oscillation period and the relative leak location, the latter may be determined as $2/\Delta\omega_r^{\text{even}} = 0.5$. The same experimental system is simulated in the current model and the even (2^{nd} and 4^{th}) harmonic LDCs are constructed to be used for leak localization, as shown in the right and top axes of Fig. 5.10 (a and b). The 2^{nd} harmonic LDC is shown in Fig. 5.10 (a), while the 4^{th} harmonic LDC is shown in Fig. 5.10 (b). In order to compare the theoretical value of the leak location to the experimental value, the former may be determined by two simple steps:

1. Determine the measured value of the relative amplitude of pressure head oscillation, h_r, from the experimental results (in the case of the 2^{nd} harmonic, for example, this value equals 0.134 as determined from the vertical axis on the left of Fig. 5.10 (a) corresponding to $\omega_r = 2$ from the bottom axis).

2. Locate h_r value on the vertical axis on the right and project a horizontal line to intersect the LDC. Project the intersection points vertically on the top axis to find the possible leak locations, L_r.

Two values of L_r (0.487 and 0.553) are obtained from the 2^{nd} harmonic LDC, while four values of L_r (0.03, 0.47, 0.537, and 0.97) are obtained from the 4^{th} harmonic LDC. However, only two values obtained from the 4^{th} harmonic LDC (0.47 and 0.537) are close to the two values obtained from the 2^{nd} harmonic LDC and may be considered for further discussion. Either of these values give a good approximation of the leak location. The difference between the actual and calculated relative leak locations may be attributed to the uncertainty in the calculations of the unsteady friction and the experimental estimation of the system parameters.

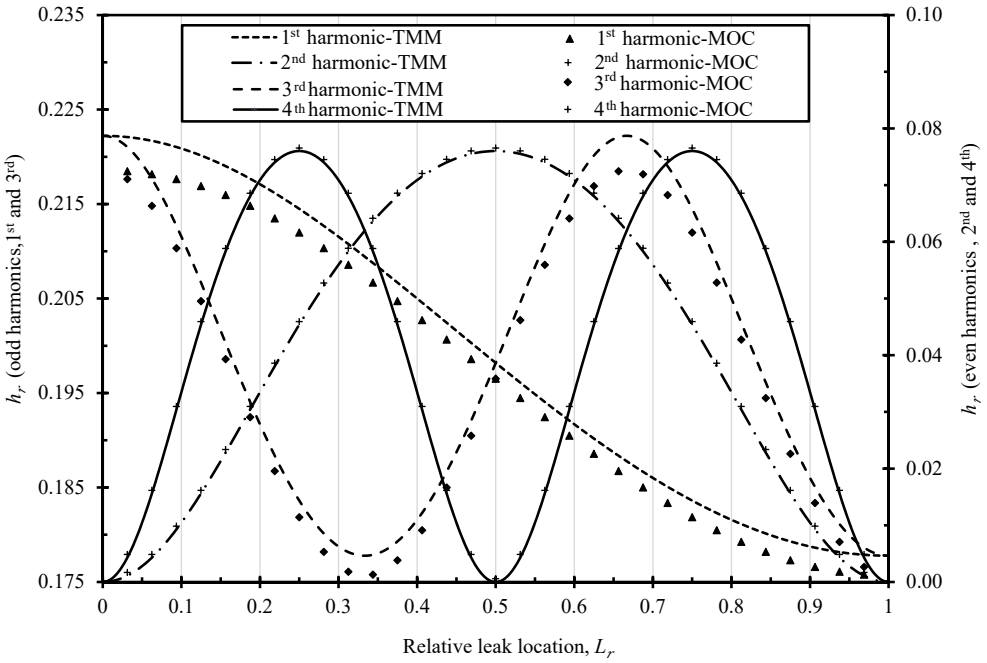

Figure 5.9 Comparison of the leak detection curves obtained by using the method of characteristics and the transfer matrix method.

5.5 Potential for Field Applications

The leak detection technique proposed in this study using the relationship between the amplitude of pressure head oscillation and leak location to detect leaks in pipelines has the potential for real-life applications. A prototype test of an intact pipe may be used to verify the system parameters. Discharge measurements at the downstream end of the pipe are carried out in order to estimate the leak discharge. A sinusoidal opening and closing of the downstream valve at the first four harmonics of the pipeline produces a sinusoidal pressure head oscillations. The relative amplitude of pressure head oscillation, h_r, at the downstream end of the pipeline is then determined. The corresponding LDC for each specific harmonic is used to determine the relative leak location, L_r. There should be one shared value of the anticipated leak location from each LDC. This value may be slightly different at each harmonic due to the estimation accuracy of the system parameters. This difference, however,

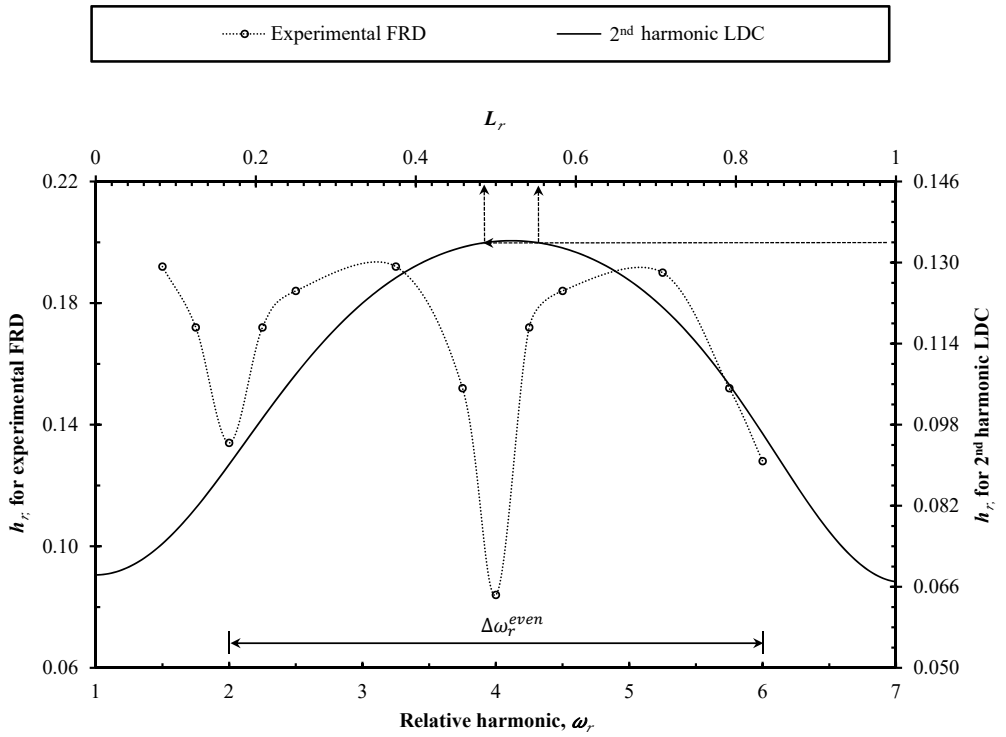

(a) 2nd harmonic

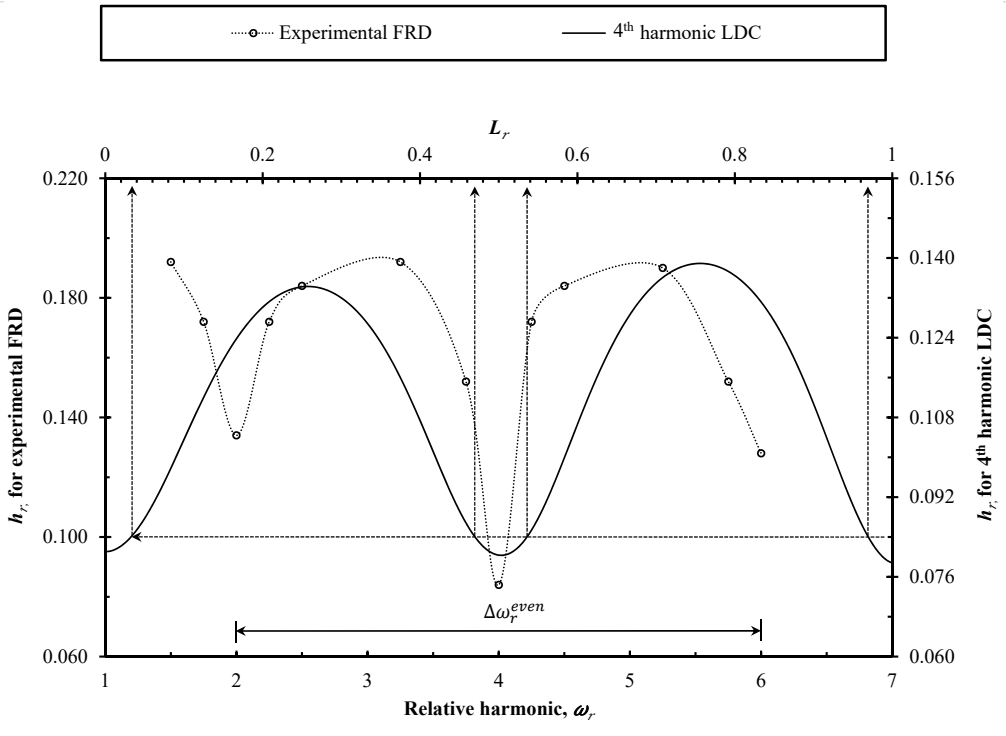

(b) 4th harmonic

Figure 5.10 Comparison of experimentally measured and theoretically computed relative leak locations.

should be small that makes it easy to determine the anticipated leak location. Other uncertainties of the system measurements and numerical assumptions may be taken into consideration for more accurate determination of leak locations.

Chapter 6

Summary and Conclusions

Following are summary and conclusion of the blockage detection approaches using pressure head oscillation and acoustic signal emission, and the leak detection approach using pressure head oscillation proposed by the current study.

6.1 Blockage Detection by Using Lower Harmonics of Pressure Oscillations

A technique to detect partial blockages in liquid pipelines is presented in this study. A simple reservoir-pipe-valve system is considered in which the downstream valve is oscillated at the first four harmonics of the pipeline to produce periodic flow. The governing equations are solved in the frequency domain using the transfer matrix method (TMM) and direct relationships between the pressure head oscillation and the blockage location are determined. These relationships are used to construct blockage detection curves the characteristics of which are discussed briefly. The effect of steady and unsteady friction on the model outputs and the formation of the pressure head oscillation nodes are discussed. As compared to the traditional frequency response diagram methods which require computing at several different frequencies, the current approach is more practical since it requires extraction of the amplitude of the pressure-head oscillation on first four harmonics to estimate the blockage location. The model results agree satisfactorily with those obtained in the time domain by the method of characteristics and with experimental measurements reported in the literature.

Model application shows that there is only one shared value of the partial blockage location among all the four modes of the downstream valve oscillations. It is found that the blockage location is independent of the blockage size if the partial blockage occurred at the location of the pressure head oscillation nodes. This limits the fact that a partial blockage in the pipeline increases the amplitude of the pressure head oscillation at even harmonics at all blockage locations rather than at the pressure head oscillation nodes. Also, it is shown that, for the 1^{st} harmonic, the rate of change of the amplitude of the pressure head oscillation decreases as the blockage size decreases.

The amplitude of the pressure head oscillations at the downstream end of the pipeline calculated in the current approach are slightly overestimated as compared to those obtained by the method of characteristics for the 1^{st} and 3^{rd} (odd) harmonics. However, there is almost full agreement between the two methods for the 2^{nd} and 4^{th} (even) harmonics. Comparing the results of the current approach with the experimental measurements shows that this approach is promising in determining the blockage location along a pipeline and may be adapted for field applications.

6.2 Blockage Detection by Continuous Emission of Acoustic Signal

This part of the current study includes exploiting the interaction between a partial blockage in a pipe and the steady-flow characteristics to detect the partial blockage. The partial blockage emits a continuous acoustic signal which can be recorded by a certain type of acoustic sensors (R6I-AST). The relationship between the accumulated signal strength and the sensor location is plotted on a curve which shows a hump in the vicinity of the blockage location. The height of the hump is proportional to the blockage size (the percent of reduction in the pipe diameter). The flow field in the primary zone of the pipe is described using a conventional CFD approach with

Reynolds-averaged Navier Stokes equations solved by using the FLUENT commercial package of Ansys software. The accumulated AE energy and the flow turbulence kinetic energy at the sensor locations are normalized using their relevant maximum values and compared on graphs in which they agreed on the hump created due to the blockage existence. This approach has the potential to be applied for gas and steam pipelines.

6.3 Leak Detection by Using Lower Harmonics of Pressure Oscillations

A leak detection technique in liquid pipelines using lower harmonics of the pipeline is presented in Chapter 5. The piping system consists of a constant-level reservoir at the upstream of the pipeline and a valve that can be closed and opened sinusoidally at the downstream. The sinusoidal movement of the downstream valve produces a sinusoidal pressure head oscillations the amplitude of which is related to the mode of oscillation. The first four harmonics of the pipeline are considered in the frequency domain analysis using the transfer matrix method (TMM). A direct relationship between the relative leak location and the amplitude of the pressure head oscillation at the downstream end of the pipeline is determined for the first four harmonics of the downstream valve oscillation. Each relationship is used to construct a leak detection curve (LDC) the characteristics of which are discussed briefly. The effect of steady and unsteady friction and the formation of the pressure head oscillation nodes are discussed. The outputs of the proposed technique show a satisfactory agreement with those obtained in the time domain using the method of characteristics (MOC). In addition, a leak in a pipeline from the literature is localized by using the 2^{nd} and 4^{th} (even) harmonics LDCs from the current approach and a good approximation of the leak location is obtained. The difference between the actual and calculated

relative leak locations may be attributed to the uncertainty in the calculation of unsteady friction and the experimental estimation of the system parameters. The current approach uses minimum efforts as compared to the traditional frequency response diagram (FRD) methods which require several runs of the valve oscillation at different frequencies to determine the leak location. The current approach has the potential to be implemented in the field, taking into consideration a number of uncertainties related to the real-life applications.

References

Al-Tofan, M., M. Elkholy, S. Khilqa, J. Caicedo, and M. H. Chaudhry (2018). Use of lower harmonics of pressure oscillations for blockage detection in liquid pipelines. *Journal of Hydraulic Engineering 145*(3), 04018090.

Black, P. (1992). A review of pipeline leak detection technology. In *Pipeline systems*, pp. 287–298. Springer.

Boaz, L., S. Kaijage, and R. Sinde (2014). An overview of pipeline leak detection and location systems. In *Proceedings of the 2nd Pan African International Conference on Science, Computing and Telecommunications (PACT 2014)*, pp. 133–137. IEEE.

Brunner, A. J. and M. Barbezat (2006). Acoustic emission monitoring of leaks in pipes for transport of liquid and gaseous media: a model experiment. In *Advanced Materials Research*, Volume 13, pp. 351–356. Trans Tech Publ.

Chaudhry, M. H. (1970). *Resonance in pressurized piping systems.* Ph. D. thesis, University of British Columbia.

Chaudhry, M. H. (2014). *Applied Hydraulic Transients,* 3rd ed. Springer, New York, NY.

Chaudhry, M. H. (2015). Analysis and control of hydraulic transients: practical aspects and considerations. In *Proc., 12th Int. Conf. on Pressure Surges, British Hydromechanic Research Assoc., Dublin, Ireland.*

Cole, E. S. (1979). Methods of leak detection: an overview. *Journal-American Water Works Association 71*(2), 73–75.

Colombo, A. F. and B. W. Karney (2002). Energy and costs of leaky pipes: toward comprehensive picture. *Journal of Water Resources Planning and Management 128*(6), 441–450.

Colombo, A. F., P. Lee, and B. W. Karney (2009). A selective literature review of transient-based leak detection methods. *Journal of Hydro-environment Research 2*(4), 212–227.

Covas, D., H. Ramos, and A. B. De Almeida (2005). Standing wave difference method for leak detection in pipeline systems. *Journal of Hydraulic Engineering 131*(12), 1106–1116.

Duan, H.-F., P. Lee, and M. Ghidaoui (2014). Transient wave-blockage interaction in pressurized water pipelines. *Procedia Engineering 70*, 573–582.

Duan, H.-F., P. J. Lee, M. S. Ghidaoui, and Y.-K. Tung (2011). Extended blockage detection in pipelines by using the system frequency response analysis. *Journal of Water Resources Planning and Management 138*(1), 55–62.

Duan, H.-F., P. J. Lee, A. Kashima, J. Lu, M. S. Ghidaoui, and Y.-K. Tung (2013). Extended blockage detection in pipes using the system frequency response: analytical analysis and experimental verification. *Journal of Hydraulic Engineering 139*(7), 763–771.

Duan, H. F., S. Meniconi, P. J. Lee, B. Brunone, and M. S. Ghidaoui (2017). Local and integral energy-based evaluation for the unsteady friction relevance in transient pipe flows. *Journal of Hydraulic Engineering 143*(7), 04017015–1–11.

Ferziger, J. H. and M. Peric (2012). *Computational methods for fluid dynamics*. Springer Science & Business Media.

Fiedler, J. (2014). An overview of pipeline leak detection technologies. *American School of Gas Measurement Technology (ASGMT), Peabody, MA, US*.

Geiger, G., D. Vogt, and R. Tetzner (2006). State-of-the-art in leak detection and localization. *Oil Gas European Magazine 32*(4), 193.

Giunta, G., S. Budano, A. Lucci, and L. Prandi (2012). Pipeline health integrity monitoring (phim) based on acoustic emission technique. In *ASME 2012 Pressure Vessels and Piping Conference*, pp. 277–283. American Society of Mechanical Engineers.

Gong, J., M. F. Lambert, A. R. Simpson, and A. C. Zecchin (2012). Single-event leak detection in pipeline using first three resonant responses. *Journal of Hydraulic Engineering 139*(6), 645–655.

Gong, J., A. C. Zecchin, A. R. Simpson, and M. F. Lambert (2013). Frequency response diagram for pipeline leak detection: Comparing the odd and even harmonics. *Journal of Water Resources Planning and Management 140*(1), 65–74.

Juliano, T. M., J. N. Meegoda, and D. J. Watts (2012). Acoustic emission leak detection on a metal pipeline buried in sandy soil. *Journal of Pipeline Systems Engineering and Practice 4*(3), 149–155.

Khilqa, S., M. Elkholy, M. Al-Tofan, J. Caicedo, and H. Chaudhry (2017). Damping rate of transient oscillations in pressurized closed conduits. In *37th IAHR World Congress, Kuala Lumpur, Malaysia 13-18 August 2017*.

Lee, P. J., J. P. Vítkovskỳ, M. F. Lambert, A. R. Simpson, and J. A. Liggett (2005a). Frequency domain analysis for detecting pipeline leaks. *Journal of Hydraulic Engineering 131*(7), 596–604.

Lee, P. J., J. P. Vítkovskỳ, M. F. Lambert, A. R. Simpson, and J. A. Liggett (2005b). Leak location using the pattern of the frequency response diagram in pipelines: a numerical study. *Journal of Sound and Vibration 284*(3), 1051–1073.

Lee, P. J., J. P. Vítkovskỳ, M. F. Lambert, A. R. Simpson, and J. A. Liggett (2008). Discrete blockage detection in pipelines using the frequency response diagram: numerical study. *Journal of Hydraulic Engineering 134*(5), 658–663.

Martins, N. M. C., B. Brunone, S. Meniconi, H. M. Ramos, and D. I. C. Covas (2017). Cfd and 1d approaches for the unsteady friction analysis of low reynolds number turbulent flows. *Journal of Hydraulic Engineering 143*(12), 04017050–1–12.

Massari, C., T.-C. Yeh, M. Ferrante, B. Brunone, and S. Meniconi (2015). A stochastic approach for extended partial blockage detection in viscoelastic pipelines: numerical and laboratory experiments. *Journal of Water Supply: Research and Technology-Aqua 64*(5), 583–595.

Massari, C., T. C. J. Yeh, M. Ferrante, B. Brunone, and S. Meniconi (2014). Detection and sizing of extended partial blockages in pipelines by means of a stochastic successive linear estimator. *Journal of Hydroinformatics 16*(2), 248–258.

Meniconi, S., B. Brunone, M. Ferrante, and C. Capponi (2016). Mechanism of interaction of pressure waves at a discrete partial blockage. *Journal of Fluids and Structures 62*, 33–45.

Meniconi, S., H. F. Duan, B. Brunone, M. S. Ghidaoui, P. J. Lee, and M. Ferrante (2014). Further developments in rapidly decelerating turbulent pipe flow modeling. *Journal of Hydraulic Engineering 140*(7), 04014028–1–9.

Meniconi, S., H. F. Duan, P. J. Lee, B. Brunone, M. S. Ghidaoui, and M. Ferrante (2013). Experimental investigation of coupled frequency and time-domain transient test–based techniques for partial blockage detection in pipelines. *Journal of Hydraulic Engineering 139*(10), 1033–1040.

Mohapatra, P., M. Chaudhry, A. Kassem, and J. Moloo (2006). Detection of partial blockage in single pipelines. *Journal of Hydraulic Engineering 132*(2), 200–206.

Mpesha, W., S. L. Gassman, and M. H. Chaudhry (2001). Leak detection in pipes by frequency response method. *Journal of Hydraulic Engineering 127*(2), 134–147.

Murvay, P.-S. and I. Silea (2012). A survey on gas leak detection and localization techniques. *Journal of Loss Prevention in the Process Industries 25*(6), 966–973.

Owowo, J. (2016). *Simulation, measurement and detection of leakage and blockage in fluid pipeline systems*. Ph. D. thesis, University of Manchester.

Papadopoulou, K., M. N. Shamout, B. Lennox, D. Mackay, A. Taylor, J. Turner, and X. Wang (2008). An evaluation of acoustic reflectometry for leakage and blockage detection. *Proceedings of the Institution of Mechanical Engineers, Part C: Journal of Mechanical Engineering Science 222*(6), 959–966.

Puust, R., Z. Kapelan, D. Savic, and T. Koppel (2010). A review of methods for leakage management in pipe networks. *Urban Water Journal 7*(1), 25–45.

Sattar, A. (2015). *Leaks and Blockages in Pipelines*. LAMBERT Academic Publishing, Saarbrucken, Germany.

Sattar, A. M. and M. H. Chaudhry (2008). Leak detection in pipelines by frequency response method. *Journal of Hydraulic Research 46*(sup1), 138–151.

Sattar, A. M., M. H. Chaudhry, and A. A. Kassem (2008). Partial blockage detection in pipelines by frequency response method. *Journal of Hydraulic Engineering 134*(1), 76–89.

Scola, I. R., G. Besançon, and D. Georges (2017). Blockage and leak detection and location in pipelines using frequency response optimization. *Journal of Hydraulic Engineering 143*(1), 04016074–1–12.

Silva, L. L., P. Monteiro, J. Vidal, and T. A. Netto (2014). Acoustic reflectometry for blockage detection in pipeline. In *ASME 2014 33rd International Conference on Ocean, Offshore and Arctic Engineering*, pp. V06AT04A027–V06AT04A027. American Society of Mechanical Engineers.

Tuck, J., P. J. Lee, M. Davidson, and M. S. Ghidaoui (2013). Analysis of transient signals in simple pipeline systems with an extended blockage. *Journal of Hydraulic Research 51*(6), 623–633.

Vardy, A. E. and J. M. B. Brown (2003). Transient turbulent friction in smooth pipe flows. *Journal of Sound and Vibration 259*(5), 1011–1036.

Vitkovsky, J. P., A. Bergant, A. R. Simpson, and M. F. Lambert (2003). Steady-osciallatory flow solution including unsteady friction. In *International Conference, Pumps, Electromechanical Devices, and Systems Applied to Urban Water Management, IAHR, IHR, and BHR Group, Granfield, U.K.*

Wang, X., M. L. Keith, A. P. Kassandra, L. Barry, and T. T. John (2012). Detection of hydrate and other blockages in gas pipelines using acoustic reflectometry. *Proceedings of the Institution of Mechanical Engineers, Part C: Journal of Mechanical Engineering Science 226*(7), 1800–1810.

Wang, X.-J., M. F. Lambert, and A. R. Simpson (2005). Detection and location of a partial blockage in a pipeline using damping of fluid transients. *Journal of Water Resources Planning and Management 131*(3), 244–249.

Yan, J., Y. Heng-hu, Y. Hong, Z. Feng, L. Zhen, W. Ping, and Y. Yan (2015). Nondestructive detection of valves using acoustic emission technique. *Advances in Materials Science and Engineering 2015*.

Zielke, W. (1968). Frequency-dependent friction in transient pipe flow. *Journal of Basic Engineering 90*(1), 109–115.

Appendix A

Derivations of the Blockage Equations

The overall extended transfer matrix, $\mathbf{U}$, for the reservoir-pipe-valve system, Fig. 3.1, may be written as

$$\mathbf{U} = \begin{bmatrix} u_{11} & u_{12} & u_{13} \\ u_{21} & u_{22} & u_{23} \\ u_{31} & u_{32} & u_{33} \end{bmatrix} = \mathbf{F}_2\ \mathbf{P}_2\ \mathbf{F}_1 \tag{A.1}$$

in which

$$\mathbf{F}_2 = \begin{bmatrix} \cos b_2\omega & -\frac{j}{C}\sin b_2\omega & 0 \\ -jC\sin b_2\omega & \cos b_2\omega & 0 \\ 0 & 0 & 1 \end{bmatrix}; \qquad \mathbf{P}_2 = \begin{bmatrix} 1 & 0 & 0 \\ -\dfrac{2\Delta H_0}{Q_0} & 1 & 0 \\ 0 & 0 & 1 \end{bmatrix} \text{ and}$$

$$\mathbf{F}_1 = \begin{bmatrix} \cos b_1\omega & -\frac{j}{C}\sin b_1\omega & 0 \\ -jC\sin b_1\omega & \cos b_1\omega & 0 \\ 0 & 0 & 1 \end{bmatrix}$$

Multiplying these matrices, u_{11} and u_{21} of the overall extended transfer matrix may be written as

$$u_{11} = \cos(b_2\omega)\ \cos(b_1\omega) + \cos(b_1\omega)\frac{j}{C}\sin(b_2\omega)\ \frac{2\Delta H_0}{Q_0} + \frac{j}{C}\sin(b_2\omega)\ jC\sin(b_1\omega) \tag{A.2}$$

For fundamental (1^{st}) harmonic, $\omega = \omega_{TH} = \dfrac{a\pi}{2L}$. Simplifying using $b_i = \dfrac{L_i}{a_i}$, $L_1 = L_b$ and $L_2 = L - L_b$ and then taking the relative blockage location, $L_r = L_b/L$ gives

$$u_{11} = \cos\left(\frac{\pi}{2}(1-L_r)\right)\cos\left(\frac{\pi}{2}L_r\right) + \cos\left(\frac{\pi}{2}L_r\right)\frac{2\Delta H_0 j}{CQ_0}\sin\left(\frac{\pi}{2}(1-L_r)\right) - \sin\left(\frac{\pi}{2}L_r\right)$$
$$\sin\left(\frac{\pi}{2}(1-L_r)\right)$$

Note that, $\cos\left(\frac{\pi}{2}(1-L_r)\right) = \sin\left(\frac{\pi}{2}L_r\right)$ and $\sin\left(\frac{\pi}{2}(1-L_r)\right) = \cos\left(\frac{\pi}{2}L_r\right)$. Hence using trigonometric identities, this equation may be simplified to

$$u_{11} = \frac{2\Delta H_0}{CQ_0}\cos^2\left(\frac{\pi}{2}L_r\right)j$$

$$u_{21} = \left(-Cj\sin(b_2\omega) - \cos(b_2\omega)\frac{2\Delta H_0}{Q_0}\right)\cos(b_1\omega)$$
$$-\cos(b_2\omega)\ Cj\ \sin(b_1\omega) \tag{A.3}$$

For fundamental (1^{st}) harmonic,

$$u_{21} = \cos\left(\frac{L_b}{a}\frac{a\pi}{2L}\right)(-Cj)\sin\left(\frac{L-L_b}{a}\frac{a\pi}{2L}\right) - \frac{2\Delta H_0}{Q_0}\cos\left(\frac{L_b}{a}\frac{a\pi}{2L}\right)\cos\left(\frac{L-L_b}{a}\frac{a\pi}{2L}\right)$$
$$-\cos\left(\frac{L-L_b}{a}\frac{a\pi}{2L}\right)(Cj)\sin\left(\frac{L_b}{a}\frac{a\pi}{2L}\right)$$

which may be further simplified to

$$u_{21} = -\frac{\Delta H_0}{Q_0}\left(2\sin\left(\frac{\pi}{2}L_r\right)\cos\left(\frac{\pi}{2}L_r\right)\right) - Cj = -\frac{\Delta H_0}{Q_0}\sin(\pi L_r) - Cj \tag{A.4}$$

Utilizing the extended point matrix and the boundary conditions at the valve

$$h^L_{n+1} = u_{21}\ q^R_1 + u_{23} \tag{A.5}$$

$$\text{where}\quad q^R_1 = -\frac{u_{23} - \frac{2H_0}{Q_0}u_{13} + \frac{2H_0 k}{\tau_0}u_{33}}{u_{21} - \frac{2H_0}{Q_0}u_{11} + \frac{2H_0 k}{\tau_0}u_{31}}$$

where τ_0 is the initial relative valve opening and k is the amplitude of the valve sinusoidal motion.

Since the oscillating valve is the only forcing function, $u_{13} = u_{23} = u_{31} = 0$, $u_{33} = 1$ and $h^L_{n+1} = \left(\frac{2H_0 k}{\tau_0}\right) / \left(\frac{2H_0}{Q_0}\frac{u_{11}}{u_{21}} - 1\right)$, then substituting for u_{11} and u_{21} in Eq. A.5 results in

$$h^L_{n+1,1} = \frac{\dfrac{2H_0 k}{\tau_0}}{\dfrac{4H_0}{Q_0}\dfrac{\dfrac{\Delta H_0}{CQ_0}\cos^2\left(\dfrac{\pi}{2}(L_r)\right)j}{-\dfrac{\Delta H_0}{Q_0}\sin(\pi L_r) - Cj} - 1} \tag{A.6}$$

Following the same steps, similar equations may be obtained for a valve oscillating at the 2nd, 3rd and 4th harmonics as follows

$$h^L_{n+1,2} = \frac{\dfrac{2H_0 k}{\tau_0}}{\dfrac{2H_0}{Q_0}\dfrac{-1 + \dfrac{\Delta H_0}{CQ_0}\sin(2\pi L_r)j}{\dfrac{2\Delta H_0}{Q_0}\cos^2(\pi L_r)} - 1} \tag{A.7}$$

$$h^L_{n+1,3} = \frac{\dfrac{2H_0 k}{\tau_0}}{\dfrac{4H_0}{Q_0}\dfrac{-\dfrac{\Delta H_0}{CQ_0}\cos^2\left(\dfrac{3\pi}{2}(L_r)\right)j}{\dfrac{\Delta H_0}{Q_0}\sin(3\pi L_r) + Cj} - 1} \tag{A.8}$$

$$h^L_{n+1,4} = \frac{\dfrac{2H_0 k}{\tau_0}}{\dfrac{2H_0}{Q_0}\dfrac{1 - \dfrac{\Delta H_0}{CQ_0}\sin(4\pi L_r)j}{-\dfrac{2\Delta H_0}{Q_0}\cos^2(2\pi L_r)} - 1} \tag{A.9}$$

in which, $h^L_{n+1,1}$, $h^L_{n+1,2}$, $h^L_{n+1,3}$ and $h^L_{n+1,4}$ are the amplitudes of the pressure head oscillations at the valve for the 1st, 2nd, 3rd and 4th harmonics, respectively. Now, the relative amplitude of the pressure head oscillation, h_r, for each lower harmonic is determined by dividing the absolute value of the complex number obtained from each of the above equations by the height of water in the upstream reservoir, H_0.

The relative amplitude of the pressure head oscillation for the first harmonic, for instance, may be determined as follows

$$\text{Let} \quad a_1 = \frac{2H_0 k}{\tau_0}; \qquad a_2 = \frac{4H_0}{Q_0}\frac{\Delta H_0}{CQ_0}\cos^2\left(\frac{\pi}{2}L_r\right);$$
$$a_3 = -\frac{\Delta H_0}{Q_0}\sin(\pi L_r); \qquad a_4 = a_1 a_3;$$
$$a_5 = -Ca_1; \qquad a_6 = a_2 + C;$$
$$a_7 = \frac{-a_3 a_4 + a_5 a_6}{{a_3}^2 + {a_6}^2}; \qquad a_8 = \frac{a_4 a_6 + a_3 a_5}{{a_3}^2 + {a_6}^2}$$

which results in

$$h^L_{n+1,1} = a_7 - a_8 j, \quad h_{r1} = \frac{\left|h^L_{n+1,1}\right|}{H_0} \tag{A.10}$$

In this expression, h_{r1} is the relative amplitude of the pressure head oscillation at the downstream end of the pipeline when the valve is oscillating at the 1st harmonic. A similar procedure is followed to obtain the relative amplitude of the pressure head oscillation at the downstream end of the pipeline for an oscillating valve at the 2nd, 3rd and 4th harmonics.

Appendix B

Derivations of the Leak Equations

The overall extended transfer matrix, $\mathbf{U}$, for the reservoir-pipe-valve system, Fig. 5.1, may be written as

$$\mathbf{U} = \begin{bmatrix} u_{11} & u_{12} & u_{13} \\ u_{21} & u_{22} & u_{23} \\ u_{31} & u_{32} & u_{33} \end{bmatrix} = \mathbf{F}_2 \ \mathbf{P}_2 \ \mathbf{F}_1 \tag{B.1}$$

This matrix may be obtained by ordered multiplication of the field matrix of the piece of the pipeline to the right of the leak, F_2, the point matrix of the leak, P_2, and the field matrix of the piece of the pipeline to the left of the leak, F_1. The oscillating valve is the only forcing function, so the following multiplication may be considered

$$= \begin{bmatrix} \cos b_2\omega & -\frac{j}{C}\sin b_2\omega \\ -jC\sin b_2\omega & \cos b_2\omega \end{bmatrix} \begin{bmatrix} 1 & -\frac{Q_{l0}}{2\Delta H_0} \\ 0 & 1 \end{bmatrix} \begin{bmatrix} \cos b_1\omega & -\frac{j}{C}\sin b_1\omega \\ -jC\sin b_1\omega & \cos b_1\omega \end{bmatrix}$$

The ordered multiplication of the above matrices gives the elements u_{11} and u_{21} of the overall transfer matrix as

$$\begin{aligned} u_{11} = & \cos b_2\omega \times \cos b_1\omega \\ & + \left[\cos b_2\omega \times \left(-\frac{Q_{l0}}{2\Delta H_0}\right) \times -\frac{j}{C}\sin b_1\omega\right] - jC\sin b_1\omega \end{aligned}$$

For fundamental (1^{st}) harmonic, $\omega = \omega_{TH} = \dfrac{a\pi}{2L}$. Simplifying using $b_i = \dfrac{L_i}{a_i}$, $L_1 = L_l$ and $L_2 = L - L_l$ and then taking the relative leak location, $L_r = L_l/L$ gives

$$\begin{aligned} u_{11} = & \cos\left(\frac{L-L_l}{L}\frac{\pi}{2}\right) \times \cos\left(\frac{L_l}{L}\frac{\pi}{2}\right) + \cos\left(\frac{L-L_l}{L}\frac{\pi}{2}\right) \times \left(-\frac{Q_{l0}}{2\Delta H_0}\right) \times \\ & - jC\sin\left(\frac{L_l}{L}\frac{\pi}{2}\right) + \frac{j}{C}\sin\left(\frac{L-L_l}{L}\frac{\pi}{2}\right) \times -jC\sin\left(\frac{L_l}{L}\frac{\pi}{2}\right) \end{aligned}$$

Using trigonometric identities gives

$$u_{11} = \sin\left(\frac{L_l}{L}\frac{\pi}{2}\right) \times \cos\left(\frac{L_l}{L}\frac{\pi}{2}\right) + \sin\left(\frac{L_l}{L}\frac{\pi}{2}\right) \times \left(-\frac{Q_{l0}Cj}{2\Delta H_0}\right) \times \sin\left(\frac{L_l}{L}\frac{\pi}{2}\right) - \cos\left(\frac{L_l}{L}\frac{\pi}{2}\right) \times \sin\left(\frac{L_l}{L}\frac{\pi}{2}\right)$$
$$= \left(-\frac{Q_{l0}Cj}{2\Delta H_0}\right) \times \sin^2 L_r\frac{\pi}{2}$$

Note that, $2\sin^2\left(L_r\frac{\pi}{2}\right) = \text{versin}\,(\pi L_r)$

$$\text{Hence} \quad u_{11} = \left(-\frac{Q_{l0}C}{4\Delta H_0}\right) \times \text{versin}\,(\pi L_r)\, j$$

$$u_{21} = -Cj\sin\left(\frac{L-L_l}{L}\frac{\pi}{2}\right) \times \cos\left(\frac{L_l}{L}\frac{\pi}{2}\right) + \left(-Cj\sin\left(\frac{L-L_l}{L}\frac{\pi}{2}\right) \times \left(-\frac{Q_{l0}}{2\Delta H_0}\right) + \cos\left(\frac{L-L_l}{L}\frac{\pi}{2}\right)\right)\left(-Cj\sin\left(\frac{L_l}{L}\frac{\pi}{2}\right)\right)$$

Using similar simplifications to that used in u_{11} derivation

$$u_{21} = \frac{Q_{l0}C^2}{4\Delta H_0} \times \sin(\pi L_r) - Cj$$

The pressure head oscillation in the downstream end of the pipeline may be related to the discharge to the left of the first section in the pipeline (immediately to the right of the reservoir-pipeline intersection) utilizing the point matrix of the leak and the boundary conditions at the valve, as follows

$$h^L_{n+1} = u_{21}q^R_1$$

$$\text{where} \quad q^R_1 = \frac{\frac{2H_0k}{\tau_0}}{\frac{2H_0}{Q_0}u_{11} - u_{21}}$$

$$\text{Hence} \quad h^L_{n+1} = \frac{\frac{2H_ok}{\tau_o}}{\frac{2H_o}{Q_o}\frac{u_{11}}{u_{21}} - 1}$$

Substitute for u_{11} and u_{21} in the last equation gives

$$h^L_{n+1,1} = \frac{\frac{2H_ok}{\tau_o}}{\frac{2H_o}{Q_o} \times \frac{\frac{CQ_{l0}}{4\Delta H_o} \times \text{versin}\,(L_r\pi)\, j}{\frac{C^2Q_{l0}}{4\Delta H_0}\sin(\pi L_r) - Cj} - 1} \tag{B.2}$$

Using the same steps, similar equations can be obtained for the case of a valve oscillating under the 2nd. 3rd, and 4th harmonics to give

$$h^L_{n+1,2} = \frac{\dfrac{2H_0k}{\tau_0}}{\dfrac{2H_0}{Q_0} \times \dfrac{-1 + \dfrac{CQ_{l0}}{4\Delta H_0} \times \sin(2\pi L_r)\, j}{\dfrac{C^2Q_{l0}}{2\Delta H_0}\sin^2(\pi L_r)} - 1} \tag{B.3}$$

$$h^L_{n+1,3} = \frac{\dfrac{2H_0k}{\tau_0}}{\dfrac{2H_0}{Q_0} \times \dfrac{-\dfrac{CQ_{l0}}{4\Delta H_0} \times \text{versin}(3\pi L_r)\, j}{\dfrac{C^2Q_{l0}}{4\Delta H_0}\sin(3\pi L_r) + Cj} - 1} \tag{B.4}$$

$$h^L_{n+1,4} = \frac{\dfrac{2H_0k}{\tau_0}}{\dfrac{2H_0}{Q_0} \times \dfrac{1 - \dfrac{CQ_{l0}}{4\Delta H_0} \times \sin(4\pi L_r)\, j}{-\dfrac{C^2Q_{l0}}{2\Delta H_0}\sin^2(2\pi L_r)} - 1} \tag{B.5}$$

where, $h^L_{n+1,1}$, $h^L_{n+1,2}$, $h^L_{n+1,3}$, and $h^L_{n+1,4}$ are amplitudes of pressure head oscillations at the downstream end of the pipeline for the 1st, 2nd, 3rd, and 4th harmonics, respectively.

Now, the relative pressure head oscillations, h_r, for each lower harmonic is determined by dividing the length of the complex number obtained from each of the above equations by the mean pressure head in the pipe, H_o. The length of the complex number for the first harmonic, as an example, may be determined as follows:

Let, $\quad a_1 = \dfrac{2H_0k}{\tau_0}; \quad a_2 = \dfrac{2H_0k}{Q_0}; \quad a_3 = \dfrac{CQ_{l0}}{4\Delta H_0} \times \text{versin}(L_r\pi); \quad a_4 = \dfrac{C^2Q_{l0}}{4\Delta H_0}\sin(\pi L_r)$

$$h^L_{n+1,1} = \frac{a_1}{a_2\dfrac{a_3 j}{a_4 - Cj} - 1} = \frac{a_1}{\dfrac{a_2a_3j - (a_4 - Cj)}{a_4 - Cj}}$$
$$= \frac{a_1(a_4 - Cj)}{-a_4 + (a_2a_3 + C)j} = \frac{a_5 - a_6 j}{a_8 + a_7 j}$$

where, $a_5 = a_1 \cdot a_4$; $a_6 = -Ca_1$; $a_7 = A_2A_3 + C$; and $a_8 = -a_4$

$$\text{Hence} \quad h^L_{n+1,1} = \frac{a_5 - a_6 j}{a_8 + a_7 j} \cdot \frac{a_8 - a_7 j}{a_8 - a_7 j}$$

where, $(a_8 - a_7 j)$ is the denominator conjugate, hence it may be written as

$$\begin{aligned} h^L_{n+1,1} &= \frac{a_5 a_8 - a_5 A_7 j - a_6 A_8 j + a_6 a_7 j^2}{{a_8}^2 - a_7 a_8 j + a_7 a_8 j - {a_7}^2 j^2} \\ &= \frac{(a_5 a_8 - a_6 a_7) - (a_5 a_7 + a_6 a_8)\, j}{{a_7}^2 + {a_8}^2} \end{aligned}$$

Let, $a_9 = \dfrac{a_5 a_8 - a_6 a_7}{{a_7}^2 + {a_8}^2}$; $a_{10} = \dfrac{a_5 a_7 + a_6 a_8}{{a_7}^2 + {a_8}^2}$ Then,

$$h^L_{n+1,1} = a_9 - a_{10} j$$

$$\left|h^L_{n+1,1}\right| = \sqrt{(a_9)^2 + (-a_{10})^2}$$

$$h_{r1} = \frac{\left|h^L_{n+1,1}\right|}{H_0}$$

where, h_{r1} is the relative pressure head oscillation at the downstream end of the pipeline when the valve is oscillated at the 1st harmonic.

A similar procedure is followed to obtain the relative pressure head oscillations at the downstream end of the pipeline when the valve is oscillated at the 2nd, 3rd, and 4th harmonics.

Appendix C

Reprint Permission

Permissions approval

PERMISSIONS <permissions@asce.org>
Fri 5/17/2019 8:38 AM
To: AL-TOFAN, MOHAMMED H <maltofan@email.sc.edu>

Dear Mahommed Al-Tofan,
Thank you for your inquiry. As an original author of an ASCE journal article or proceedings paper, you are permitted to reuse your own content (including figures and tables) for another ASCE or non-ASCE publication, including your dissertation, provided it does not account for more than 25% of the new work. This email serves as permission to reuse your work shown below.

- "Use of Lower Harmonics of Pressure Oscillations for Blockage Detection in Liquid Pipelines", *Journal of Hydraulic Engineering*, (145/3), https://doi.org/10.1061/(ASCE)HY.1943-7900.0001568

A full credit line must be added to the material being reprinted. For reuse in non-ASCE publications, add the words "With permission from ASCE" to your source citation. For Intranet posting, add the following additional notice: "This material may be downloaded for personal use only. Any other use requires prior permission of the American Society of Civil Engineers. This material may be found at [URL/link of abstract in the ASCE Library or Civil Engineering Database]."

Each license is unique, covering only the terms and conditions specified in it. Even if you have obtained a license for certain ASCE copyrighted content, you will need to obtain another license if you plan to reuse that content outside the terms of the existing license. For example: If you already have a license to reuse a figure in a journal, you still need a new license to use the same figure in a magazine. You need a separate license for each edition.

For more information on how an author may reuse their own material, please view:
http://ascelibrary.org/page/informationforasceauthorsreusingyourownmaterial

Sincerely,

Leslie Connelly
Senior Marketing Coordinator
American Society of Civil Engineers
1801 Alexander Bell Drive
Reston, VA 20191

PERMISSIONS@asce.org

703-295-6169
Internet: www.asce.org/pubs | www.ascelibrary.org | http://ascelibrary.org/page/rightsrequests